グループ1

神経細胞の機能維持メカニズムの解明ならびに創薬への展開

高度神経細胞機能の維持メカニズムの解明ならびに創薬への展開

同志社大学生命医科学研究科　　西川喜代孝
同志社大学生命医科学部　　高橋美帆
東京大学大学院・理学研究科　　菅　裕明

１．はじめに

中枢神経系の高次機能は厳密な制御の下で維持されており、そのバランスが崩れると、認知障害、発達障害、Angelman 症候群、パーキンソン病等のさまざまな神経疾患が発症する。本研究では、以下に示す２つの局面からその制御機構の一端を分子生物学的に解明すること、その上で新たな創薬の分子標的を同定すること、さらにその制御分子ならびに制御法を確立し、これら精神神経疾患の治療に役立てることを目的とする。

２．研究の目的と概要

A) 高次神経機能維持におけるCa^{2+}-カルモデュリン依存性蛋白リン酸化酵素の作用解明とその制御法の確立

中枢神経系の機能維持にはさまざまなキナーゼが関与しているが、その中でもCa^{2+}-カルモデュリン依存性蛋白リン酸化酵素（CaMK）はシナプス伝達や可塑性に代表される高次神経機能調節において中心的な役割を果たしている。CaMKにはCaMKI, II, IVの３種のアイソザイムが知られているが、基質特異性、局在性、活性化機構が異なっており、それぞれが個別の機能を果たしていると考えられている。一方で、その活性化の異常が認知障害、学習障害、痙攣、Angelman症候群、パーキンソン病等の精神神経疾患に関連していることが指摘されている。本研究では、独自に開発した手法（PCT出願/JP2005/012286）を用いて各CaMKサブタイプ（CaMKI, II, IV）に対する特異的阻害剤を開発し、ユニークな視点から各アイソザイムの機能を解明するとともに、これまで不可能だったアイソザイムレベルでの厳密な活性制御法を確立し、各種神経疾患の新規治療薬としての確立を目指す。

B) 神経機能維持に関わる細胞内小胞輸送の制御法の確立

細胞内での小胞輸送の厳密な制御は、さまざまな場面で生体の恒常性の維持に貢献している。特に、神経細胞においては神経情報伝達物質の貯蔵、輸送、放出の一連の現象に重要な役割を果たしている。その一方で、アルツハイマー病の病原因子であるamyloid-β（Aβ）ならびにその前駆体であるβ-amyloid precursor protein(APP)等の

各種疾患関連分子群の輸送にも小胞輸送が密接に関与している。本研究では、神経細胞内での小胞輸送を、さまざまな段階で制御できる新規手法を確立する。具体的には、細胞内骨格、ならびに細胞内小胞輸送に影響をあたえることが知られている各種毒素分子に着目し、その毒素分子に結合してその作用を修飾する分子を開発してゆく。得られた毒素分子と修飾分子を組み合わせる事によって、各ステージ特異的小胞輸送制御法を確立する。本系を用いて小胞輸送制御機構を明らかにし、さらにその制御を基盤とした関連疾患に対する治療薬開発へと発展させる。

３．結果および考察

A) 高次神経機能維持におけるCaMKの作用解明とその制御法の確立

３-A-１　CaMKII 阻害ペプチドによるマクロファージの活性化の制御

CaMKII は、脳での神経伝達物質の合成や分泌、長期増強の誘導などの高次神経機能の制御、さらに炎症細胞での Toll 様受容体(TLR)を介したサイトカイン産生制御など、多岐に渡る生命現象に深く関与している。我々はこれまでに、CaMKⅡの触媒部位を標的とし、多価型ペプチドライブラリー法を用い、基質情報に依存しない新たな CaMKⅡ特異的阻害ペプチド（M1-M6）を開発することに成功している（特許第 5754008 号、2015/6/5)。そこで、CaMKⅡが関与する細胞内情報伝達に及ぼすこれら阻害ペプチドの効果を検討する目的で、LPS 刺激による TLR4 を介したマクロファージからの炎症性サイトカインの産生に及ぼす影響を検討した。

得られたペプチド(M1-M6)の他、これらのペプチドに膜透過性を付与する目的で M1, M3, M6 の N 末端にミリストイル基（myr）を導入したペプチド(myr-M1, myr-M3、myr-M6)を作製した。これら一連の化合物を用いて、マクロファージ系細胞である Raw264 細胞に LPS(10 ng/ml, 24h)刺激を加えた時に産生される炎症性サイトカイン（TNFα）量に及ぼす効果を検討した。その結果、LPS による TLR4 刺激に伴う TNFαの産生増大は、5 μM の M6 によって 90%以上, myr-M3 によって 80%以上、それぞれ阻害されることを見出した。この時、myr 化されていない M3 では阻害効果は 60%であることから、阻害ペプチドの配列によっては効率のよい膜透過能を持たないことがあること、その場合でも myr 化によって十分な膜透過能を付与できることが示された。

次に、M6 ならびに myr-M3 が実際に細胞内の CaMKII の活性化を阻害することによって TNFαを抑制しているのかを検討した。CaMKII は Ca/CaM の結合によって Thr286 が自己リン酸化されることよって活性化することが知られている。そこでリン酸化 Thr286 を特異的に認識する抗体を用い、western blot 法によって、CaMKII の活性化に与える M6 ならびに myr-M3 を検討した。その結果、LPS(10 ng/ml)刺激 30 分後に観察される顕

著なCaMKIIの自己リン酸化をM6ならびにmyr-M3ともに容量依存的に有意に抑制することが示された。このことから、これら阻害薬はRaw264細胞内においてLPS刺激によるCaMKIIの活性化を直接阻害しているものと考えられた。

Raw264細胞はLPS刺激によってTNFα以外にも様々な炎症性サイトカインを産生することが知られている。そこで、LPS(10 ng/ml, 3h)刺激によって誘導される一連の炎症性サイトカイン(TNFα, IL1β, IL-6, IL-15, MIP1α, MIP1β, IL-12b)のmRNAレベルの増強に及ぼすM6ならびにmyr-M3の効果を検討した。その結果、これら全てのサイトカンmRNAレベルはLPSによって著しく増強されるが、M6は全てのサイトカンmRNAレベルの増強を完全に抑制すること、を見出した。myr-M3はM6に比較すると抑制効果は減弱するものの、TNFα, IL1β, IL-6, IL-12bのmRNAレベルの増強を有意に阻害することが明らかとなった。

以上の結果から、我々が同定したCaMKII阻害ペプチドのうち、M6ならびにmyr-M3は、代表的な炎症性細胞であるマクロファージにおいて、LPS刺激によって誘導されるCaMKIIの活性化を顕著に抑制し、その下流に位置する各種炎症性サイトカイン産生の誘導を効率よく阻害する能力を有していることが示された。

<u>３-A-2　CaMKII阻害ペプチドによるミクログリア活性化の制御</u>

脳や脊髄に存在するマクロファージ様免疫細胞であるミクログリアは中枢神経系を構成する全グリア細胞の約5-20%を占め、脳損傷部位の清掃機能、炎症の惹起、抗原提示機能などを有している。その一方で、ミクログリアは神経変性疾患の病態進行に関与していることが示されている。最近、脊髄内のミクログリアの活性化が慢性疲労症候群で見られる異常な痛みの主要な原因であることが明らかにされたことから、ミクログリアの異常な活性化を制御する薬剤はいまだ有効な治療薬のない本疾患に対する新規治療薬として期待される。これまでの検討で、M6ならびにmyr-M3はマクロファージの活性化を効率よく抑制する能力を有することことから、ミクログリアのin vitroならびにin vivoの活性化に及ぼすこれらペプチドの阻害効果を検討した。

ミクログリアは新生児マウスの全脳より取得した、初代培養ミクログリアを使用した。ミクログリア特異的タンパクであるIbaIの発現をFACSにより定量し、ミクログリアの純度は90%以上であることを確認した。本初代培養ミクログリアをLPS(10 ng/ml, 24h)刺激すると、顕著なTNFα産生の増強が見られることを確認した。そこで、このTNFα産生に及ぼすM6ならびにmyr-M3の阻害効果を検討したところ、10 μMのM6によって95%以上, myr-M3によって70%以上、それぞれ阻害されることを見出した。この時、M6はCaMKIIの自己リン酸化、すなわち活性化を有意に抑制していることが示された

（図１）。さらに、LPS(10 ng/ml, 3h)刺激によって誘導される一連の炎症性サイトカイン(TNFα, IL1β, IL-6, IL-15, MIP1α, MIP1β, IL-12b)の mRNA レベルの増強に及ぼす効果を検討したところ、M6 は全てのサイトカン mRNA レベルの増強を完全に抑制すること、myr-M3 は IL1β, IL-6, IL-12b の mRNA レベルの増強を有意に阻害すること、が明らかとなった。

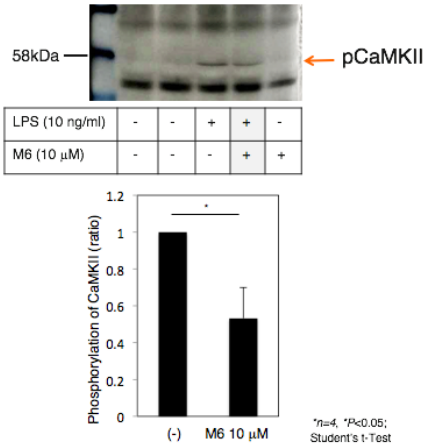

図 1

近年、脳での炎症時、あるいは障害時には、TNF や IL-6 などの炎症生サイトカイン、が産生され、特に IL-6 は脳においてパーキンソン病やアルツハイマー病、多発性硬化症等様々な疾患の発症に関与していることが明らかにされてきている（**Int. J. Biol. Sci.**, 2012, 8, 1254-）。興味深いことに、その産生細胞はアストロサイト、そしてミクログリアが主とされている。そこで、LPS の腹腔内投与によって誘導される、脳内部の炎症性サイトカイン産生に及ぼす M6 の効果を検討することにした。これは全身性の敗血症モデルであり、その際脳内での炎症反応をモニタリングするのに適した系である（**Mol. Cell. Biol.**, 2015, 35, 3590-）。8 週齢の Balb/c マウスに 500 μg の M6 存在、あるいは非存在下で、1 mg/kg の LPS を腹腔内投与し、４時間後の血清ならびに脳を採取し、各種炎症生サイトカイン量ならびに mRNA 量を定量した。その結果、LPS 刺激によって血清中の TNFα及び IL-6 量は著しく増加するが、M6 はこれらのサイトカインの増加を減少させる傾向を示すものの有意な差は認められなかった。その一方で、脳内で著しい増加を示す一連の炎症性サイトカイン mRNA のうち、M6 は TNFα, IL1β, IL-6, IL-15, IL-12b の増加をいずれも顕著に抑制することを見出した（図２）。これらのサイトカン mRNA 産生の増加がミクログリアの活性化を介しているかを検証するため、現在脳内のミクログリアの活性化に対する M６の抑制効果を同系を用いて形態学的に検討中である。

以上の結果から、M6 は生体内においても有効に作用しうることが示された。今後、活性化ミクログリアの脊髄後角への投与によって誘導される神経障害性疼痛モデル、坐骨神経部分障害モデル等、各種神経疾患モデルでの M6 の効果を検証し、CaMKII の活性化制御を作用機構とする新たな治療戦略の確立を目指す。

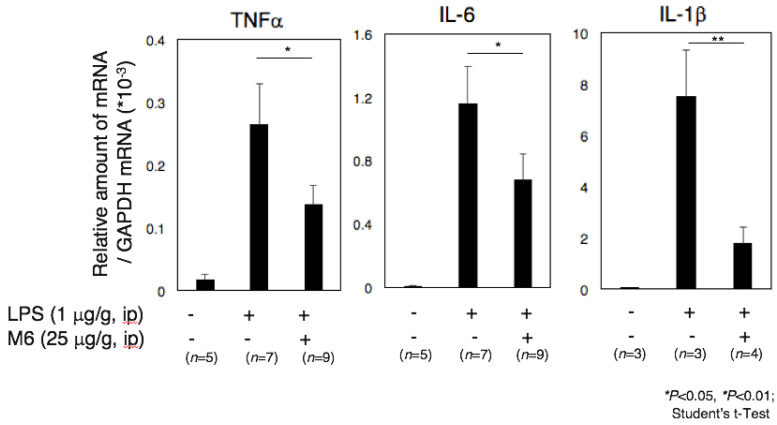

図２

３-A-３　CaMKIV ならびに CaMKIγを標的とした特異的阻害ペプチドの同定

CaMKI, II, IV の各アイソザイムは基質特異性が非常に類似していることから、各々を峻別する特異的阻害薬の開発は困難であるとされていた。そこで、CaMKI, IV についても CaMKII と同様に多価型ペプチドライブラリー法を用いて部分的な阻害モチーフ情報を取得することを目的とした。さらに、最近、最大 384 種の多価型ペプチドをセルロース膜ならびにスライドグラスにスポット合成する技術を開発しており（**Appl. Environ. Microbiol.**, 2015, 81, 1092-, 特許第 5718574 号;2015/3/7）、本技術と多価型ペプチドライブラリー法により取得した阻害モチーフ情報を組み合わせることにより、CaMKI, IV それぞれに特異的な阻害モチーフの同定を試みた。

CaMKIV ならびに CaMKIγについて、各々の kinase domain をバキュロウイルス発現ベクターに組み入れ、Bac to Bac バキュロウイルス発現系を用い、各組み替えタンパク質の大量調製系を確立した。本系を用い、高純度の CaMKIV、ならびに CaMKIγを、数百 μg 取得することができた。本標品を用い、CaMKIV ならびに CaMKIγの触媒部位を標的として多価型ペプチドライブラリーをスクリーニングすることにより、それぞれ 12 アミノ酸からなる候補モチーフを同定することができた。その中心部には CaMKII 阻害モチーフとは大きく異なる特徴的な配列が存在することが明らかとなった（出願準備中）。しかしながら同定されたモチーフそのままでは細胞毒性が懸念されたため、CaMKII 阻害ペプチドである M1-6 のモチーフに上記 CaMKIV ならびに CaMKIγ特徴的配列を移植し

た一連のペプチドをスライドグラス上にスポット合成した。本スライドグラスを各CaMKアイソザイムでブロットし、CaMKII の結合強度に対する CaMKIV ならびに CaMKIγそれぞれの結合比をベースに補正することにより、CaMKIV ならびに CaMKIγそれぞれに高い特異性を示す新規高親和性結合配列を数種同定することができた。特に、CaMKIV 特異的結合ペプチド５種については、M1-M6 のうち最も CaMKIV に対してキナーゼ活性阻害効果の強かった M1 よりも CaMKIV に対し強い阻害能を示すこと、一方で CaMKII に対してはこれら５種のペプチドは、CaMKII に対して高い阻害能を示す M6 よりも全て阻害能が減弱していること、すなわち極めて高い CaMKIV 特的阻害能を有していることが示された（図３）。これは CaMK アイソザイムを峻別する初めての阻害ペプチドである。これまでに、骨髄細胞から骨を破壊する破骨細胞へと分化する際に、CaMKIV が重要な役割を果たしていることが知られている。そこで、これら CaMKIV 特異的阻害ペプチドについて、この破骨細胞分化系に及ぼす効果を検討することにした。これまでに数種のペプチドについて検討を開始しており、このうちの１つに顕著な阻害効果があることを確認している。

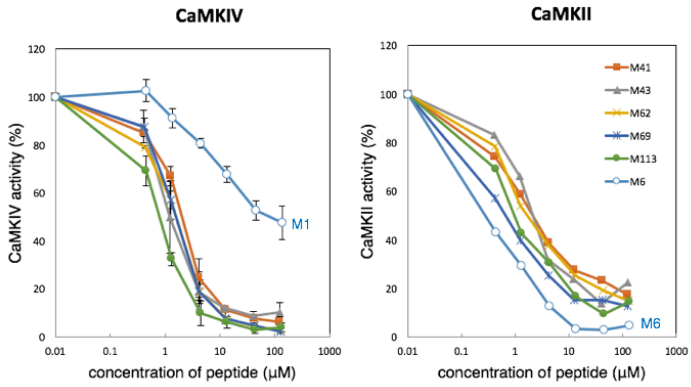

図３

B) 神経機能維持に関わる細胞内小胞輸送の制御法の確立

３-B-１ 細菌毒素を用いた小胞輸送制御分子の開発

Shiga toxin (Stx)やコレラ毒素(CT)は受容体結合後、小胞輸送によってゴルジ体、さらに ER へと輸送されることで毒性を発揮する。本経路は通常の分泌タンパク質の輸送とは逆方向であることから、逆行輸送経路と呼ばれている。この小胞輸送は、多くの細胞内情報伝達の起点として重要な機能を果たしている脂質ラフトを介して起こる事から、これらの毒素の受容体結合領域に結合し、その輸送を制御する分子は、小胞輸送に関わる様々なシグナル伝達に影響を与えると考えられる。本研究では、これら毒素の標的細胞への結合を担う B サブユニット５量体を標的として、その受容体との結合、な

らびにその後のシグナルに影響を及ぼすペプチド性化合物を同定し、小胞輸送制御分子として確立することを目的とする。

Stx は Stx1 ならびに Stx2 の２種のファミリーから構成され、さらに各には複数のバリアントが存在する。Stx の B サブユニット 5 量体は受容体である糖脂質 Gb3 のグロボ３糖部を特異的に認識するが、この時１つの B サブユニットにはサイト１−３の３種のグロボ３糖結合部位が存在している。これまでに Stx2 B サブユニットのサイト３を標的とし、多価型ペプチドライブラリー法を用いて特異的阻害薬 PPP-tet を開発している（**FASEB J.**, 2006, 20, 2597-）。本研究では、多価型ペプチドライブラリー法ならびに多価型ペプチドシートスクリーニング法を用いることにより、Stx1 B サブユニットのサイト１を標的として、新規 Stx1 阻害薬 MMA-tet を、さらに Stx2 のバリアントの一つであり強毒性であることが知られている Stx2d の B サブユニットのサイト１を標的として、Stx2d 特異的阻害薬 LMA-tet ならびに MMM-tet を、それぞれ同定することができた（**Infect. Immun.**, 2013, 81, 2133-, **Infect. Immun.**, 2016, 84, 2653-）。興味深いことに、PPP-tet ならびに MMA-tet は各 Stx の受容体結合部位に結合するものの、細胞への侵入は阻害しないこと、その代わり PPP-tet は Stx2 のゴルジ体から ER への逆行輸送を、MMA-tet は Stx1 の A サブユニットの ER からの離脱を、それぞれ阻害すること、すなわち逆行性小胞輸送を異なる段階で制御することを明らかにした。

コレラ毒素の B サブユニット 5 量体(CTB)に結合する分子開発についても、多価型ペプチドライブラリー法、ならびに多価型ペプチドシートスクリーニング法を用い、新規阻害薬 GNR-tet を同定した。GNR-tet は細胞レベルで CT 刺激による cAMP 産生増強を効率よく阻害すること、さらにマウス個体においても CT によって誘導される腸管内水分貯留を顕著に阻害すること、を見出した。GNR-tet は個体において有効性が確認された初めてのペプチド性 CT 阻害薬である。興味深いことに、GNR-tet も CT の受容体結合部位に結合するものの、細胞への侵入は阻害しないこと、一方で GNR-tet は CT のリサイクリングエンドソームからゴルジ体への逆行輸送を顕著に遅延させること、それが CT 阻害の分子機構であることを見出した。

以上の結果から、Stx、CT の他、Stx1 と MMA-tet、Stx2 と PPP-tet、CT と GNR-tet の各複合体を用いることにより、様々な段階でラフトを介した逆行性小胞輸送を制御する系を確立することができた。

<u>３-B-２ 細菌毒素ならびにその阻害ペプチドとの複合体を用いたアミロイド β 産生制御法の開発</u>

アルツハイマー病の病原因子と考えられている amyloidβ-protein （アミロイド

β;Aβ)の前駆体、β-Amyloid precursor protein (APP)は生体由来分子として逆行輸送経路をたどる数少ない分子の一つである。小胞体で生合成されたAPPはゴルジ体へ輸送され、一部のAPPは細胞膜へ順行輸送される。この細胞膜上のAPPはエンドサイトーシスにより再び細胞内に取り込まれ、ゴルジ体から小胞体へ逆行輸送される。さらに一部のAPPはリサイクリングエンドソームを介して細胞膜、あるいはエンドソームからリソソームへと輸送される。この一連の輸送過程でAPPはβ及びγセクレターゼによる切断を受けAβが産生され、Aβは細胞外へ放出される。本研究では、APPがStxやCTと共通した逆行輸送機構を有する点に注目し、これら毒素ならびに各々の阻害ペプチドとの複合体を用い、新たなAPPの細胞内輸送及びAβ産生量の制御法を確立する。

まず、Aサブユニットに変異を導入し無毒化したStx2変異体(mStx2)を使用し、APPを発現させたStx感受性CHO細胞(CHO 1D)における細胞内APPと培養上清中のAβをwestern blot法により測定した。その結果、mStx2の濃度依存的に細胞内APPが有意に減少すること、培養上清中のAβも減少傾向にあることが明らかになった（図４）。いずれの濃度のmStx2存在下でもCHO 1D細胞の生存率、及び同時に導入したGFPの発現量には影響がないことから、mStx2により特異的にAPPの輸送異常が生じてAPP分解が亢進し、その結果Aβ産生量が低下したと考えられた。現在、APPとStxの細胞内局在を解析中であり、APPの分解亢進のメカニズムを明らかにする予定である。また、Stx1やCT単独、さらに各毒素と特異的阻害ペプチドとの複合体を用いて同様の検討を行い、もっとも効率のよいAβ産生の制御法の確立を目指す。

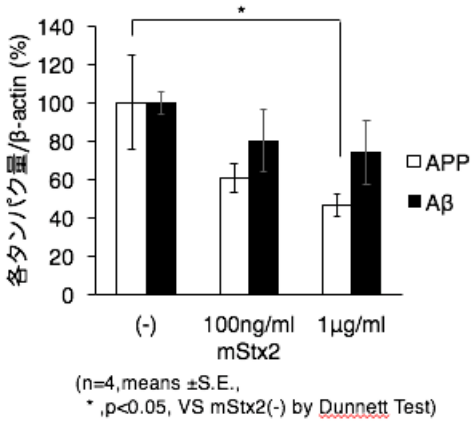

図４

４）研究業績

１）原著論文(* ; corresponding author)

1) Mitsui T., Watanabe-Takahashi M., Shimizu E., Zhang B., Funamoto S., Shinji Yamasaki S., Nishikawa K.*, Affinity-based screening of tetravalent peptides identifies subtype-selective neutralizers of Shiga toxin 2d, a highly virulent subtype, by targeting a unique amino acid involved in its receptor recognition, **Infect. Immun.**, 2016, 84, 2653-2661, doi: 10.1128/IAI.00149-16.

2) Hattori T., Watanabe-Takahashi M., Shiina I., Ohashi Y., Dan S., Nishikawa K., Yamori T., and Naito M., M-COPA, a novel disruptor of Golgi system suppresses apoptosis induced by Shiga toxin, **Genes Cells**, 2016, 21, 901-906, doi: 10.1111/gtc.12386.

3) Ogawa R., Nagao K., Taniuchi K., Kato U., Hara Y., Inaba T., Kobayashi T., Sasaki Y., Akiyoshi K., Watanabe-Takahashi M., Nishikawa K., and Umeda M., Development of a novel tetravalent synthetic peptide that binds to phosphatidic acid, **PLoS One**, 2015 Jul 6;10(7):e0131668. doi: 10.1371/journal.pone.0131668. eCollection 2015, PMID: 26147860.

4) Hattori T., Watanabe-Takahashi M., Ohoka N., Hamabata T., Furukawa K., Nishikawa K., and Naito M., Inhibition of Proteasome Prevents Cell Death and Prolongs Survival of Mice Challenged by Shiga Toxin, **FEBS Open Bio.**, 2015, 5, 605-614, doi: 10.1016/j.fob.2015.06.005, PMID: 26273560.

5) Watanabe-Takahashi M.[#], Kato M.[#], Shimizu E., and Nishikawa K.*, Identification of a wide range of motifs inhibitory to Shiga toxin by affinity-driven screening of customized divalent peptides synthesized on a membrane, **Appl. Environ. Microbiol.**, 2015, 81, 1092-1100. doi: 10.1128/AEM.03517-14, PMID: 25452283. [#]Equal contribution.

6) Funamoto S., Sasaki T., Ishihara S., Nobuhara M., Nakano M., Watanabe-Takahashi M., Saito T., Kakuda N., Miyasaka T., Nishikawa K., Saido TC, and Ihara Y., Substrate ectodomain is critical for substrate preference and inhibition of γ-secretase, **Nature Commun**., 2013, 4:2529. doi: 10.1038/ncomms3529.

7) Watanabe-Takahashi M.[#], Tsutsuki K.[#], Takenaka Y., Kita E. and Nishikawa K.*, Identification of a peptide-based neutralizer that potently inhibits both Shiga toxins 1 and 2 by targeting specific receptor-binding regions, **Infect. Immun.**, 2013, 81, 2133-2138. [#]Equal contribution.

8) Ribosome-mediated synthesis of natural product-like peptides via cell-free translation. R. Maini; S. Umemoto; H. Suga. Current opinion in chemical biology, 2016, 34, 44-52.

２）図書

なし

３）学会発表

国外

Invited

1) Peptide-based Stx-neutralizers of treatment of STEC infections., Nishikawa, K., Seminar Series Fall 2015, Pathology and Laboratory Medicine, Boston Univ. Sch. Med, 2015.9.17, Boston, US.
2) Peptide-based Stx-neutralizers of treatment of STEC infections., Nishikawa, K.
   International Symposium “New trends of anti-infection strategy” on The 86th Annual Meeting of Japanese Society For Microbiology, 2013.3.20, Chiba, Japan.
3) Peptide-based neutralizers of Shiga toxin., Nishikawa, K. (invited speaker and convener)
   International Union of Microbiological Societies 2011 Congress (IUMS2011), 2011.9.8, Sapporo, Japan.

Oral/Poster presentation

1) M-COPA, a novel disruptor of Golgi system suppresses apoptosis induced by Shiga toxin, Naiton M., Hattori T., Watanabe-Takahashi M., Shiina I., Ohashi Y., Dan S., Nishikawa K., Yamori T., the 41th FEBS Congress, 03-08 Sep., 2016, in Ephesus, Turkey. Poster presentation.
2) Affinity-driven screening of customized divalent peptides synthesized on a membrane identifies a wide range of inhibitory motifs against Shiga toxin, Watanabe-Takahashi M, Kato M., Shimizu E., Nishikawa K., the 9th International Symposium on Shiga toxin (Verocytotoxin) Producing *Escherichia coli* Infections, 13-16 Sep. 2015, in Boston, US. Poster presentation.
3) Peptide-based Stx-neutralizers for treatment of STEC infections, Watanabe-Takahashi, M., Tsutsuki, K., Kita, E., Nishikawa, K.*(presenter), the 8th International Symposium on Shiga toxin (Verocytotoxin) Producing *Escherichia coli* Infections, 6-9 May 2012 in Amsterdam, the Netherlands., * The prize for the Best Poster on Prevention , Control and Treatment: Animal and Human.

国内

国内学会招待講演・シンポジウム等

1）演題名「感染症・炎症・疼痛を適応疾患としたペプチド創薬」、西川喜代孝、第３回同志社大学「新ビジネス」フォーラム、同志社大学東京サテライト・キャンパス、

2016/12/8

2) テーマ「食中毒のリスクを低下させる科学−食中毒の制御に向けた新たな取り組みの現状と展望」、演題名「細菌毒素を標的とした発症制御への取り組み」、西川喜代孝、共同開催フォーラム第６回（大阪府立大学食品安全科学研究センター、東京大学食の安全研究センター、神戸大学食の安全・安心科学センター、岩手大学動物医学食品安全教育研究センター、東北大学食と農免疫国際教育研究センター）、大阪府立大学 I-site なんば、2016/11/24

3) テーマ「細菌学会から発信する新規感染症治療薬創生の提案」、演題名「AB5 型細菌毒素に対する多価型ペプチド性阻害薬の開発」、西川喜代孝、第８８回日本細菌学会総会、長良川国際会議場、2015/3/26-28

4) 演題名「新規腸管出血性大腸菌感染症治療薬の開発」、西川喜代孝、第６３回日本薬学会近畿支部総会、同志社女子大学京田辺キャンパス、2013/10/12

5) 演題名「腸管出血性大腸菌感染症の新たな治療薬」、西川喜代孝、バイオビジネスアワード JAPAN（大阪商工会議所・大阪医薬品協会等主催）、大阪産業創造館、2013/2/15

6) 演題名「クラスター効果に基づく蛋白質の強い相互作用を阻害する新技術」、西川喜代孝、近畿経済産業局　地域企業立地促進等事業費補助事業　（関西地域健康長寿成長産業振興・発展対策支援事業） 第３回フォローアップ勉強会（2012、１月２０日、大阪科学技術センター、近畿バイオインダストリー振興会議主催）

一般公演

1) 第 20 回腸管出血性大腸菌感染症研究会（富山県民共生センターサンフォルテ、2016/11/10-11）X 線結晶構造解析によるペプチド性 Stx 阻害薬の新たな阻害機構の解明、玉田真一、高橋美帆、千田美紀、奥田明子、宮澤淳夫、千田俊哉、○西川喜代孝

2) 第 20 回腸管出血性大腸菌感染症研究会（富山県民共生センターサンフォルテ、2016/11/10-11）志賀毒素耐性 THP-1 細胞の単離と解析、○服部隆行、高橋美帆、西川喜代孝、内藤幹彦

3) 第 89 回日本生化学会大会（仙台国際センター、2016/9/25-27）、新規ペプチド性コレラ毒素阻害薬のマウス腸管水分貯留に対する阻害効果、○雲井香保里、高橋美帆、山本洋、濱端崇、西川喜代孝

4) 第 2 回日本骨免疫学会（ホテルモントレー沖縄スパ＆リゾート、2016/7/6-8）、Ca^{2+}/カルモジュリン依存性プロテインキナーゼ阻害ペプチドを用いた破骨細胞分化制御、○西川喜代孝、田口祐、大西 弘晃、藤原誠、西園貴志、西村浩輝、小林俊彦、反町

典子、高柳広、尾藤晴彦、井上純一郎、高橋美帆

5) 第８９回日本細菌学会総会（大阪国際交流センター、2016/3/23-25)、耐熱性エンテロトキシンに対するペプチド性阻害薬の開発、○近江 純平、高橋 美帆、宮坂 知宏、山崎 伸二、日高 雄二、杤尾 豪人、濱端 崇、西川喜代孝

6) BMB2015（第 38 回日本分子生物学会年会、第 88 回日本生化学会大会 合同大会）(2015/12/1-4)、新規小胞輸送阻害薬を用いた志賀毒素のアポトーシス死誘導活性の抑制、○服部　隆行、高橋　美帆、椎名　勇、大橋　愛美、旦　慎吾、西川　喜代孝、内藤　幹彦

7) 第１９回腸管出血性大腸菌感染症研究会（国立医薬品食品衛生研、2015/7/9-10）、新規小胞輸送阻害薬を用いた志賀毒素による細胞死の抑制、○服部隆行，高橋美帆，椎名勇，大橋愛美，旦慎吾，西川喜代孝，内藤幹彦

8) 第８８回日本細菌学会総会（岐阜、長良川国際会議場、2015/3/26-28)、異なった受容体結合部位を標的とする Stx 阻害薬の併用による相乗効果、○高橋美帆、清水英子、加藤美帆子、西川喜代孝

9) 第８８回日本細菌学会総会（岐阜、長良川国際会議場、2015/3/26-28)、耐熱性エンテロトキシンに対するペプチド性阻害薬開発、○近江 純平、高橋 美帆、宮坂 知宏、山崎 伸二、日高 雄二、杤尾 豪人、濱端 崇、西川喜代孝

10) 第８８回日本細菌学会総会（岐阜、長良川国際会議場、2015/3/26-28)、新規ペプチド性コレラ毒素阻害薬の in vivo での効果、○雲井香保里、高橋美帆、山本洋、濱端崇、西川喜代孝

11) 日本薬学会第 135 回年会（神戸、2015/3/25-28)、新規小胞輸送阻害薬による志賀毒素の細胞死誘導活性の抑制、○服部　隆行，高橋　美帆，椎名　勇、大橋　愛美、旦　慎吾、西川　喜代孝，内藤　幹彦

12) 第１８回腸管出血性大腸菌感染症研究会（同志社大学・寒梅館、2014/7/15-16）、プロテアソーム阻害薬による志賀毒素誘導性細胞死の抑制、○服部隆行、高橋美帆、大岡伸通、西川喜代孝、内藤幹彦

13) 第１８回腸管出血性大腸菌感染症研究会（同志社大学・寒梅館、2014/7/15-16）、受容体結合部位特異的 Stx 阻害薬の組み合わせによる阻害効果の増強、○高橋美帆、清水英子、加藤美帆子、西川喜代孝

14) 第１８回日本がん分子標的治療学会学術集会（仙台情報・産業プラザ、2014/6/25-27）、プロテアソーム阻害薬によるシガトキシン誘導性アポトーシスの抑制（Inhibition of Stx-induced Apoptosis by Proteasome Inhibitor）、○服部隆行、大岡伸通、内藤幹彦、西川喜代孝（学会会員外共同研究者)、高橋美帆（学会会員外

共同研究者）

15）第８７回日本細菌学会総会（タワーホール船堀、2014/3/26-28、ポスター発表）、受容体結合部位を標的とした易熱性エンテロトキシン阻害薬の開、○谷川 哲也、高橋美帆、山本洋、濱端崇、西川喜代孝

16）日本薬学会第 134 回年会（熊本大学、2014/3/27-30）、志賀毒素耐性 THP-1 細胞クローンの単離と解析、○服部　隆行，高橋　美帆，西川　喜代孝，内藤　幹彦

17）第３６回日本分子生物学会年会（神戸ポートアイランド、2013/12／3-6，ポスター発表）、Inhibition of Stx-induced cell death by proteasome inhibitor, ○ Hattori, T., Takahashi, M., Ohoka, N., Nishikawa, K., Naito, M.

18）第３６回日本分子生物学会年会（神戸ポートアイランド、2013/12／3-6，ポスター発表）、志賀毒素の分子動力学シミュレーション，○尾又一実(国立国際医療研究センター)、奥村久士(分子研、総研大)、森義治(分子研)、西川喜代孝

19）CBI 学会 2013 年大会（タワーホール船堀、2013/10/28-31）、Molecular Dynamics Simulation of Shiga Toxin, Omata K., Okumura H., Mori Y., and Nishikawa K.

20）第８６回日本細菌学会総会（千葉、幕張メッセ、2013/3/18-20、ポスター発表）、受容体結合部位を標的とした新規コレラ毒素阻害薬の開発、○山本洋、高橋美帆、濱端崇、西川喜代孝

21）第８５回日本生化学会大会（博多、福岡国際会議場、2012/12/16、口頭発表）、Ca^{2+}/カルモジュリン依存性プロテインキナーゼⅡ阻害ペプチドの開発、○西園貴志、西村浩輝、小林俊彦、高橋美帆、反町典子、高柳広、尾藤晴彦、西川喜代孝

22）第１６回腸管出血性大腸菌感染症研究会（秋田、パーティーギャラリーイヤタカ、2012/7/19、口頭発表）、Stx 阻害薬 MMA-tet の作用メカニズムの解明、○竹中康章*、高橋美帆，西川喜代孝（*若手奨励賞受賞）

23）第１６回腸管出血性大腸菌感染症研究会（秋田、パーティーギャラリーイヤタカ、2012/7/19、口頭発表）、新規ペプチド性 Stx 阻害薬 MMA-tet と Stx との結合様式の解析、○高橋美帆*　津々木一恵　飯田将太　西川喜代孝（*奨励賞受賞）

24）BIOtech2012 アカデミックフォーラム（東京ビッグサイト、2012/425-27、口頭発表およびポスター発表）、基質情報に依存しない特異的プロテインキナーゼ阻害ペプチド同定技術、○西川喜代孝

４）その他の研究成果等

・特許（取得・申請）

出願

1)特願 2014-128632、発明者；西川喜代孝、高橋美帆、谷川哲也、名称；LT 阻害４価ペプチドおよび ETEC 感染症治療薬、出願人；学校法人同志社、提出日； 2014 年 6 月 23 日

2)特願 2013-13746、発明者；西川喜代孝、高橋美帆、三井貴瑛、清水英子、山崎伸二、名称；Stx2 阻害４価ペプチドおよびこの Stx2 阻害４価ペプチドを含む治療薬、出願人；学校法人同志社、公立大学法人大阪府立大学、提出日；2013 年 1 月 28 日

3)特願 2014-050828、発明者；西川喜代孝、高橋美帆、山本洋、濱端崇、名称；CT 阻害４価ペプチドおよびコレラ治療薬、出願人；学校法人同志社、独立行政法人国立国際医療研究センター、提出日； 2014 年 3 月 13 日

取得特許

1） 発明人；西川喜代孝、高橋美帆、加藤美帆子、名称；Stx1 毒性阻害４価ペプチドおよびこれを含む疾患治療薬、出願人；学校法人同志社、出願日；2010 年 1 月 29 日、登録番号：特許第 5897178 号、登録日：2016 年 3 月 11 日

2) US Patent, No.US 9,103,820 B2, Publication Date: 11 Aug. 2015, Inventor(s): Nishikawa, Kiyotaka., Assignee: Japan Science and Technology Agency, Title of Invention: Method of screening toxin-neutralizing peptide, STX2 inhibitory peptide and vero toxin-neutralizing agent., Patent Expiration Date: 7 May 2030 (extended or adjusted under 35 U.S.C. 154(b) by 1774 days).

3） 発明者；西川喜代孝、高橋美帆、西村浩輝、高柳広、尾藤晴彦、名称；ＣａＭＫＩＩ阻害ペプチドおよびこれを含有するＣａＭＫＩＩ阻害剤、出願人；学校法人同志社、国立大学法人東京医科歯科大学、出願日；2010 年 1 月 29 日、登録番号：特許第 5754008 号、登録日：2015 年 6 月 5 日

4） 発明人；西川喜代孝、高橋美帆、加藤美帆子、名称；ペプチドのスクリーニング方法、出願人；学校法人同志社、出願日；2010 年 1 月 29 日、登録番号：特許第 5718574 号、登録日：2015 年 3 月 27 日

5） 発明人；西川喜代孝、高橋美帆、津々木一恵、名称；Stx 毒性阻害ペプチドおよび Stx に起因する疾患の治療薬、出願人；学校法人同志社、出願日；2010 年 1 月 29 日、登録番号：特許第 5635779 号、登録日：2014 年 10 月 24 日

6）EP Patent (GB, DE, FR, IT, CH) No.1782820, Publication Date: 30 Jul. 2014, Inventor(s): Nishikawa, Kiyotaka., Assignee: Japan Science and Technology Agency., Title of Invention: Method of screening toxin-neutralizing peptide, STX2 inhibitory peptide and vero toxin-neutralizing agent., Patent Expiration Date: 28 June 2025

7）China Patent No.ZL200910205690.3, Publication Date: 5 Jun. 2013, Inventor(s): Nishikawa, Kiyotaka., Assignee: Japan Science and Technology Agency., Title of Invention: STX2 inhibitory peptide and vero toxin-neutralizing agent, Patent Expiration Date: 28 June 2025

8）Canada Patent No.2575768, Publication Date: 4 Dec. 2012, Inventor(s): Nishikawa, Kiyotaka., Assignee: Japan Science and Technology Agency., Title of Invention: Method of screening toxin-neutralizing peptide, STX2 inhibitory peptide and vero toxin-neutralizing agent, Patent Expiration Date: 28 June 2025

受賞

1）バイオビジネスアワード JAPAN 彩都賞、西川喜代孝、腸管出血性大腸菌感染症の新たな治療薬、2013.2.15、大阪産業創造館；バイオビジネスアワード JAPAN 実行委員会（構成；大阪医薬品協会、財団法人大阪科学技術センター、株式会社大阪証券取引所、大阪商工会議所、大阪府、国際文化公園都市株式会社、彩都建設推進協議会、公益財団法人千里ライフサイエンス振興財団、公益財団法人都市活力研究所）

2）K. Nishikawa, the prize for the Best Poster on Prevention, Control and Treatment: Animal and Human at the 8th International Symposium on Shiga toxin (Verocytotoxin) Producing *Escherichia coli* Infections, 6-9 May 2012 in Amsterdam, the Netherlands.

3）第１６回腸管出血性大腸菌感染症研究会（秋田、パーティーギャラリーイヤタカ、2012/7/19、口頭発表)、新規ペプチド性 Stx 阻害薬 MMA-tet と Stx との結合様式の解析、○高橋美帆* 津々木一恵 飯田将太 西川喜代孝（*奨励賞受賞）

新聞等報道

1） 読売新聞（2012 年４月８日）0157（ベロ毒素）無毒化−分解促す化合物開発

IAI Journals.ASM.org

Identification of a Peptide-Based Neutralizer That Potently Inhibits Both Shiga Toxins 1 and 2 by Targeting Specific Receptor-Binding Regions

Kazue Tsutsuki,[a] Miho Watanabe-Takahashi,[a] Yasuaki Takenaka,[a] Eiji Kita,[b] Kiyotaka Nishikawa[a]

Faculty of Life and Medical Sciences, Doshisha University, Kyoto, Japan[a]; Department of Bacteriology, Nara Medical University, Nara, Japan[b]

Shiga toxin (Stx) is a major virulence factor of enterohemorrhagic *Escherichia coli* that occasionally causes fatal systemic complications. We recently developed a tetravalent peptide (PPP-tet) that neutralizes the cytotoxicity of Stx2 using a multivalent peptide library approach. In this study, we used this technique to identify a series of tetravalent peptides that bound to Stx1, another major Stx family member, with high affinity by targeting one receptor-binding site of the B subunit. One peptide, MMA-tet, markedly inhibited Stx1 and Stx2 cytotoxicity with greater potency than PPP-tet. After forming a complex with Stx1 through its specific receptor-binding region, MMA-tet did not affect vesicular transport of the toxin to the endoplasmic reticulum but substantially rescued inhibition of the protein synthesis induced by Stx1. Oral application of MMA-tet protected mice from a fatal dose of an *E. coli* O157:H7 strain producing both toxins. MMA-tet may be a promising therapeutic agent against the infection.

Infection by enterohemorrhagic *Escherichia coli* (EHEC) causes bloody diarrhea and hemorrhagic colitis in humans that is occasionally followed by fatal systemic complications, such as acute encephalopathy and hemolytic-uremic syndrome (1–4). Because Shiga toxin (Stx) is a major virulence factor of EHEC, Stx neutralizers can be practical therapeutic agents against EHEC infections.

Stx can be classified into two subgroups, Stx1 and Stx2 (5). Stx consists of a catalytic A subunit and a B-subunit pentamer. The former has 28S rRNA *N*-glycosidase activity and inhibits eukaryotic protein synthesis, whereas the latter is responsible for the high-affinity binding of the toxin to the functional cell surface receptor Galα(1-4)-Galβ(1-4)-Glcβ-ceramide (Gb3) (4, 6, 7). The crystal structure of Stx reveals the presence of three distinctive binding sites for the trisaccharide moiety of Gb3 (i.e., sites 1, 2, and 3 on each B-subunit monomer) (8, 9). Highly selective and potent binding of Stx to Gb3 is mainly attributed to the multivalent interaction of the B-subunit pentamer with the trisaccharide moiety of Gb3. This is occasionally referred to as the "clustering effect." On the basis of this, several synthetic Stx neutralizers with clustered trisaccharides that can bind to Stx with high affinity and inhibit its cytotoxicity have been developed (10–15). However, the clinical application of these neutralizers has been substantially hampered by the synthetic complexity of the trisaccharide moiety.

Recently, we developed a multivalent peptide library technique and identified a novel peptide-based neutralizer against Stx2 (16, 17), which is more closely related to the severity of EHEC infections (18, 19). In this approach, a library of novel tetravalent peptides designed to exert the clustering effect was screened for high-affinity binding to one of the trisaccharide binding sites, site 3, of the Stx2 B subunit. We identified four tetravalent peptides that bind to Stx2 with high affinity and effectively inhibit its cytotoxicity. One of the tetravalent peptides, named PPP-tet, protected mice from a fatal dose of *E. coli* O157:H7 (16) and, furthermore, inhibited the lethal effect of intravenously administered Stx2 in a nonhuman primate model (20). In stark contrast to the Stx neutralizers with assembled trisaccharides, which competitively inhibit the binding of Stx to target cells, PPP-tet did not inhibit Stx binding, but instead, it induced the aberrant intracellular transport of the toxin (16). After binding to Gb3, Stx is first transported in a retrograde manner to the Golgi complex and then to the endoplasmic reticulum (ER), where the catalytic A subunit is released into the cytosol to inhibit protein synthesis (21). After forming a complex with Stx2, PPP-tet specifically inhibits the process of vesicular transport of Stx2 from the Golgi complex to the ER, followed by the effective degradation of Stx2 in an acidic compartment (16). Recently, other synthetic compounds or chemicals that similarly affect the intracellular transport of Stx have been reported (22–24), further confirming the usefulness of these transport modulators as Stx neutralizers.

PPP-tet, however, did not efficiently inhibit the cytotoxicity of Stx1, another major Stx family member, indicating an urgent need to identify a peptide-based neutralizer against Stx1. In this study, using the multivalent peptide library approach, we identified a tetravalent peptide that markedly inhibited the cytotoxicity of both Stx1 and Stx2. This tetravalent peptide, named MMA-tet, rescued mice from the lethality of *E. coli* O157:H7 infection with marked efficacy. We also elucidated the unique mechanism by which MMA-tet exerts its inhibitory effect on the toxins in target cells.

MATERIALS AND METHODS

Materials. Recombinant Stx1 and Stx2, histidine-tagged Stx1 B subunit (1BH), histidine-tagged Stx2 B subunit (2BH), 1BH with single amino acid substitutions (1BH-D17E, 1BH-D18E, 1BH-F30A, 1BH-G62A, and 1BH-W34A), 1BH with double amino acid substitutions (1BH-D17E/

Received 10 November 2012 Returned for modification 18 December 2012
Accepted 20 March 2013
Published ahead of print 1 April 2013
Editor: B. A. McCormick
Address correspondence to Kiyotaka Nishikawa, knishika@mail.doshisha.ac.jp.
K.T. and M.W.-T. contributed equally to this article.

doi:10.1128/IAI.01256-12

W34A, 1BH-D18E/G62A, and 1BH-G62A/W34A), and 1BH with a triple amino acid substitution (1BH-D17E/G62A/W34A) were prepared as described previously (14, 16). The Gb3 polymer and rabbit anti-Stx antiserum were obtained as described previously (15, 16). AlphaScreen reagent and l-[4,5-^{3}H(N)]Leu were purchased from PerkinElmer (Tokyo, Japan).

Peptides and peptide library screening. Tetravalent peptides and tetravalent peptide libraries were synthesized as described previously (16). Recombinant 1BH or 1BH-F30A (0.5 mg of protein) bound to Ni^{2+} beads was incubated with 300 μg of a given library peptide in phosphate-buffered saline (PBS) overnight at 4°C. After extensive washing, bound peptides were sequenced on an Applied Biosystems model 477A protein sequencer. To calculate the relative amino acid preference at each degenerate position, the corrected quantities of amino acids in the peptides recovered from the 1BH beads were compared with those of amino acids in the peptides recovered from the 1BH-F30A beads to calculate the abundance ratios of amino acids (16).

Kinetic analysis of binding between inhibitory peptides and immobilized Stx B subunit. The binding of tetravalent peptides to immobilized 1BH or 2BH was quantified using a Biacore T100 system instrument (GE Healthcare Sciences) as described previously (16). The resonance unit is an arbitrary unit used by the Biacore system.

Cytotoxicity assay. Subconfluent Vero cells cultured in a 96-well plate in Dulbecco's modified Eagle's medium (DMEM) supplemented with 10% fetal calf serum were treated with Stx1 or Stx2 (1 pg/ml) in the absence or presence of a given tetravalent peptide for 72 h at 37°C. Each peptide was added simultaneously with Stx1 or Stx2. The relative number of living cells was determined using a Cell Counting Kit-8 (Dojindo, Japan), which allows the sensitive determination of cell viability based on the production of an orange formazan dye from 2-(2-methoxy-4-nitrophenyl)-3-(4-nitrophenyl)-5-(2,4-disulfophenyl)-2H-tetrazolium, monosodium salt (WST-8), by the intracellular dehydrogenases.

Analysis of binding between 1BH or a 1BH mutant and inhibitory peptides by AlphaScreen assay. The indicated amounts of the biotinylated tetravalent peptide and 1BH or its mutant (10 μg/ml) were incubated in each well of an OptiPlate-384 microplate (PerkinElmer) for 1 h at room temperature. The plate was incubated with nickel chelate acceptor donor beads (20 μg/ml) for 30 min, followed by incubation with streptavidin donor beads (20 μg/ml) for 1 h at room temperature under protection from light. After excitation at 680 nm, the emission at 615 nm was measured by an EnVision system (PerkinElmer). The signal intensity (cps) is an arbitrary unit used by the system.

ELISA of the binding between 1BH and inhibitory peptides. The indicated tetravalent peptides (1.7 μM dissolved in PBS) were coated onto each well of a 96-well enzyme-linked immunosorbent assay (ELISA) plate and incubated for 24 h at 4°C. After blocking, the plate was incubated with 1BH (1 μg/ml) for 1 h at room temperature. Bound 1BH was detected using rabbit anti-Stx1 antiserum as described previously (16).

^{125}I-Stx binding assay. Vero cells cultured in a 24-well plate were treated with ^{125}I-Stx1 or ^{125}I-Stx2 (1×10^6 to 2×10^6 cpm/μg protein, 1 μg/ml) in the absence or presence of a given compound for 30 min at 4°C. Each compound was added simultaneously with ^{125}I-Stx1 or ^{125}I-Stx2. After extensive washing, the recovered radioactivity was measured by a gamma counter.

Intracellular localization of Stx1. Subconfluent Vero cells in a glass base dish (35 mm) were treated with Stx1 (1 μg/ml) in the absence or presence of MMA-tet (52 μM) for 1 h at 37°C. MMA-tet was added simultaneously with Stx1. After incubation, the cells were fixed with 3% paraformaldehyde. Immunostaining of Stx1, GM130, Vti1a, GS28, HSP47, calnexin, and ribophorin was performed using rabbit anti-Stx1 polyclonal antibody, mouse anti-GM130 IgG monoclonal antibody (BD Biosciences, NJ), mouse anti-Vti1a IgG monoclonal antibody (BD Biosciences), mouse anti-GS28 monoclonal antibody (BD Biosciences), mouse anti-HSP47 IgG monoclonal antibody (Enzo Life Sciences, Inc., NY), rabbit anticalnexin polyclonal antibody (Santa Cruz Biotechnology, Inc., CA), and goat antiribophorin IgG polyclonal antibody (Santa Cruz Biotechnology), respectively, followed by detection using Alexa Fluor-labeled secondary antibodies. The cells were analyzed by confocal laser scanning microscopy (Olympus, Tokyo, Japan).

Assay for protein synthesis inhibition. Vero cells cultured in a 96-well plate in DMEM supplemented with 10% fetal calf serum were pretreated with the indicated amount of MMA-tet for 1 h and then treated with Stx1 (100 pg/ml) for 1.5 h. After extensive washing, the cells were incubated with 2 μCi/well [^{3}H]Leu in Leu-free minimal essential medium Eagle (MEME; Sigma, Tokyo, Japan) at 37°C for 30 min, and the radioactivity incorporated into cellular proteins was counted as described previously (25).

Mouse infection protocol. Specific-pathogen-free 3-week-old female C57BL/6 mice (Charles River Breeding Laboratories, Wilmington, MA) were maintained on a low-protein diet to induce calorie malnutrition (26). At 5 weeks of age, mice were infected intragastrically with 2×10^6 CFU of *E. coli* O157:H7 strain N-9 as described elsewhere (26). The indicated amount of the acetylated form of MMA-tet (Ac-MMA-tet) or saline was administered intragastrically to the mice twice a day from day 2 to day 5. Data were analyzed by Kaplan-Meier survival analysis or by Fisher's exact test when no mice had died by the end of the observation period. All animal experiments were approved by the animal ethics committee of Nara Medical University prior to their commencement.

RESULTS

Tetravalent peptide library screening identified peptide motifs with high affinity for the Stx1 B subunit. In this study, we used a tetravalent peptide library composed of tetravalent peptides containing a polylysine core bifurcating at both ends with four randomized peptides (16). The tetravalent peptide library was screened for the capability to bind to wild-type 1BH but not to 1BH-F30A, which has a mutation in receptor-binding site 1, because this site has been demonstrated to play an essential role in the receptor binding of Stx1 (27). A tetravalent peptide library with Arg fixed at position 4 (XRX library) was used for the first round of selection on the basis of the previous observation that the Stx2 neutralizer PPP-tet, which has clustered Args in its motif, can also bind to the Stx1 B subunit (data not shown). As shown in Fig. 1A, Arg was strongly selected at positions 5 to 7 and hydrophobic amino acids were preferred at positions 1 to 3. On the basis of this result, second sets of tetravalent peptide libraries with clustered Args (RXR and XRR libraries) were screened to further refine peptide selection. Preferred selection of Arg at positions 5 and 7 was confirmed with the RXR library. Furthermore, Met was strongly selected at positions 1 and 2 with both libraries, and Ala was relatively preferred at position 3 with the XRR library. Based on these results, we identified four candidate motifs: MMARRRR, MAARRRR, AMARRRR, and AAARRRR. Tetravalent forms of these peptides with the same core structure, which were referred to as MMA-tet, MAA-tet, AMA-tet, and AAA-tet, respectively, were synthesized and examined for their capability to bind to 1BH and 2BH. As shown in Fig. 1B, all of these tetravalent peptides, especially AAA-tet and MMA-tet, bound to both B subunits with high affinity, whereas MA-tet, which has the same core structure but lacks any Stx binding motifs, did not bind to either B subunit.

MMA-tet efficiently inhibits the cytotoxicity of both Stx1 and Stx2. The ability of the four tetravalent peptides to inhibit the cytotoxicity of Stx1 and Stx2 in Vero cells was examined (Fig. 2). Among the tetravalent peptides, MMA-tet inhibited the cytotoxicity of both toxins with the highest potency, followed by AMA-tet. MAA-tet and AAA-tet displayed less potency. Interestingly, MMA-tet inhibited Stx2 more efficiently than did PPP-tet, indi-

A

1st-library	Position 1	2	3	4	5	6	7
$(MA\text{-}XXXRXXX\text{-}AU)_4$-3Lys ; XRX-library	W/P/F/W (1.1)	F(1.2)	P(1.2)	R	R(1.5) P(1.2)	R(1.8)	R(1.7) M(1.2)

2nd-libraries	Position 1	2	3	4	5	6	7
$(MA\text{-}XXXRXRX\text{-}AU)_4$-3Lys ; RXR-library	M(1.3) A/P(1.2)	M(1.3) P(1.2)	M/P(1.2)	R	R(1.3) M/A(1.2)	R	M/R(1.3)
$(MA\text{-}XXXRRRR\text{-}AU)_4$-3Lys ; XRR-library	M(1.5) A(1.4)	M(1.4) A(1.3)	A(1.3) M(1.2)	R	R	R	R

B

tetrameric peptide	Stx1BH K_D(nM) mean ± SE (n=3)	Stx1BH Rumax(AU) mean ± SE (n=3)	Stx2BH K_D(nM) mean ± SE (n=3)	Stx2BH Rumax(AU) mean ± SE (n=3)
MMA-tet; $(MA\text{-}MMARRRR\text{-}AU)_4$-3Lys	64 ± 11	1860 ± 66	91 ± 10	2200 ± 83
MAA-tet; $(MA\text{-}MAARRRR\text{-}AU)_4$-3Lys	134 ± 9.4	1870 ± 30	139 ± 8	2030 ± 28
AMA-tet; $(MA\text{-}AMARRRR\text{-}AU)_4$-3Lys	146 ± 2.2	1800 ± 40	158 ± 5	2120 ± 26
AAA-tet; $(MA\text{-}AAARRRR\text{-}AU)_4$-3Lys	20 ± 4.1	1450 ± 145	21 ± 2	1480 ± 9
MA-tet; $(MA\text{-}AU)_4$-3Lys	-	-	-	-

FIG 1 Identification of peptide motifs with high affinity for the Stx B subunit using tetravalent peptide library screening. (A) The tetravalent peptide library was composed of tetravalent peptides with a polylysine core bifurcating at both ends with four randomized peptides. The peptide library for the first screening has a sequence of Met-Ala-X-X-X-R-X-X-X-Ala-U, in which U indicates aminohexanoic acid and X indicates any amino acid except Cys. Screening of the library was performed to identify tetravalent peptides that bound to 1BH but not to 1BH-F30A. For the second screening, a peptide library with fixed Args at positions 4 and 6 (RXR library) or fixed Args at positions 4 to 7 (XRR library) was used. Values in parentheses indicate the relative selectivities for the amino acids. Boldface letters indicate amino acids that were strongly selected. Each screening was performed twice; representative values are shown. (B) The kinetics of the binding of each tetravalent peptide with each identified binding motif to immobilized 1BH or 2BH was analyzed using the Biacore system. K_D, dissociation constant; Rumax, maximum resonance unit. −, binding was not detected.

cating that this tetravalent peptide is promising as a universal neutralizer against both toxins.

MMA-tet binds to 1BH through specific receptor-binding regions. To elucidate the mechanism by which MMA-tet binds to 1BH, the binding between MMA-tet and a series of 1BH mutants with mutations in the trisaccharide binding sites was examined using the AlphaScreen assay. Using this system, we detected high-affinity binding between MMA-tet and 1BH (Fig. 3A). Under the

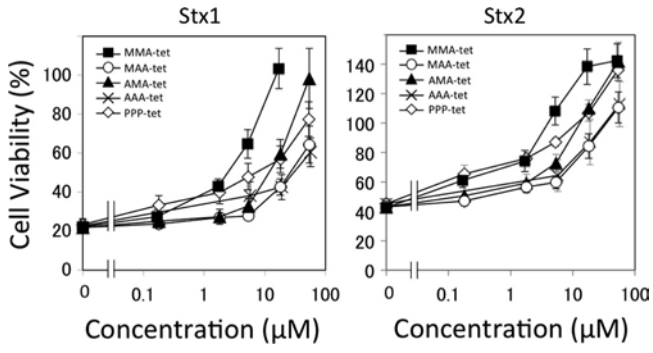

FIG 2 Inhibitory effects of the tetravalent peptides on the cytotoxicity of Stx1 or Stx2 in Vero cells. The effects of the tetravalent peptides on the cytotoxicity of Stx1 (1 pg/ml) or Stx2 (1 pg/ml) in Vero cells were examined by the cytotoxicity assay. Data are presented as a percentage of the control value (mean ± standard error, n = 3).

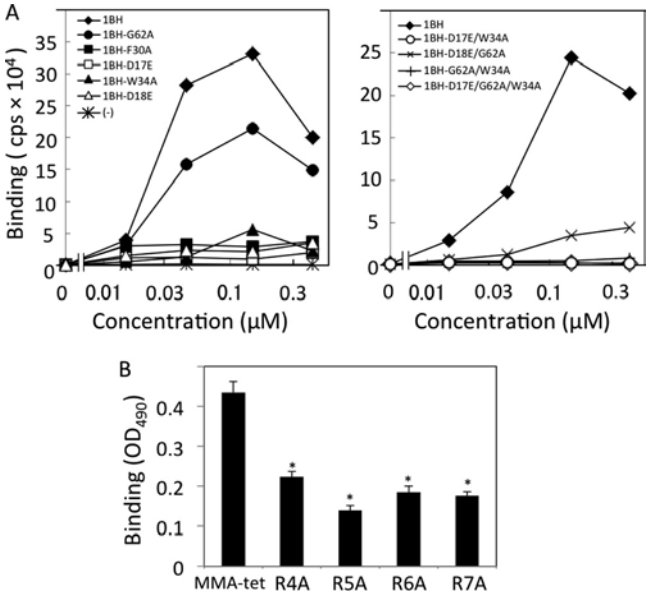

FIG 3 Analysis of the binding of MMA-tet with the Stx1 B subunit. (A) The binding between MMA-tet and a series of 1BH mutants (10 μg/ml) was examined using the AlphaScreen assay. Data are presented as signal intensity (cps). Each experiment was performed three times, and representative data are shown. (B) The binding of 1BH (1 μg/ml) with MMA-tet or Ala-substituted MMA-tet was examined using ELISA (mean ± standard error, n = 3; *, $P < 0.001$, Tukey's test). R4A, R5A, R6A, and R7A, MMA-tet with a substitution of Arg to Ala at positions 4, 5, 6, and 7, respectively. OD_{490}, optical density at 490 nm.

same conditions, the maximum binding of MMA-tet to 1BH-G62A, a site 2 mutant, was 65% of that of 1BH, whereas the levels of binding of MMA-tet to 1BH-F30A and 1BH-D17E, both of which are site 1 mutants, were markedly reduced to 11 and 10%, respectively, consistent with the fact that MMA-tet was identified by targeting Phe30 in site 1. Interestingly, the maximum binding of MMA-tet to 1BH-D18E and 1BH-W34A, both of which are site 3 mutants, was also markedly reduced to the same level (Fig. 3A, left). Furthermore, the maximum binding of MMA-tet to 1BH-D18E/G62A, a site 2 and 3 double mutant, was reduced to 18%, and the binding of MMA-tet to 1BH-D17E/W34A (a site 1 and 3 double mutant), 1BH-G62A/W34A (a site 2 and 3 double mutant), and 1BH-D17E/G62A/W34A (a site 1, 2, and 3 triple mutant) was completely diminished (Fig. 3A, right). These results indicate the substantial contribution of both sites 1 and 3, but not site 2, to the binding of MMA-tet to the Stx1 B subunit.

To evaluate the importance of the Arg cluster present in MMA-tet, the effect of mutating each Arg to Ala on the binding of MMA-tet to 1BH was examined. As shown in Fig. 3B, all of these substitutions, especially substitution of the second Arg, significantly reduced the binding of MMA-tet to 1BH, suggesting the possible electrostatic interaction of the Arg cluster with the acidic amino acid cluster present on the receptor-binding surface of the B subunit, including Asp16, Asp17, and Asp18. In fact, among them, Asp17 and Asp18, which constitute sites 1 and 3, respectively, have been demonstrated to have essential roles in the binding of MMA-tet to the B subunit.

MMA-tet did not inhibit the uptake of Stx and its subsequent vesicular transport to the ER. MMA-tet and the other identified tetravalent peptides did not inhibit the cell surface binding of ^{125}I-

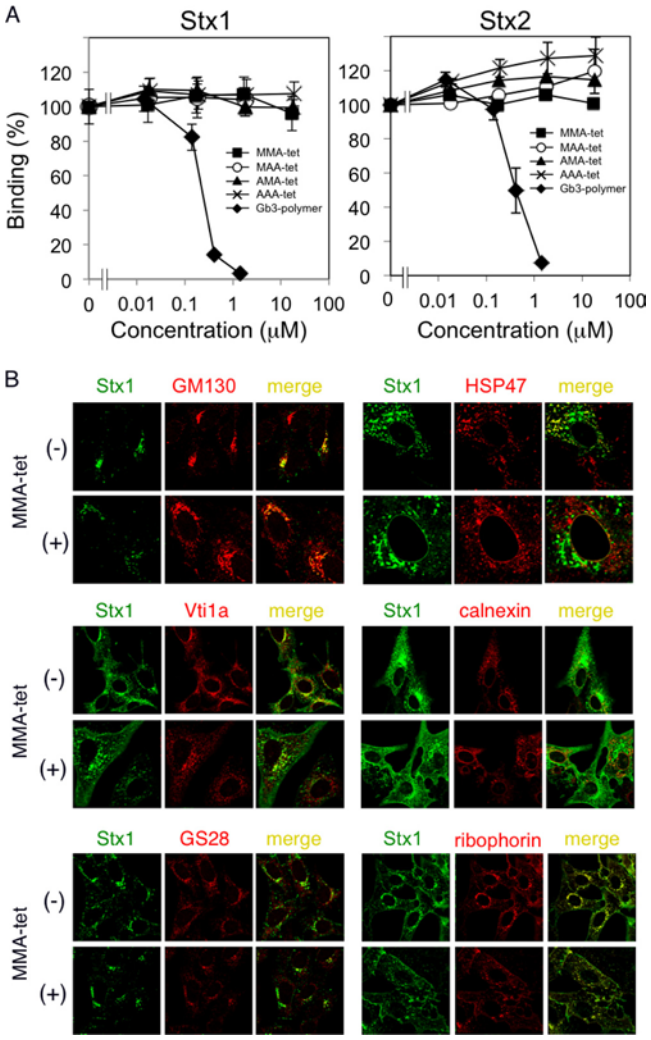

FIG 4 MMA-tet did not affect the uptake and subsequent intracellular transport of Stx1 to the ER. (A) Binding of ^{125}I-Stx1 or ^{125}I-Stx2 (1 μg/ml) to Vero cells. Data are presented as a percentage of the control value (mean ± standard error, $n = 3$). (B) Colocalization of Stx1 (1 μg/ml) with GM130, Vti1a, GS28, HSP47, calnexin, and ribophorin in the absence or presence of MMA-tet (52 μM) was examined by immunocytochemical staining.

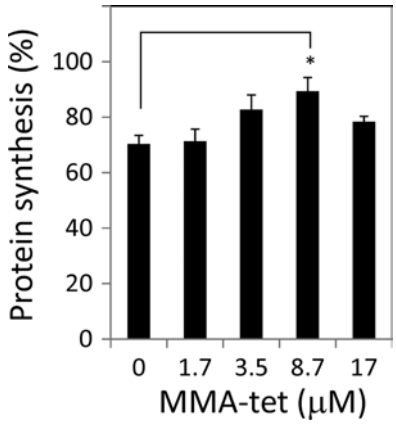

FIG 5 Effect of MMA-tet on Stx1-induced protein synthesis inhibition. Vero cells cultured in DMEM supplemented with 10% fetal calf serum were pretreated with each amount of MMA-tet for 1 h and then treated with Stx1 (100 pg/ml) for 1.5 h. After extensive washing, the cells were incubated with 2 μCi/well [^{3}H]Leu in Leu-free MEME at 37°C for 30 min. The relative amounts of radioactivity incorporated into cellular proteins are presented as percentages of the control value without Stx1 (mean ± standard error, $n = 3$; *, $P < 0.05$, Tukey's test).

Stx1 or ^{125}I-Stx2, although the Gb3 polymer (15), an Stx neutralizer with clustered trisaccharides, efficiently inhibited this binding (Fig. 4A). We previously demonstrated that PPP-tet does not inhibit the binding of Stx2 to the cell surface receptor, but it induces the aberrant cellular transport of Stx2, allowing it to exert its inhibitory effect (16). Thus, the effect of MMA-tet on the intracellular transport of Stx1 was examined. The retrograde transport of Stx1 to the Golgi complex and then to the ER was confirmed by the colocalization of Stx1 with GM130 (a *cis*-Golgi complex marker), Vti1a (a *trans*-Golgi complex marker), GS28 (a *trans*-Golgi complex marker), and ER markers, such as HSP47, calnexin, and ribophorin. As shown in Fig. 4B, MMA-tet did not affect the colocalization of Stx1 with any of these markers, suggesting that even in a complex with MMA-tet, Stx1 can be transported to the ER through the Golgi complex.

MMA-tet rescued the inhibition of protein synthesis caused by Stx1 following its ER localization. The Stx1 A subunit has been demonstrated to translocate from the ER to the cytosol to exert its 28S rRNA *N*-glycosidase activity, resulting in the inhibition of protein synthesis. After 1.5 h of incubation of Vero cells with Stx1, i.e., during the early stage of this translocation, [^{3}H]Leu uptake into newly synthesized proteins was inhibited by 30% (Fig. 5). The inhibition of [^{3}H]Leu uptake was substantially recovered by the presence of MMA-tet in a dose-dependent manner, suggesting that MMA-tet negatively affects the translocation of the A subunit from the ER to the cytosol.

Acetylated MMA-tet protected mice from the lethality caused by *E. coli* O157:H7 infections. The inhibitory effects of MMA-tet on the lethality of *E. coli* O157:H7 infections in mice with protein-calorie malnutrition (26), which are very susceptible to infection, were examined. To prevent proteolytic degradation in the gastrointestinal tract, an acetylated form of MMA-tet (Ac-MMA-tet) was synthesized. Intragastrically administered Ac-MMA-tet completely inhibited the lethality of *E. coli* O157:H7 infections at an amount of 4.2 nmol/g ($P < 0.0001$) and rescued mice with high potency at an amount of 1.25 nmol/g ($P < 0.005$) (Fig. 6).

DISCUSSION

Using a tetravalent peptide library approach, we identified four tetravalent peptides that exhibit high affinities for the Stx1 B subunit and inhibit Stx1 cytotoxicity by targeting one of the receptor-binding sites, namely, site 1. Interestingly, one of these tetravalent peptides, MMA-tet, markedly inhibited both Stx1 and Stx2 with even more potency than PPP-tet, a previously identified Stx2 neutralizer (16). In the previous study, it was revealed that both sites 1 and 2 of Stx1 play essential roles in receptor binding, whereas site 3 has a lower contribution to the binding but cooperatively enhances effective binding through site 1 and/or site 2 (27). In this study, MMA-tet was found to bind to the Stx1 B subunit through both sites 1 and 3, possibly contributing to the potent inhibitory effect of MMA-tet against cytotoxicity. Conversely, AAA-tet, which has the lowest K_D (dissociation constant) value for 1BH

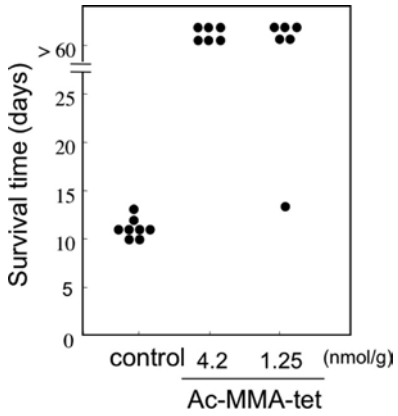

FIG 6 Ac-MMA-tet protects mice from the lethality of *E. coli* O157:H7 infection. Mice with protein-calorie malnutrition were infected intragastrically with a fatal dose of *E. coli* O157:H7 strain N-9 on day 0. The indicated amount of Ac-MMA-tet was administered intragastrically twice a day from day 2 to day 5. The survival time of each animal after Ac-MMA-tet (1.25 nmol/g of body weight, $n = 6$; 4.2 nmol/g of body weight, $n = 6$) or saline ($n = 8$) administration is shown.

binding among the identified tetravalent peptides, did not efficiently inhibit cytotoxicity. Binding analysis between AAA-tet and 1BH by ELISA indicated that the contribution of site 3, including Asp18 and Trp34, is less than that of site 1 (K. Tsutsuki unpublished data), further supporting the importance of occupation of both sites 1 and 3 to function as an effective Stx1 neutralizer.

All four Args present in MMA-tet were revealed to be involved in its effective binding to the Stx1 B subunit, suggesting an electrostatic interaction of these Args with the acidic amino acid cluster present on the receptor-binding surface of the Stx1 B subunit (8). The superior inhibitory effect of MMA-tet on Stx1 compared to the effects of the other tetravalent peptides with the same clustered Args may be explained by the presence of the consecutive Mets at positions 1 and 2, both of which could be involved in forming hydrophobic interactions with the B subunit through Phe30 (site 1) and Trp34 (site 3), as mentioned previously. AMA-tet and MAA-tet, each of which lacks one of these Mets, inhibited the cytotoxicity of Stx1 with less potency than MMA-tet, confirming the importance of the hydrophobic interaction for the inhibitory efficacy, in addition to the electrostatic interaction through clustered Args.

Although MMA-tet did not inhibit the uptake of Stx1 or its subsequent retrograde transport to the ER through the Golgi complex, the inhibition of protein synthesis caused by Stx1 was substantially recovered in the presence of MMA-tet. Because the translocation of the A subunit from the ER to the cytosol is considered crucial for the inhibition of protein synthesis (28, 29), MMA-tet may prevent or retard the translocation of the A subunit, which is mediated by the retrotranslocation system (21, 30, 31). As described previously, MMA-tet binds to the Stx1 B subunit through both sites 1 and 3, possibly allowing site 2 to facilitate retrograde transport of the Stx1/MMA-tet complex to the ER. In addition, as previously demonstrated with PPP-tet (16), the Arg cluster present in MMA-tet may also contribute to the effective binding of the complex to target cells due to its cell-permeant nature (32, 33); conversely, in the absence of the peptides, any dysfunction of each receptor-binding site results in a marked reduction of the cell association of Stx1 (14, 27). This type of interaction of the complex with target cells, however, may impair signal transduction, affecting the subsequent retrotranslocation of the A subunit. Although the precise mechanism remains to be elucidated, some of the signal transduction pathways induced by the association of the Stx1 B subunit (34–38), such as the mitogen-activated protein kinase pathway, were found to be impaired in the presence of MMA-tet (Y. Takenaka unpublished data), further supporting this contention.

Finally, Ac-MMA-tet, a stable form of MMA-tet, was found to completely protect mice from a fatal dose of *E. coli* O157:H7 strain N-9, which produces both Stx1 and Stx2, even when administered after an established infection. This marked protective effect of Ac-MMA-tet may be attributed to its unique property to function in its target cells through its cell-permeant nature, broadening the window for active treatment. Thus, the approach of screening a multivalent peptide library for activity against the specific receptor-binding region of Stx1 successfully identified a peptide-based Stx neutralizer functioning against both Stx1 and Stx2 with remarkable therapeutic potency exceeding that of the previously identified Stx2 neutralizer PPP-tet.

ACKNOWLEDGMENTS

This work was supported by a grant from the National Center for Global Health and Medicine, Japan (21S106); a grant from the MEXT-Supported Program for the Strategic Research Foundation at Private Universities, 2012-2016; grants from the Ministry of Education, Culture, Sports, Science and Technology, Japan (scientific research grants 10017944 and 24390035); and a grant from the Ministry of Health, Labor and Welfare, Japan (scientific research grant 10103178).

REFERENCES

1. **Karmali MA, Steele BT, Petric M, Lim C.** 1983. Sporadic cases of haemolytic-uraemic syndrome associated with fecal cytotoxin and cytotoxin-producing *Escherichia coli* in stools. Lancet **i**:619–620.
2. **Riley LW, Remis RS, Helgerson SD, McGee HB, Wells JG, Davis BR, Hebert RJ, Olcott ES, Johnson LM, Hargrett NT, Blake PA, Cohen ML.** 1983. Hemorrhagic colitis associated with a rare *Escherichia coli* serotype. N. Engl. J. Med. **308**:681–685.
3. **O'Brien AD, Holmes RK.** 1987. Shiga and Shiga-like toxins. Microbiol. Rev. **51**:206–220.
4. **Paton JC, Paton AW.** 1998. Pathogenesis and diagnosis of Shiga toxin-producing *Escherichia coli* infections. Clin. Microbiol. Rev. **11**:450–479.
5. **Scheutz F, Teel LD, Beutin L, Piérard D, Buvens G, Karch H, Mellmann A, Cprioli A, Tozzoli R, Morabito S, Strockbine NA, Melton-Celsa AR, Sanchez M, Persson S, O'Brien AD.** 2012. Multicenter evaluation of a sequence-based protocol for subtyping Shiga toxins and standardizing Stx nomenclature. J. Clin. Microbiol. **50**:2951–2963.
6. **Karmali MA, Petric M, Lim C, Fleming PC, Arbus GS, Lior H.** 1985. The association between idiopathic hemolytic uremic syndrome and infection by verotoxin-producing *Escherichia coli*. J. Infect. Dis. **151**: 775–782.
7. **Melton-Celsa AR, O'Brien AD.** 1998. Structure, biology, and relative toxicity of Shiga toxin family members for cells and animals, p 121–128. *In* Kaper JB, O'Brien AD (ed.), *Escherichia coli* O157:H7 and other Shiga toxin-producing *E. coli* strains. ASM Press, Washington, DC.
8. **Ling H, Boodhoo A, Hazes B, Cummings MD, Armstrong GD, Brunton JL, Read RJ.** 1998. Structure of the Shiga-like toxin I B-pentamer complexed with an analogue of its receptor Gb3. Biochemistry **37**:1777–1788.
9. **Fraser ME, Fujinaga M, Cherney MM, Melton-Celsa AR, Twiddy EM, O'Brien AD, James MNG.** 2004. Structure of Shiga toxin type 2 (Stx2) from *Escherichia coli* O157:H7. J. Biol. Chem. **279**:27511–27517.
10. **Kitov PI, Sadowska JM, Mulvey G, Armstrong GD, Ling H, Pannu NS, Read RJ, Bundle DR.** 2000. Shiga-like toxins are neutralized by tailored multivalent carbohydrate ligands. Nature **403**:669–672.
11. **Paton AW, Morona R, Paton JC.** 2000. A new biological agent for treatment of Shiga toxigenic *Escherichia coli* infections and dysentery in humans. Nat. Med. **6**:265–270.

12. **Nishikawa K, Matsuoka K, Kita E, Okabe N, Mizuguchi M, Hino K, Miyazawa S, Yamasaki C, Aoki J, Takashima S, Yamakawa Y, Nishijima M, Terunuma D, Kuzuhara H, Natori Y.** 2002. A therapeutic agent with oriented carbohydrates for treatment of infections by Shiga toxin-producing *Escherichia coli* O157:H7. Proc. Natl. Acad. Sci. U. S. A. **99**: 7669–7674.
13. **Mulvey GL, Marcato P, Kitov PI, Sadowska J, Bundle DR, Armstrong GD.** 2003. Assessment in mice of the therapeutic potential of tailored, multivalent Shiga toxin carbohydrate ligands. J. Infect. Dis. **187**:640–649.
14. **Nishikawa K, Matsuoka K, Watanabe M, Igai K, Hino K, Hatano K, Yamada A, Abe N, Terunuma D, Kuzuhara H, Natori Y.** 2005. Identification of the optimal structure required for a Shiga toxin neutralizer with oriented carbohydrates to function in the circulation. J. Infect. Dis. **191**: 2097–2105.
15. **Watanabe M, Matsuoka K, Kita E, Igai K, Higashi N, Miyagawa A, Watanabe T, Yanoshita R, Samejima Y, Terunuma D, Natori Y, Nishikawa K.** 2004. Oral therapeutic agents with highly clustered globotriose for treatment of Shiga toxigenic *Escherichia coli* infections. J. Infect. Dis. **189**:360–368.
16. **Nishikawa K, Watanabe M, Kita E, Igai K, Omata K, Yaffe MB, Natori Y.** 2006. A multivalent peptide library approach identifies a novel Shiga toxin inhibitor that induces aberrant cellular transport of the toxin. FASEB J. **20**:2597–2599.
17. **Watanabe-Takahashi M, Sato T, Dohi T, Noguchi N, Kano F, Murata M, Hamabata T, Natori Y, Nishikawa K.** 2010. An orally applicable Shiga toxin neutralizer functions in the intestine to inhibit the intracellular transport of the toxin. Infect. Immun. **78**:177–183.
18. **Ostroff SM, Tarr PI, Neill MA, Lewis JH, Hargrett-Bean N, Kobayashi JM.** 1989. Toxin genotypes and plasmid profiles as determinants of systemic sequelae in *Escherichia coli* O157:H7 infections. J. Infect. Dis. **160**: 994–998.
19. **Tesh VL, Burris JA, Owens JW, Gordon VM, Wadolkowski EA, O'Brien AD, Samuel JE.** 1993. Comparison of the relative toxicities of Shiga-like toxins type I and type II for mice. Infect. Immun. **61**:3392–3402.
20. **Stearns-Kurosawa DJ, Collins V, Freeman S, Debord D, Nishikawa K, Oh SY, Leibowitz CS, Kurosawa S.** 2011. Rescue from lethal Shiga toxin 2-induced renal failure with a cell-permeable peptide. Pediatr. Nephrol. **26**:2031–2039.
21. **Johannes L, Römer W.** 2010. Shiga toxins—from cell biology to biomedical applications. Nat. Rev. Microbiol. **8**:105–116.
22. **Spooner RA, Watson P, Smith DC, Boal F, Amessou M, Johannes L, Clarkson GJ, Lord JM, Stephens DJ, Roberts LM.** 2008. The secretion inhibitor Exo2 perturbs trafficking of Shiga toxin between endosomes and the trans-Golgi network. Biochem. J. **414**:471–484.
23. **Stechmann B, Bai SK, Gobbo E, Lopez R, Merer G, Pinchard S, Panigai L, Tenza D, Raposo G, Beaumelle B, Sauvaire D, Gillet D, Johannes L, Barbier J.** 2010. Inhibition of retrograde transport protects mice from lethal ricin challenge. Cell **141**:231–242.
24. **Mukhopadhyay S, Linstedt AD.** 2012. Manganese blocks intracellular trafficking of Shiga toxin and protects against Shiga toxicosis. Science **335**:332–335.
25. **Yamasaki C, Nishikawa K, Zeng XT, Katayama Y, Natori Y, Komatsu N, Oda T, Natori Y.** 2004. Induction of cytokines by toxins that have an identical RNA *N*-glycosidase activity: Shiga toxin, ricin, and modeccin. Biochim. Biophys. Acta **1671**:44–50.
26. **Kurioka T, Yunou Y, Kita E.** 1998. Enhancement of susceptibility to Shiga toxin-producing *Escherichia coli* O157:H7 by protein calorie malnutrition in mice. Infect. Immun. **66**:1726–1734.
27. **Soltyk AM, MacKenzie CR, Wolski VM, Hirama T, Kitov PI, Bundle DR, Brunton JL.** 2002. A mutational analysis of the globotriaosylceramide-binding sites of verotoxin VT1. J. Biol. Chem. **277**:5351–5359.
28. **LaPointe P, Wei X, Gariépy J.** 2005. A role for the protease-sensitive loop region of Shiga-like toxin 1 in the retrotranslocation of its A1 domain from the endoplasmic reticulum lumen. J. Biol. Chem. **280**:23310–23318.
29. **Tam PJ, Lingwood CA.** 2007. Membrane cytosolic translocation of verotoxin A1 subunit in target cells. Microbiology **153**:2700–2710.
30. **Tsai B, Ye Y, Rapoport TA.** 2002. Retro-translocation of proteins from the endoplasmic reticulum into the cytosol. Nat. Rev. Mol. Cell Biol. **3**:246–255.
31. **Li S, Spooner RA, Hampton RY, Lord JM, Roberts LM.** 2012. Cytosolic entry of Shiga-like toxin A chain from the yeast endoplasmic reticulum requires catalytically active Hrd1p. PLoS One **7**:e41119. doi:10.1371/journal.pone.0041119.
32. **Derossi D, Chassaing G, Prochiantz A.** 1998. Trojan peptides: the penetratin system for intracellular delivery. Trends Cell Biol. **8**:84–87.
33. **Wadia JS, Dowdy SF.** 2002. Protein transduction technology. Curr. Opin. Biotechnol. **13**:52–56.
34. **Katagiri YU, Mori T, Nakajima H, Katagiri C, Taguchi T, Takeda T, Kiyokawa N, Fujimoto J.** 1999. Activation of Src family kinase Yes induced by Shiga toxin binding to globotriaosyl ceramide (Gb3/CD77) in low density, detergent-insoluble microdomains. J. Biol. Chem. **274**: 35278–35282.
35. **Mori T, Kiyokawa N, Katagiri YU, Taguchi T, Suzuki T, Sekino T, Sato N, Ohmi K, Nakajima H, Takeda T, Fujimoto J.** 2000. Globotriaosyl ceramide (CD77/Gb3) in the glycolipid-enriched membrane domain participates in B-cell receptor-mediated apoptosis by regulating Lyn kinase activity in human B cells. Exp. Hematol. **28**:1260–1268.
36. **Lauvrak SU, Wälchli S, Iversen TG, Slagsvold HH, Torgersen ML, Spilsberg B, Sandvig K.** 2006. Shiga toxin regulates its entry in a Syk-dependent manner. Mol. Biol. Cell **17**:1096–1109.
37. **Torgersen ML, Wälchli S, Grimmer S, Skånland SS, Sandvig K.** 2007. Protein kinase Cδ is activated by Shiga toxin and regulates its transport. J. Biol. Chem. **282**:16317–16328.
38. **Tesh VL.** 2012. Activation of cell stress response pathways by Shiga toxins. Cell. Microbiol. **14**:1–9.

AEM
Journals.ASM.org

Identification of a Wide Range of Motifs Inhibitory to Shiga Toxin by Affinity-Driven Screening of Customized Divalent Peptides Synthesized on a Membrane

Mihoko Kato, Miho Watanabe-Takahashi, Eiko Shimizu, Kiyotaka Nishikawa

Faculty of Life and Medical Sciences, Doshisha University, Kyoto, Japan

Shiga toxin (Stx), a major virulence factor of enterohemorrhagic *Escherichia coli*, binds to target cells through a multivalent interaction between its B-subunit pentamer and the cell surface receptor globotriaosylceramide, resulting in a remarkable increase in its binding affinity. This phenomenon is referred to as the "clustering effect." Previously, we developed a multivalent peptide library that can exert the clustering effect and identified Stx neutralizers with tetravalent peptides by screening this library for high-affinity binding to the specific receptor-binding site of the B subunit. However, this technique yielded only a limited number of binding motifs, with some redundancy in amino acid selectivity. In this study, we established a novel technique to synthesize up to 384 divalent peptides whose structures were customized to exert the clustering effect on the B subunit on a single cellulose membrane. By targeting Stx1a, a major Stx subtype, the customized divalent peptides were screened to identify high-affinity binding motifs. The sequences of the peptides were designed based on information obtained from the multivalent peptide library technique. A total of 64 candidate motifs were successfully identified, and 11 of these were selected to synthesize tetravalent forms of the peptides. All of the synthesized tetravalent peptides bound to the B subunit with high affinities and effectively inhibited the cytotoxicity of Stx1a in Vero cells. Thus, the combination of the two techniques results in greatly improved efficiency in identifying biologically active neutralizers of Stx.

Infection with enterohemorrhagic *Escherichia coli* (EHEC) causes bloody diarrhea and hemorrhagic colitis, sometimes followed by fatal systemic complications, such as acute encephalopathy and hemolytic-uremic syndrome (HUS) (1–6). In 2011, unprecedented outbreaks of *E. coli* O104:H4 occurred in the European Union (EU), particularly in Germany, with more than 4,000 cases of infection and 50 fatalities (7, 8). Since antibiotic use is controversial (9–11), novel therapeutic strategies against the infection are urgently required. EHEC produces Shiga toxin (Stx) as a major virulence factor; therefore, one of the most promising approaches is to develop an Stx neutralizer that effectively binds to and inhibits Stx.

Stx, a typical ribotoxin, is present in various forms that can be classified into two subgroups, Stx1 and Stx2, each of which has various closely related subtypes: Stx1a, -1c, and -1d and Stx2a, -2b, -2c, -2d, -2e, -2f, and -2g, respectively (12–14). Each Stx subtype consists of a catalytic A subunit and a B-subunit pentamer, which is responsible for high-affinity binding to the functional cell surface receptor Gb3 [Galα(1-4)-Galβ(1-4)-Glcβ-ceramide] (4, 15, 16), or Gb4 [GalNAcβ(1-3)-Galα(1-4)-Galβ(1-4)-Glcβ-ceramide], which is preferred by Stx2e (17). Each B subunit has three distinctive binding sites (sites 1, 2, and 3) for the trisaccharide moiety of Gb3 (18, 19), resulting in the formation of a multivalent interaction between the B-subunit pentamer and Gb3. This type of interaction is known to markedly increase the binding affinity a millionfold and is generally known as the "clustering effect."

Previously, we developed a multivalent peptide library that can exert the clustering effect and identified Stx neutralizers with tetravalent peptides by screening this library based on high-affinity binding to specific receptor-binding sites (20–22). By targeting one of the receptor-binding sites (site 3) of subtype Stx2a which is most closely associated with high disease severity (23, 24), we identified four tetravalent peptides that bind to Stx2a with high affinity and specificity as novel peptide-based neutralizers (20). One of the neutralizers, PPP-tet, protected mice from a fatal dose of *E. coli* O157:H7 (20) and inhibited the lethal effect of intravenously administered Stx2a in a nonhuman primate model (25). Recently, by targeting receptor-binding site 1 of Stx1a, the most frequently observed subtype, we identified tetravalent peptide MMA-tet (22). Interestingly, MMA-tet strongly inhibited Stx1a and Stx2a with greater potency than that of PPP-tet as well as rescuing mice from the lethality caused by the infection by *E. coli* O157:H7, which produces both toxins. This multivalent peptide library technique, however, can yield only a limited number of binding motifs for the intended receptor-binding region of the B subunit, with redundancy of amino acid selectivity at some positions.

In this study, we established a novel technique to determine a wide range of binding motifs for the B subunit by directly screening hundreds of divalent peptides on a membrane whose struc-

Received 25 October 2014 **Accepted** 21 November 2014

Accepted manuscript posted online 1 December 2014

Citation Kato M, Watanabe-Takahashi M, Shimizu E, Nishikawa K. 2015. Identification of a wide range of motifs inhibitory to Shiga toxin by affinity-driven screening of customized divalent peptides synthesized on a membrane. Appl Environ Microbiol 81:1092–1100. doi:10.1128/AEM.03517-14.

Editor: H. L. Drake

Address correspondence to Kiyotaka Nishikawa, knishika@mail.doshisha.ac.jp.

M.K. and M.W.-T. contributed equally to this article.

Supplemental material for this article may be found at http://dx.doi.org/10.1128/AEM.03517-14.

doi:10.1128/AEM.03517-14

tures were customized to exert the clustering effect. By targeting one of the receptor-binding sites (site 2) of the Stx1a B subunit, a site which plays a significant role in the receptor binding of Stx1a (18, 26), we successfully identified 11 peptide-based neutralizers of Stx1a using this novel technology combined with multivalent peptide library screening. Screening the multivalent peptide library alone could not identify a biologically active inhibitor of this site. Thus, the combination of the two techniques will provide a powerful strategy to develop customized neutralizers for a restricted area of the receptor-binding region of the B subunit, enabling the identification of tailored neutralizers for each Stx subtype with highly conserved structural similarity.

MATERIALS AND METHODS

Materials. Recombinant Stx1a, histidine-tagged Stx1a B subunit (1BH), and 1BH with a single-amino-acid substitution (1BH-G62A) were prepared as described previously (27). The amino-PEG_{500}-UC540 membrane (Intavis Bioanalytical Instruments AG, Germany) used for the spot synthesis of peptides was purchased from PerkinElmer, Tokyo, Japan. Porcine erythrocyte Gb3 and egg phosphatidylcholine (PC) were purchased from Wako Pure Industries, Osaka, Japan.

Peptides and peptide library screening. Tetravalent peptides and tetravalent peptide libraries were synthesized using *N*-α-9-fluorenylmethoxy carbonyl (FMOC)-protected amino acids and standard BOP [benzotriazol-1-yloxytris(dimetylamino)phosphonium hexafluorophosphate]/HOB (1-hydroxybenzotriazole hydrate) coupling chemistry as described previously (20). A Met-Ala sequence was included at the amino terminus of each library peptide to verify the identity and origin of the peptides being sequenced and to qualify the peptides. Recombinant 1BH or 1BH-G62A (0.5 mg protein) bound to Ni^{2+} beads was incubated with 300 μg of a given library peptide in phosphate-buffered saline (PBS) overnight at 4°C. After extensive washing, the bound peptides were sequenced on an Applied Biosystems model 477A protein sequencer. To calculate the relative amino acid preference at each degenerate position, the corrected quantities of amino acids in the peptides recovered from the 1BH beads were compared with those recovered from the 1BH-G62A beads to calculate the abundance ratios of amino acids (20).

ELISA of the binding between 1BH and inhibitory peptides. The indicated amounts of the tetravalent peptide dissolved in PBS were applied as a coating onto each well of a 96-well enzyme-linked immunosorbent assay (ELISA) plate and incubated for 24 h at 4°C. After blocking, the plate was incubated with 1BH or 1BH-G62A (1 μg/ml) for 1 h at room temperature. Bound 1BH was detected using rabbit anti-Stx1a antiserum as described previously (20).

Cytotoxicity assay. Subconfluent Vero cells were cultured in a 96-well plate in Dulbecco's modified Eagle's medium (DMEM) supplemented with 10% fetal calf serum and treated with Stx1a (1 pg/ml) in the absence or presence of a given tetravalent peptide for 72 h at 37°C. The relative number of living cells was determined using cell counting kit 8 (Dojindo, Kumamoto, Japan) as described previously (22).

Spot synthesis of peptides on cellulose membrane. Basic spot synthesis of peptides on a cellulose membrane was performed as described previously (28, 29) using the ResPep SL spot synthesizer (Intavis Bioanalytical Instruments AG, Cologne, Germany). The density of peptides synthesized on a membrane was controlled by using a mixture of FMOC-βAla-OH and Boc-βAla-OH (Watanabe Chemical Industries, Japan) at different ratios (100:0, 30:70, or 10:90, respectively) for the first cycle. *t*-Butyloxycarbonyl (Boc) is resistant to the deprotection procedure and inhibits the subsequent elongation reaction. The spacer length of the peptide was controlled by the number of amino hexanoic acids following the first βAla. After the addition of amino hexanoic acid(s), FMOC-Lys(FMOC)-OH (Watanabe Chemical Industries) was used for the next cycle to bifurcate the peptide chain for subsequent motif synthesis. This step was omitted for monovalent peptide synthesis. The successful synthesis of each peptide was confirmed by staining the membrane using bromophenol blue (1% in *N*,*N*′-dimethylformamide), which reacts to free amino residues. Free amino residues are produced only after the completion of all the reactions and before the deprotection of the side chain residues. After destaining with *N*,*N*′-dimethylformamide, the membrane was used in the binding assay. As a positive control for Stx B-subunit binding, Gb3 (0.1 μg) mixed with PC (1 μg) was directly spotted on the membrane.

Binding assay of 1BH or 1BH-G62A to divalent peptides synthesized on the membrane. After blocking with 5% skim milk in PBS, the membrane (prepared as described above) was blotted with the indicated concentration of ^{125}I-1BH or ^{125}I-1BH-G62A (1×10^6 to 2×10^6 cpm/μg protein) for 1 h at room temperature. After extensive washing, the radioactivity bound to each peptide spot was quantitated as a pixel value using a BAS 2500 bioimaging analyzer system (GE Healthcare, Amersham, United Kingdom). In another detection system, the membrane was blotted with 1.0 μg/ml 1BH for 1 h at room temperature. After extensive washing, bound 1BH was detected using rabbit anti-Stx1a antiserum as described previously (22) and quantitated as a pixel value using ImageQuant LAS 500 (GE Healthcare).

Kinetic analysis of the binding between inhibitory peptides and immobilized 1BH. The binding of tetravalent peptides to immobilized 1BH was quantified using a Biacore T100 system instrument (GE Healthcare Sciences, USA) as described previously (20). The resonance unit is an arbitrary unit (AU) used by the Biacore system. Binding kinetics were analyzed using Biaevaluation software, v1.1.1 (GE Healthcare).

RESULTS

Tetravalent peptide library screening identified a peptide motif that specifically binds 1BH through site 2. A tetravalent peptide library is comprised of peptides containing a polylysine core that bifurcates at both ends with four randomized peptides (20). The library was screened for the ability to bind to wild-type 1BH but not to 1BH-G62A, which contains a mutation in one of the receptor-binding sites (site 2). Site 2 has been shown to play an essential role in the receptor binding of Stx1a (26). A tetravalent peptide library with a fixed Arg at position 4 (the XRX library) was used for the first round of selection, based on the previous observation that Stx1a prefers clustered Args in its binding motifs (22). As shown in Fig. 1A, Arg was strongly selected at positions 1, 5, and 7, and His was selected at position 5. Based on this result, a second tetravalent peptide library with clustered Args (the XRR library) was screened to further refine peptide selection. Lys was strongly selected at position 1, and both Arg and His were selected at position 3. Based on these results, we identified KRRRRRR as a candidate motif. A tetravalent form of this peptide with the same core structure was synthesized and referred to as KRR-tet. As shown in Fig. 1B, KRR-tet bound efficiently to 1BH, whereas the binding to 1BH-G62A was less efficient. Under the same conditions, MA-tet, which has the same core structure but lacks the binding motif, did not bind to either of the B subunits (data not shown). These results indicate that KRR-tet specifically binds to the B subunit through site 2. KRR-tet, however, was found to be cytotoxic due to its highly basic nature (Fig. 1C) and thus did not inhibit the cytotoxicity of Stx1a in Vero cells, in contrast to MMA-tet (Fig. 1D).

Establishment of a technique to synthesize peptides on a membrane that can exert the clustering effect on the Stx1a B subunit. KRR-tet has an Arg cluster at positions 4 to 7; this cluster is also observed in MMA-tet, indicating that the motif is commonly required for the efficient binding to the Stx1a B subunit. Based on this motif, we tried to identify a series of site 2-targeted binding motifs by establishing a novel technique in which hun-

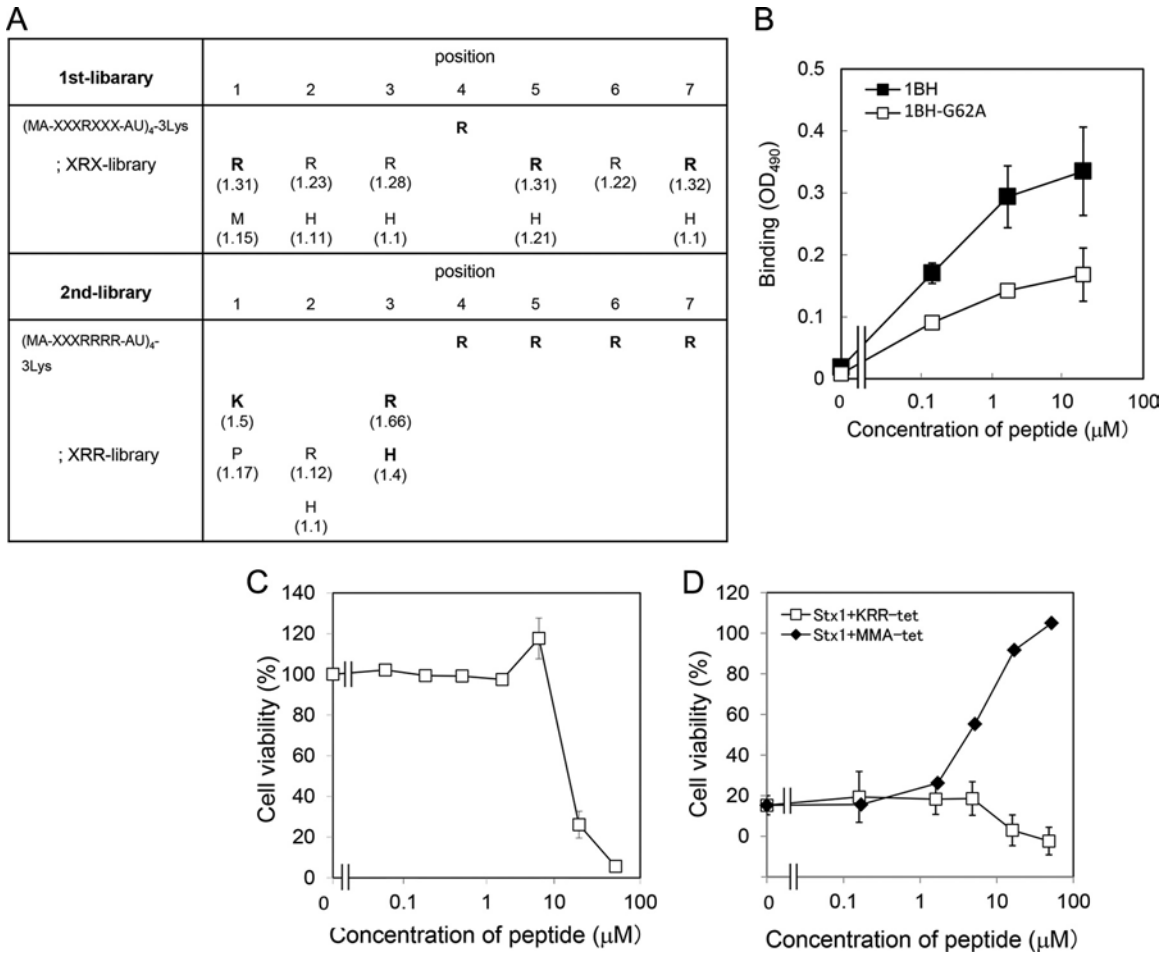

FIG 1 Identification of a peptide motif that specifically binds to Stx1a B subunit through site 2 by using tetravalent peptide library screening. (A) The tetravalent peptide library was comprised of tetravalent peptides with a polylysine core bifurcating at both ends with four randomized peptides. The peptide library for the first screening had the sequence Met-Ala-X-X-X-R-X-X-X-Ala-U (U, amino hexanoic acid), where X indicates all amino acids except Cys. Screening of the library was performed to identify tetravalent peptides that bound to 1BH but not to 1BH-G62A. For the second screening, a peptide library with fixed Args at positions 4 to 7 (XRR library) was used. Values in parentheses indicate relative selectivities for the amino acids. Bold letters indicate amino acids that were strongly selected. Each screening was performed twice; representative values are shown. (B) The binding of 1BH or 1BH-G62A (1 μg/ml) to KRR-tet at the indicated concentrations was examined using ELISA (mean ± standard error, $n = 3$). (C) The effect of KRR-tet on the cell viability in Vero cells was examined by the cytotoxicity assay. Data are presented as a percentage of the control value (mean ± standard error, $n = 4$). (D) The effect of KRR-tet or MMA-tet on the cytotoxic activity of Stx1a (1 pg/ml) in Vero cells was examined by the cytotoxicity assay (mean ± standard error, $n = 4$).

dreds of peptides with the Arg cluster were synthesized in a divalent form on a cellulose membrane and screened for high-affinity binding to 1BH but not to 1BH-G62A. We also optimized the structure of the peptide synthesized on the membrane (Fig. 2A). A divalent form of the peptide, KRRRRRR, was found to exert the clustering effect and exhibited markedly increased binding to 1BH compared to the monovalent form (Fig. 2B). Under the same conditions, Gb3 blotted on the membrane was specifically detected by 1BH. Using the divalent peptide, we found that a spacer of one amino hexanoic acid functioned most efficiently and that the higher density yielded higher binding efficacy (Fig. 2B). We further examined the binding of other divalent peptides. The divalent form of MMARRRR, a binding motif present in MMA-tet, also efficiently bound to 1BH in a dose-dependent manner when one amino hexanoic acid was used as a spacer (Fig. 2C). Similar density dependency was observed for the divalent peptide (Fig. 2B). The divalent form of AAARRRR, another binding motif previously determined for 1BH (22), could still efficiently bind to 1BH. In contrast, the divalent form of AAADDDD, in which all Args of AAARRRR were replaced with Asps, completely lost binding activity (Fig. 2C), confirming the requirement of the Arg cluster in the binding motif.

Screening of divalent peptides synthesized on a membrane successfully identified a wide range of peptide motifs that specifically bind to the Stx1a B subunit through site 2. Using the optimized conditions identified above, 380 divalent peptides containing the Arg cluster and shuffled amino acids at motif positions 1 to 3 were synthesized on a cellulose membrane. One group had the XXA-RRRR motif, and the other group had the AAX-RRRR motif, respectively, where X indicates a fixed amino acid as indicated (Fig. 3A). The divalent peptide with the original motif KRR-RRRR was also synthesized. The membrane was blotted with ^{125}I-1BH or ^{125}I-1BH-G62A (Fig. 3B), and the radioactivity bound to each peptide spot was quantitated and analyzed. Divalent peptides

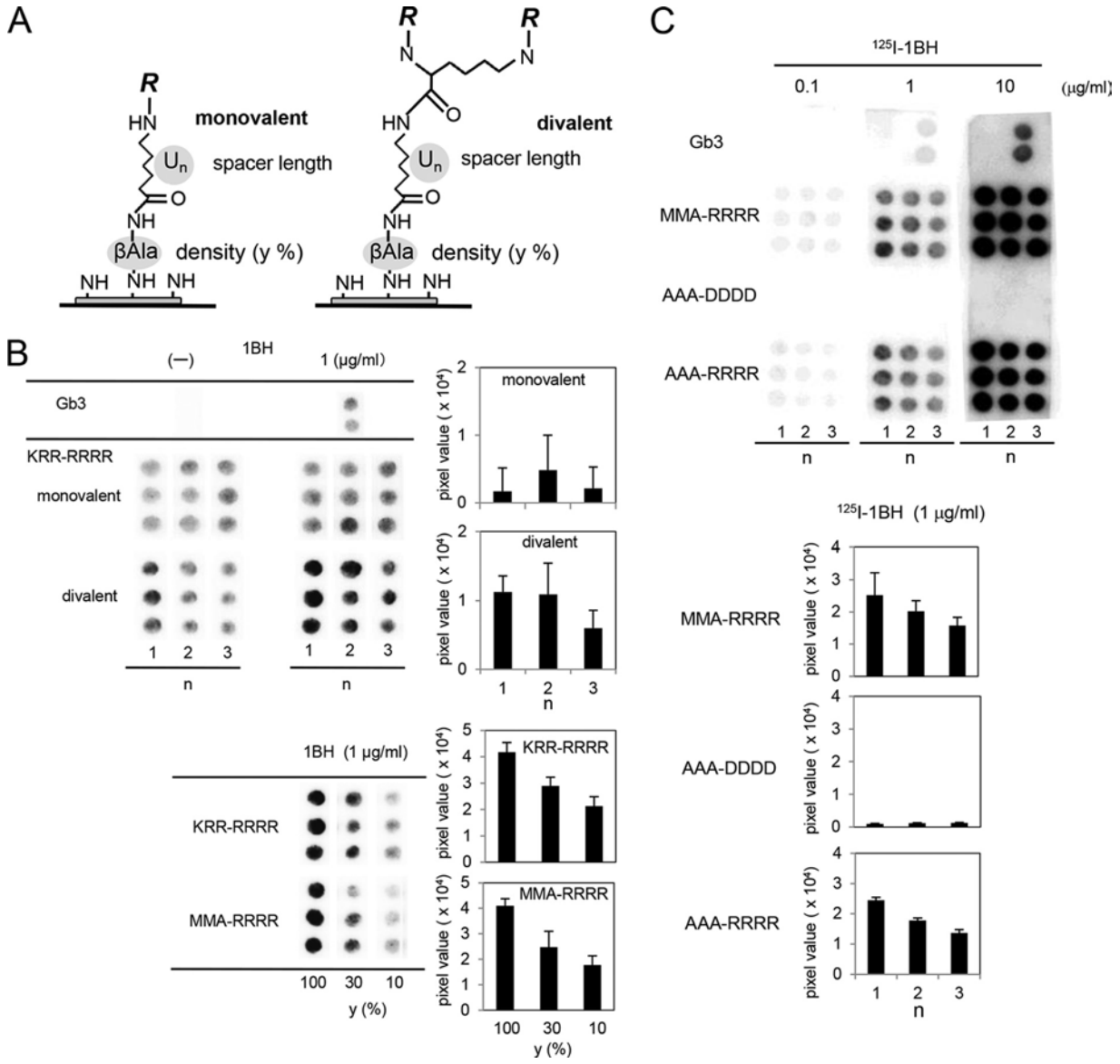

FIG 2 Optimization of the structure of the peptides synthesized on a membrane to exert the clustering effect. (A) The structure of a monovalent or a divalent peptide synthesized on a cellulose membrane is shown as described in Materials and Methods (density: $y = 10$, 30, or 100%; spacer length: $n = 1$, 2, or 3; U indicates amino hexanoic acid; ***R*** = Met-Ala-[indicated motif]-Ala). (B) The monovalent or the divalent form of the KKKRRRR motif was synthesized with different spacer lengths in triplicate ($y = 100\%$, upper panel). The divalent form of the KKKRRRR or MMARRRR motif was synthesized with different densities ($n = 1$, lower panel). The membrane was blotted with 1.0 μg/ml of 1BH. Bound 1BH was detected using rabbit anti-Stx1a antiserum and quantitated as a pixel value. Each value is shown after subtraction of the control value obtained without 1BH. (C) Divalent peptides with the MMARRRR, AAADDDD, or AAARRRR motif were synthesized on a membrane with different spacer lengths ($y = 100\%$). The membrane was blotted with the indicated concentration of ^{125}I-1BH, and the radioactivity bound to each peptide was detected (upper panel) and quantitated. Data obtained with 1.0 μg/ml of ^{125}I-1BH are shown (lower panel).

with a normalized value of ^{125}I-1BH binding (1BH-binding value) greater than 1.14 were selected and then resorted in descending order of the product (1BH × ratio) of the 1BH-binding value and the normalized ratio (1BH/G62A ratio), as shown in Table S1 in the supplemental material. A total of 64 peptides with 1BH × ratio values greater than 1.3 were identified as candidate motifs. These 64 divalent peptides were synthesized on a membrane (Fig. 4A) and blotted with different concentrations of ^{125}I-1BH or ^{125}I-1BH-G62A (Fig. 4B). The radioactivity bound to each peptide was quantitated and analyzed (see Fig. S1 in the supplemental material). Among these divalent peptides, 11 motifs were selected based on the binding intensity and specificity of 1BH, excluding peptide motifs that had tandem basic amino acids in the first three amino acids (e.g., KHA or KKA). The exclusion was implemented to avoid selecting potentially cytotoxic motifs.

Tetravalent peptides with the identified motifs bind to 1BH through site 2 with high affinities. Tetravalent peptides with the 11 motifs identified above were synthesized using the same core structure as described in Materials and Methods and were referred to as NKA-tet, IIA-tet, KGA-tet, KMA-tet, KFA-tet, FRA-tet,

A

	1	2	3	4	5	6	7	8	9	10	11	12	13	14	15	16	17	18	19	20	21	22	23	24
A					AAA	ARA	ANA	ADA	AQA	AEA	AGA	AHA	AIA	ALA	AKA	AMA	AFA	APA	ASA	ATA	AWA	AYA	AVA	RAA
B	RRA	RNA	RDA	RQA	REA	RGA	RHA	RIA	RLA	RKA	RMA	RFA	RPA	RSA	RTA	RWA	RYA	RVA	RAA	NRA	NNA	NDA	NQA	NEA
C	NGA	NHA	NIA	NLA	NKA	NMA	NFA	NPA	NSA	NTA	NWA	NYA	NVA	DAA	DRA	DNA	DDA	DQA	DEA	DGA	DHA	DIA	DLA	DKA
D	DMA	DFA	DPA	DSA	DTA	DWA	DYA	DVA	QAA	QRA	QNA	QDA	QQA	QEA	QGA	QHA	QIA	QLA	QKA	QMA	QFA	QPA	QSA	QTA
E	QWA	QYA	QVA	EAA	ERA	ENA	EDA	EQA	EEA	EGA	EHA	EIA	ELA	EKA	EMA	EFA	EPA	ESA	ETA	EWA	EYA	EVA	GAA	GRA
F	GNA	GDA	GQA	GEA	GGA	GHA	GIA	GLA	GKA	GMA	GFA	GPA	GSA	GTA	GWA	GYA	GVA	HAA	HRA	HNA	HDA	HQA	HEA	HGA
G	HHA	HIA	HLA	HKA	HMA	HFA	HPA	HSA	HTA	HWA	HYA	HVA	IAA	IRA	INA	IDA	IQA	IEA	IGA	IHA	IIA	ILA	IKA	IMA
H	IFA	IPA	ISA	ITA	IWA	IYA	IVA	LAA	LRA	LNA	LDA	LQA	LEA	LGA	LHA	LIA	LLA	LKA	LMA	LFA	LPA	LSA	LTA	LWA
I	LYA	LVA	KAA	KRA	KNA	KDA	KQA	KEA	KGA	KHA	KIA	KLA	KKA	KMA	KFA	KPA	KSA	KTA	KWA	KYA	KVA	MAA	MRA	MNA
J	MDA	MQA	MEA	MGA	MHA	MIA	MLA	MKA	MMA	MFA	MPA	MSA	MTA	MWA	MYA	MVA	FAA	FRA	FNA	FDA	FQA	FEA	FGA	FHA
K	FIA	FLA	FKA	FMA	FFA	FPA	FSA	FTA	FWA	FYA	FVA	PAA	PRA	PNA	PDA	PQA	PEA	PGA	PHA	PIA	PLA	PKA	PMA	PFA
L	PPA	PSA	PTA	PWA	PYA	PVA	SAA	SRA	SNA	SDA	SQA	SEA	SGA	SHA	SIA	SLA	SKA	SMA	SFA	SPA	SSA	STA	SWA	SYA
M	SVA	TAA	TRA	TNA	TDA	TQA	TEA	TGA	THA	TIA	TLA	TKA	TMA	TFA	TPA	TSA	TTA	TWA	TYA	TVA	WAA	WRA	WNA	WDA
N	WQA	WEA	WGA	WHA	WIA	WLA	WKA	WMA	WFA	WPA	WSA	WTA	WWA	WYA	WVA	YAA	YRA	YNA	YDA	YQA	YEA	YGA	YHA	YIA
O	YLA	YKA	YMA	YFA	YPA	YSA	YTA	YWA	YYA	YVA	VAA	VRA	VNA	VDA	VQA	VEA	VGA	VHA	VIA	VLA	VKA	VMA	VFA	VPA
P	VSA	VTA	VWA	VYA	VVA	AAR	AAN	AAD	AAQ	AAE	AAG	AAH	AAI	AAL	AAK	AAM	AAF	AAP	AAS	AAT	AAW	AAY	AAV	KRR

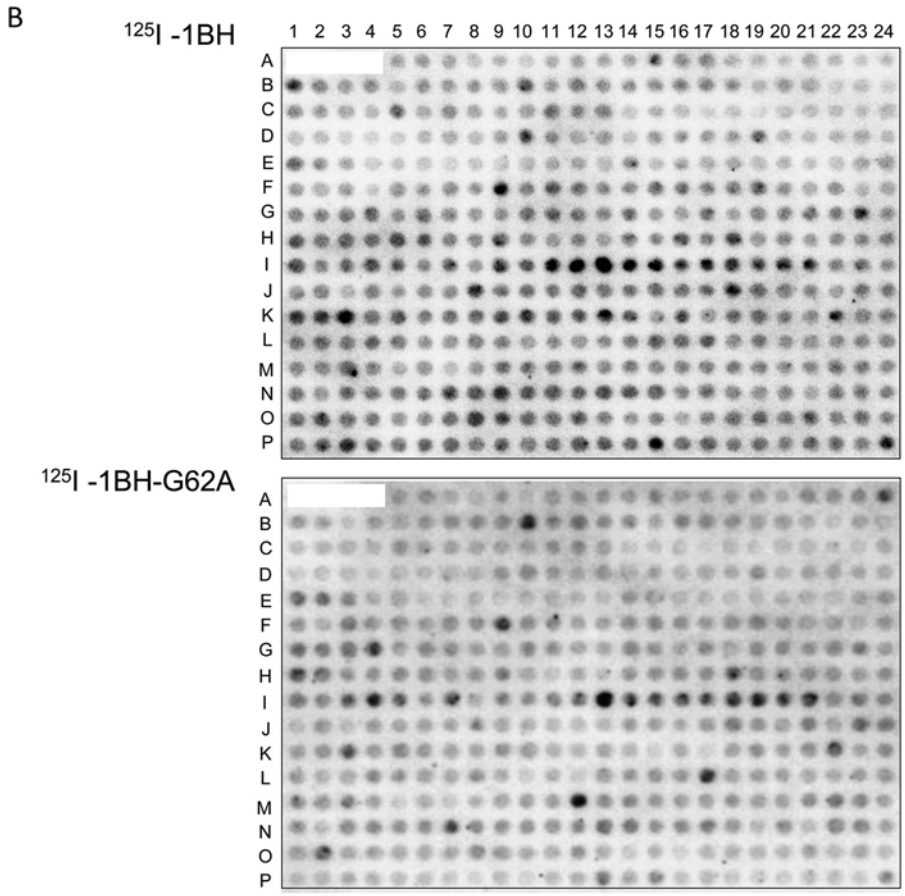

FIG 3 Screening of divalent peptides synthesized on a membrane based on binding to 1BH but not to 1BH-G62A. (A) The structure of the divalent peptide synthesized on a membrane was the same as that shown in Fig. 2A. The density of the peptides (*y*) was 100%, and the spacer length (*n*) was 1. The first three amino acids present in the XXA-RRRR or AAX-RRRR motif are shown at positions A5 to P5 or positions P6 to P23, respectively. The divalent peptide with the original motif, KRR-RRRR, was synthesized at position P24. The gray boxes indicate the 64 candidate motifs that were selected after the binding analysis. (B) The membrane was blotted with ^{125}I-1BH or ^{125}I-1BH-G62A (1 μg/ml), and the radioactivity bound to each peptide spot was quantitated and analyzed as shown in Table S1 in the supplemental material.

A

	1	2	3	4	5	6	7	8
A	RRA	NKA	QRA	GKA	GFA	GPA	GWA	GYA
B	HRA	HWA	HYA	IIA	IKA	ISA	LRA	LIA
C	LYA	KGA	KHA	KIA	KLA	KKA	KMA	KFA
D	MKA	MMA	MFA	MSA	MYA	FRA	FNA	FLA
E	FKA	FSA	FTA	FWA	FYA	FVA	PAA	PRA
F	PNA	PQA	SIA	TRA	WMA	WFA	WSA	WVA
G	YTA	YWA	YYA	VAA	VIA	VTA	VWA	VVA
H	AAR	AAN	AAG	AAH	AAL	AAK	AAM	AAF

B

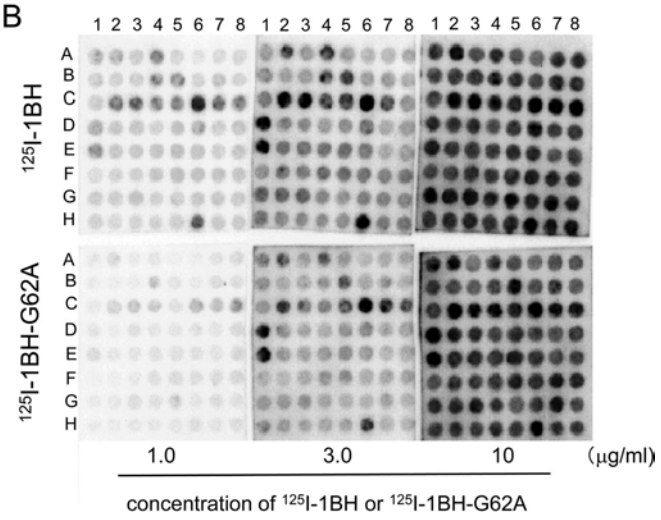

FIG 4 Binding analysis of the divalent peptides with 64 candidate motifs synthesized on a membrane to 1BH or 1BH-G62A. (A) The structure of the divalent peptide synthesized on a membrane was the same as that shown in Fig. 3A. The 64 divalent peptides with candidate motifs, the first three amino acids of which are shown in the panel, were synthesized at the indicated positions. The gray boxes indicate the 11 candidate motifs selected after the binding analysis as shown in Fig. S1 in the supplemental material. (B) The membrane was blotted with the indicated amounts of ^{125}I-1BH or ^{125}I-1BH-G62A, and the radioactivity bound to each peptide spot was quantitated and analyzed (see Fig. S1 in the supplemental material).

PQA-tet, YTA-tet, VIA-tet, AAL-tet, and AAK-tet. The binding of these tetravalent peptides to 1BH or 1BH-G62A was examined (Fig. 5). All of the tetravalent peptides bound to 1BH with more potency than to 1BH-G62A, indicating that site 2 is involved in the binding of these peptides. Under the same conditions, MMA-tet, which binds to sites 1 and 3 of 1BH but not site 2 (22), bound to 1BH-G62A with similar affinity as that of 1BH (data not shown), further confirming the binding specificity of the identified tetravalent peptides. As shown in Table 1, all of these tetravalent peptides bound to 1BH with high affinities.

Tetravalent peptides with the identified motifs efficiently inhibit the cytotoxicity of Stx1a. The ability of the identified tetravalent peptides to inhibit the cytotoxicity of Stx1a in Vero cells was examined (Fig. 6). MMA-tet was used as a positive control. Among the 11 tetravalent peptides, KGA-tet, KFA-tet, FRA-tet, PQA-tet, YTA-tet, VIA-tet, and AAL-tet inhibited Stx1a cytotoxicity as efficiently as MMA-tet, although the inhibitory effects of KFA-tet and FRA-tet were reduced at 52 μM because of their own cytotoxicity (data not shown). NKA-tet, IIA-tet, KMA-tet, and AAK-tet exerted inhibitory effects with lower efficiency.

DISCUSSION

In this study, we established a novel technique to synthesize, on a single cellulose membrane, divalent peptides that could exert the clustering effect on the Stx1a B subunit. By targeting one of the receptor-binding sites (site 2) of the B subunit, we screened divalent peptides whose sequences were designed based on information obtained by multivalent peptide library screening. We successfully identified 11 peptide-based neutralizers of Stx1a. Thus, the combination of these two techniques enables us to identify a wide range of biologically active neutralizers of Stx1a, whereas the multivalent peptide library technique yielded only one motif, which was found to be cytotoxic.

Previously, we developed a series of carbosilane dendrimers with clustered trisaccharides of Gb3, named SUPER TWIGs, as Stx neutralizers (27, 30). One of these compounds, SUPER TWIG (1)2, which has a divalent form of the trisaccharide, was found to sufficiently exert the clustering effect on the Stx B subunit to markedly increase binding affinity. Their K_D (dissociation constant) values toward the Stx1a B subunit and Stx2a B subunit were determined to be 88 and 68 μM, respectively, using the Biacore system; no binding was observed with free trisaccharide up to 1.6 mM (20, 27). These observations provide a theoretical rationale for the use of membrane-synthesized divalent (but not monomeric) peptides during screening of high-affinity binding motifs against the B subunit. Furthermore, our finding that higher density and shorter spacer length of the divalent peptide resulted in higher binding efficacy clearly demonstrates that a spatially condensed configuration of the divalent peptide enables each motif to exert the clustering effect.

Here, we focused on site 2 as a target region to develop an Stx1a neutralizer because this site has already been shown to play an essential role in the receptor binding of Stx1a (26, 31, 32). One of the Stx neutralizers with clustered trisaccharides, the STARFISH compound, containing 10 trisaccharides assembled into a single glucose core through bifurcated spacers, was found to exclusively occupy site 2 of the Stx1a B subunit, further confirming the importance of site 2 as a target region (33). The 11 Stx1a neutralizers that we identified here are the first peptide-based neutralizers to target site 2, while PPP-tet and MMA-tet, which were identified by targeting site 3 of Stx2a and site 1 of Stx1a, respectively, did not touch site 2 on each B subunit (Fig. 5) (20, 22). Among these inhibitors, KGA-tet, PQA-tet, YTA-tet, VIA-tet, and AAL-tet inhibited the cytotoxicity of Stx1a with potency similar to that of MMA-tet (Fig. 6).

All the divalent peptides synthesized on a membrane have the RRRR motif at positions 4 to 7: this motif was introduced based on information obtained from multivalent peptide library screening. The addition of even a single acidic amino acid (Asp or Glu) to this motif at position 1, 2, or 3 markedly reduced the binding of ^{125}I-1BH and ^{125}I-1BH-G62A (positions C14 to D8, E4 to E22, F23, G16, G18, H11, H13, I6, I8, J1, J3, K15, K17, M5, M7, N2, and N21, in Fig. 3B), and surprisingly, no acidic amino acids were selected in the data shown in Table S1 in the supplemental material. This significant finding about the negative selectivity of acidic amino acids cannot be theoretically obtained by using the multivalent peptide library technique. In accordance with this observation, all the motifs with 1BH-binding values and 1BH-G62A values greater than 2.2 have at least one Lys in positions 1 to 3 (see Table S1 in the supplemental material), demonstrating that the

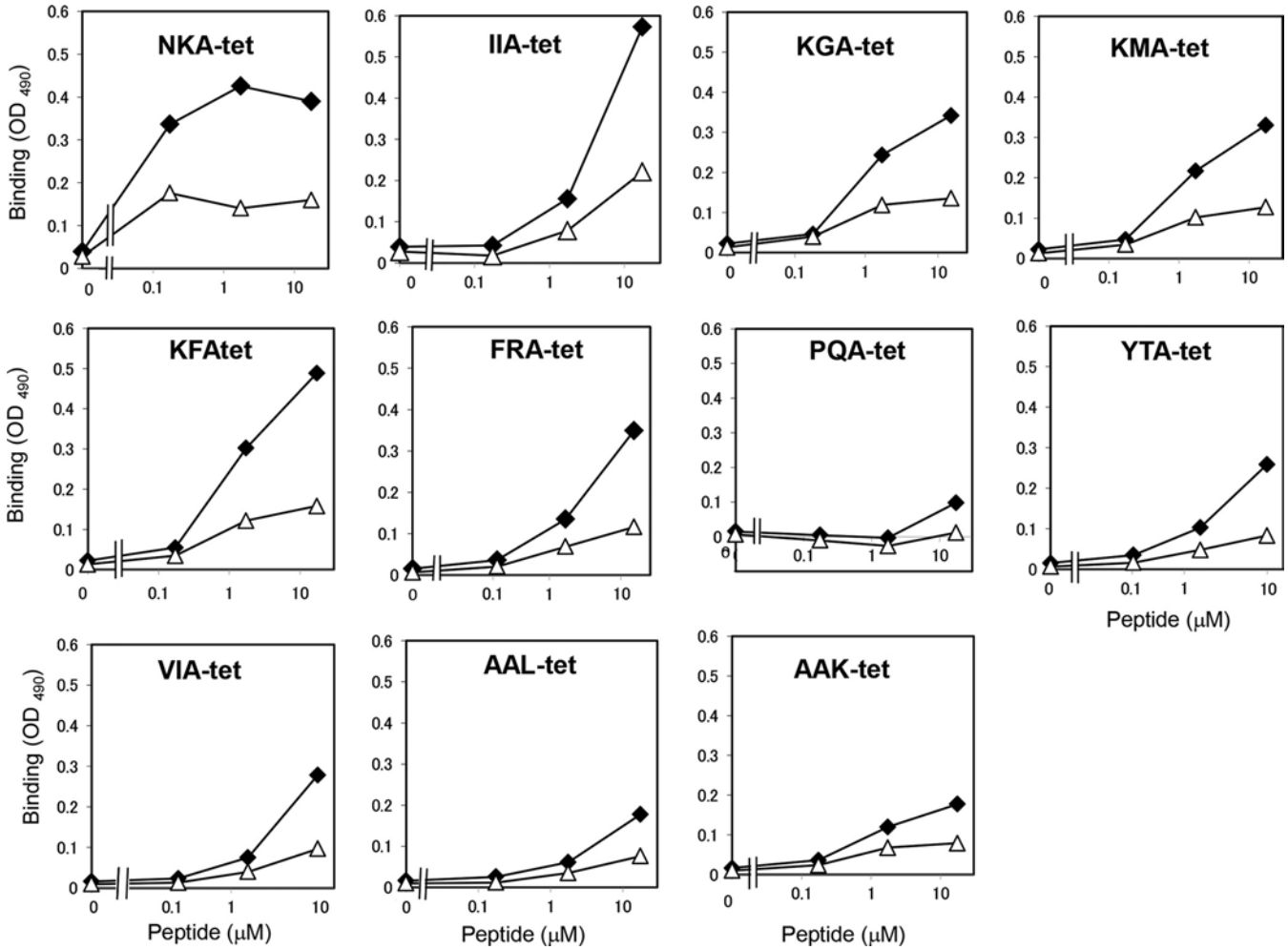

FIG 5 Analysis of the binding of the identified tetravalent peptides with 1BH or 1BH-G62A. The binding of 1BH (closed diamonds) or 1BH-G62A (open triangles) (1 μg/ml) with the indicated amounts of the tetravalent peptides was examined using ELISA.

basic amino acid cluster is required to efficiently bind to the B subunit, irrespective of the presence of Gly 62. It is possible that this basic amino acid cluster interacts with the acidic amino acids present on the receptor-binding surface of the B subunit (Asps 16, 17, and 18) (18) through electrostatic interactions. Thus, amino acids in other positions may contribute to binding site specificity. Specifically, 8 out of 11 identified Stx neutralizers have at least one hydrophobic amino acid in positions 1 to 3 (e.g., Ile, Met, Phe, Val, Pro, Tyr, or Leu) which might be involved in hydrophobic interactions at site 2, where hydrophobic interactions with the trisaccharide are prominent during receptor recognition compared to the other receptor-binding sites (18).

TABLE 1 Binding kinetics of the identified tetravalent peptides[a]

Tetravalent peptide	K_D (μM), mean ± SE (n = 3)	RU_{max} (AU), mean ± SE (n = 3 to 4)
NKA-tet	0.28 ± 0.01	2,460 ± 57
IIA-tet	0.51 ± 0.05	3,580 ± 52
KGA-tet	0.21 ± 0.01	1,390 ± 77
KMA-tet	0.43 ± 0.03	2,510 ± 71
KFA-tet	0.55 ± 0.04	3,630 ± 44
FRA-tet	0.63 ± 0.11	3,910 ± 95
PQA-tet	0.57 ± 0.01	2,140 ± 19
YTA-tet	0.34 ± 0.03	2,170 ± 364
VIA-tet	0.40 ± 0.01	2,050 ± 202
AAL-tet	1.00 ± 0.14	2,400 ± 175
AAK-tet	0.35 ± 0.02	2,630 ± 35

[a] The binding kinetics of the identified tetravalent peptides to immobilized 1BH were analyzed using the Biacore system. K_D, dissociation constant; RU_{max}, maximum resonance unit.

The novel membrane-screening technique established here substantially overcomes the problems of the multivalent peptide library technique, where only a limited number of binding motifs are determined and redundancy of amino acid selectivity may be observed in some positions in the motif. In this technique, hundreds of divalent peptides synthesized on a membrane with known sequences can be screened quantitatively, thus yielding a wide variety of binding motifs that could successfully distinguish a small change in amino acid sequence, such as Gly to Ala. Various closely related subtypes for Stx1 (Stx1a, -1c, and -1d) and Stx2 (Stx2a, -2b, -2c, -2d, -2e, -2f, and -2g) are present (12–14), but their modes of globosugar recognition are shown to be substantially different because of the minute differences present on the receptor-binding surface of the B subunits (34). Thus, the combi-

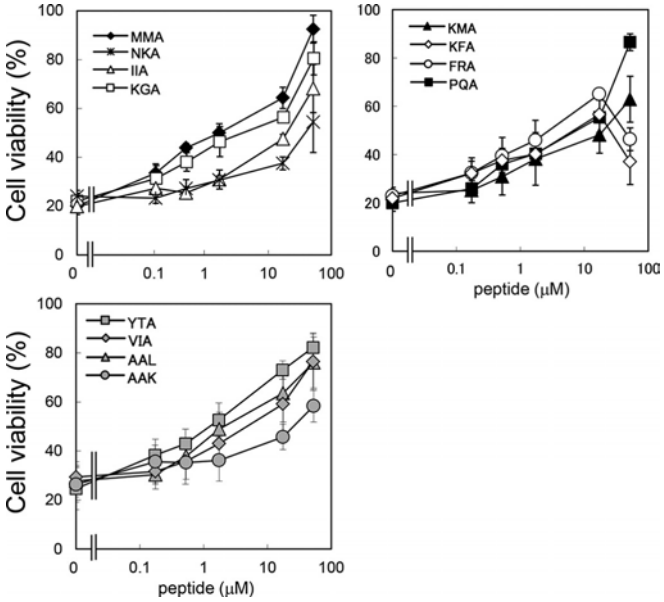

FIG 6 Inhibitory effects of the identified tetravalent peptides on the cytotoxicity of Stx1a in Vero cells. The effects of the identified tetravalent peptides on the cytotoxicity of Stx1a (1 pg/ml) in Vero cells were examined by the cytotoxicity assay. Data are presented as a percentage of the control value (mean ± standard error, $n = 3$).

nation of the two techniques presented here will provide a powerful strategy to develop optimal neutralizers against specific subtypes, enabling customized therapy that targets individual Stx subtypes produced by various EHEC strains.

ACKNOWLEDGMENTS

We thank Mika Fukumoto (Doshisha University) for her technical assistance.

This work was supported by a grant from the National Center for Global Health and Medicine, Japan; a grant from the MEXT-Supported Program for the Strategic Research Foundation at Private Universities; grants from the Ministry of Education, Culture, Sports, Science and Technology, Japan; and a grant from the Ministry of Health, Labor and Welfare, Japan.

REFERENCES

1. **Karmali MA, Steele BT, Petric M, Lim C.** 1983. Sporadic cases of haemolytic uraemic syndrome associated with fecal cytotoxin and cytotoxin-producing Escherichia coli in stools. Lancet **i:**619–620.
2. **Riley LW, Remis RS, Helgerson SD, McGee HB, Wells JG, Davis BR, Hebert RJ, Olcott ES, Johnson LM, Hargrett NT, Blake PA, Cohen ML.** 1983. Hemorrhagic colitis associated with a rare *Escherichia coli* serotype. N Engl J Med **308:**681–685. http://dx.doi.org/10.1056/NEJM198303243081203.
3. **O'Brien AD, Holmes RK.** 1987. Shiga and Shiga-like toxins. Microbiol Rev **51:**206–220.
4. **Paton JC, Paton AW.** 1998. Pathogenesis and diagnosis of Shiga toxin-producing *Escherichia coli* infections. Clin Microbiol Rev **11:**450–479.
5. **Tarr PI, Gordon CA, Chandler WL.** 2005. Shiga-toxin-producing Escherichia coli and haemolytic uraemic syndrome. Lancet **365:**1073–1086. http://dx.doi.org/10.1016/S0140-6736(05)71144-2.
6. **Trachtman H, Austin C, Lewinski M, Stahl RA.** 2012. Renal and neurological involvement in typical Shiga toxin-associated HUS. Nat Rev Nephrol **8:**658–669. http://dx.doi.org/10.1038/nrneph.2012.196.
7. **Frank C, Werber D, Cramer JP, Askar M, Faber M, an der Heiden M, Bernard H, Fruth A, Prager R, Spode A, Wadl M, Zoufaly A, Jordan S, Kemper MJ, Follin P, Müller L, King LA, Rosner B, Buchholz U, Stark K, Krause G, HUS Investigation Team.** 2011. Epidemic profile of Shiga-toxin-producing Escherichia coli O104:H4 outbreak in Germany. N Engl J Med **365:**1771–1780. http://dx.doi.org/10.1056/NEJMoa1106483.
8. **Hauswaldt S, Nitschke M, Sayk F, Solbach W, Knobloch JK.** 2013. Lessons learned from outbreaks of Shiga toxin producing Escherichia coli. Curr Infect Dis Rep **15:**4–9. http://dx.doi.org/10.1007/s11908-012-0302-4.
9. **Ikeda K, Ida O, Kimoto K, Takatorige T, Nakanishi N, Tatara K.** 1999. Effect of early fosfomycin treatment on prevention of hemolytic uremic syndrome accompanying Escherichia coli O157:H7 infection. Clin Nephrol **52:**357–362.
10. **Wong CS, Jelacic S, Habeeb RL, Watkins SL, Tarr PI.** 2000. The risk of the hemolytic-uremic syndrome after antibiotic treatment of Escherichia coli O157:H7 infections. N Engl J Med **342:**1930–1936. http://dx.doi.org/10.1056/NEJM200006293422601.
11. **Wong CS, Mooney JC, Brandt JR, Staples AO, Jelacic S, Boster DR, Watkins SL, Tarr PI.** 2012. Risk factors for the hemolytic uremic syndrome in children infected with Escherichia coli O157:H7: a multivariable analysis. Clin Infect Dis **55:**33–41. http://dx.doi.org/10.1093/cid/cis299.
12. **Gyles CL.** 2007. Shiga toxin-producing Escherichia coli: an overview. J Anim Sci **85:**E45–E62. http://dx.doi.org/10.2527/jas.2006-508.
13. **Fuller CA, Pellino CA, Flagler MJ, Strasser JE, Weiss AA.** 2011. Shiga toxin subtypes display dramatic differences in potency. Infect Immun **79:**1329–1337. http://dx.doi.org/10.1128/IAI.01182-10.
14. **Scheutz F, Teel LD, Beutin L, Piérard D, Buvens G, Karch H, Mellmann A, Caprioli A, Tozzoli R, Morabito S, Strockbine NA, Melton-Celsa AR, Sanchez M, Persson S, O'Brien AD.** 2012. Multicenter evaluation of a sequence-based protocol for subtyping Shiga toxins and standardizing Stx nomenclature. J Clin Microbiol **50:**2951–2963. http://dx.doi.org/10.1128/JCM.00860-12.
15. **Karmali MA, Petric M, Lim C, Fleming PC, Arbus GS, Lior H.** 1985. The association between idiopathic hemolytic uremic syndrome and infection by verotoxin-producing Escherichia coli. J Infect Dis **151:**775–782. http://dx.doi.org/10.1093/infdis/151.5.775.
16. **Melton-Celsa AR, O'Brien AD.** 1998. Structure, biology, and relative toxicity of Shiga toxin family members for cells and animals, p 121–128. *In* Kaper JB, O'Brien AD (ed), *Escherichia coli* O157:H7 and other Shiga toxin-producing *E. coli* strains. ASM Press, Washington, DC.
17. **DeGrandis S, Law H, Brunton J, Gyles C, Lingwood CA.** 1989. Globotetraosylceramide is recognized by the pig edema disease toxin. J Biol Chem **264:**12520–12525.
18. **Ling H, Boodhoo A, Hazes B, Cummings MD, Armstrong GD, Brunton JL, Read RJ.** 1998. Structure of the Shiga-like toxin I B-pentamer complexed with an analogue of its receptor Gb3. Biochemistry **37:**1777–1788. http://dx.doi.org/10.1021/bi971806n.
19. **Fraser ME, Fujinaga M, Cherney MM, Melton-Celsa AR, Twiddy EM, O'Brien AD, James MNG.** 2004. Structure of Shiga toxin type 2 (Stx2) from *Escherichia coli* O157:H7. J Biol Chem **279:**27511–27517. http://dx.doi.org/10.1074/jbc.M401939200.
20. **Nishikawa K, Watanabe M, Kita E, Igai K, Omata K, Yaffe MB, Natori Y.** 2006. A multivalent peptide library approach identifies a novel Shiga toxin inhibitor that induces aberrant cellular transport of the toxin. FASEB J **20:**2597–2599. http://dx.doi.org/10.1096/fj.06-6572fje.
21. **Watanabe-Takahashi M, Sato T, Dohi T, Noguchi N, Kano F, Murata M, Hamabata T, Natori Y, Nishikawa K.** 2010. An orally applicable Shiga toxin neutralizer functions in the intestine to inhibit the intracellular transport of the toxin. Infect Immun **78:**177–183. http://dx.doi.org/10.1128/IAI.01022-09.
22. **Tsutsuki K, Watanabe-Takahashi M, Takenaka Y, Kita E, Nishikawa K.** 2013. Identification of a peptide-based neutralizer that potently inhibits both Shiga toxins 1 and 2 by targeting specific receptor-binding regions. Infect Immun **81:**2133–2128. http://dx.doi.org/10.1128/IAI.01256-12.
23. **Ostroff SM, Tarr PI, Neill MA, Lewis JH, Hargrett-Bean N, Kobayashi JM.** 1989. Toxin genotypes and plasmid profiles as determinants of systemic sequelae in *Escherichia coli* O157:H7 infections. J Infect Dis **160:**994–998. http://dx.doi.org/10.1093/infdis/160.6.994.
24. **Tesh VL, Burris JA, Owens JW, Gordon VM, Wadolkowski EA, O'Brien AD, Samuel JE.** 1993. Comparison of the relative toxicities of Shiga-like toxins type I and type II for mice. Infect Immun **61:**3392–3402.
25. **Stearns-Kurosawa DJ, Collins V, Freeman S, Debord D, Nishikawa K, Oh SY, Leibowitz CS, Kurosawa S.** 2011. Rescue from lethal Shiga toxin 2-induced renal failure with a cell-permeable peptide. Pediatr Nephrol **26:**2031–2039. http://dx.doi.org/10.1007/s00467-011-1913-y.

26. **Soltyk AM, MacKenzie CR, Wolski VM, Hirama T, Kitov PI, Bundle DR, Brunton JL.** 2002. A mutational analysis of the globotriaosylceramide-binding sites of verotoxin VT. J Biol Chem **277:**5351–5359. http://dx.doi.org/10.1074/jbc.M107472200.
27. **Nishikawa K, Matsuoka K, Watanabe M, Igai K, Hino K, Terunuma D, Kuzuhara H, Natori Y.** 2005. Identification of the optimal structure for a Shiga toxin neutralizer with oriented carbohydrates to function in the circulation. J Infect Dis **191:**2097–2105. http://dx.doi.org/10.1086/430388.
28. **Frank R.** 1992. Spot-synthesis: an easy technique for the positionally addressable, parallel chemical synthesis on a membrane support. Tetrahedron **48:**9217–9232. http://dx.doi.org/10.1016/S0040-4020(01)85612-X.
29. **Frank R.** 2002. The SPOT-synthesis technique. Synthetic peptide arrays on membrane supports—principles and applications. J Immunol Methods **267:**13–26. http://dx.doi.org/10.1016/S0022-1759(02)00137-0.
30. **Nishikawa K, Matsuoka K, Kita E, Okabe N, Mizuguchi M, Hino K, Miyazawa S, Yamasaki C, Aoki J, Takashima S, Yamakawa Y, Nishijima M, Terunuma D, Kuzuhara H, Natori Y.** 2002. A therapeutic agent with oriented carbohydrates for treatment of infections by Shiga toxin-producing *Escherichia coli* O157:H7. Proc Natl Acad Sci U S A **99:**7669–7674. http://dx.doi.org/10.1073/pnas.112058999.
31. **Wolski VM, Soltyk AM, Brunton JL.** 2001. Mouse toxicity and cytokine release by verotoxin 1B subunit mutants. Infect Immun **69:**579–583. http://dx.doi.org/10.1128/IAI.69.1.579-583.2001.
32. **Flagler MJ, Mahajan SS, Kulkarni AA, Iyer SS, Weiss AA.** 2010. Comparison of binding platforms yields insights into receptor binding differences between Shiga toxins 1 and 2. Biochemistry **49:**1649–1657. http://dx.doi.org/10.1021/bi902084y.
33. **Kitov PI, Sadowska JM, Mulvey G, Armstrong GD, Ling H, Pannu NS, Read RJ, Bundle DR.** 2000. Shiga-like toxins are neutralized by tailored multivalent carbohydrate ligands. Nature **403:**669–672. http://dx.doi.org/10.1038/35001095.
34. **Yosief HO, Iyerb SS, Weiss AA.** 2013. Binding of Pk-trisaccharide analogs of globotriaosylceramide to Shiga toxin variants. Infect Immun **81:**2753–2760. http://dx.doi.org/10.1128/IAI.00274-13.

AMERICAN SOCIETY FOR MICROBIOLOGY | Infection and Immunity

Affinity-Based Screening of Tetravalent Peptides Identifies Subtype-Selective Neutralizers of Shiga Toxin 2d, a Highly Virulent Subtype, by Targeting a Unique Amino Acid Involved in Its Receptor Recognition

Takaaki Mitsui,[a] Miho Watanabe-Takahashi,[a] Eiko Shimizu,[a] Baihao Zhang,[a] Satoru Funamoto,[b] Shinji Yamasaki,[c] Kiyotaka Nishikawa[a]

Departments of Molecular Life Sciences[a] and Neuropathology,[b] Graduate School of Life and Medical Sciences, Doshisha University, Kyoto, Japan; International Prevention of Epidemics, Graduate School of Life and Environmental Sciences, Osaka Prefecture University, Osaka, Japan[c]

Shiga toxin (Stx), a major virulence factor of enterohemorrhagic *Escherichia coli* (EHEC), can be classified into two subgroups, Stx1 and Stx2, each consisting of various closely related subtypes. Stx2 subtypes Stx2a and Stx2d are highly virulent and linked with serious human disorders, such as acute encephalopathy and hemolytic-uremic syndrome. Through affinity-based screening of a tetravalent peptide library, we previously developed peptide neutralizers of Stx2a in which the structure was optimized to bind to the B-subunit pentamer. In this study, we identified Stx2d-selective neutralizers by targeting Asn16 of the B subunit, an amino acid unique to Stx2d that plays an essential role in receptor binding. We synthesized a series of tetravalent peptides on a cellulose membrane in which the core structure was exactly the same as that of peptides in the tetravalent library. A total of nine candidate motifs were selected to synthesize tetravalent forms of the peptides by screening two series of the tetravalent peptides. Five of the tetravalent peptides effectively inhibited the cytotoxicity of Stx2a and Stx2d, and notably, two of the peptides selectively inhibited Stx2d. These two tetravalent peptides bound to the Stx2d B subunit with high affinity dependent on Asn16. The mechanism of binding to the Stx2d B subunit differed from that of binding to Stx2a in that the peptides covered a relatively wide region of the receptor-binding surface. Thus, this highly optimized screening technique enables the development of subtype-selective neutralizers, which may lead to more sophisticated treatments of infections by Stx-producing EHEC.

Shiga toxin (Stx) is a major virulence factor of enterohemorrhagic *Escherichia coli* (EHEC), which causes bloody diarrhea, hemorrhagic colitis, and sometimes life-threatening systemic complications such as acute encephalopathy and hemolytic-uremic syndrome (HUS) (1–6). To date, numerous EHEC strains that produce various Stx subtypes have been reported (7, 8). These Stxs can be classified into two subgroups, Stx1 and Stx2, each consisting of various closely related subtypes, such as Stx1a, -1c, and -1d and Stx2a, -2b, -2c, -2d, -2e, -2f, and -2g (7–9). Stx2a (10, 11) and Stx2d, which is activated by elastase derived from the intestinal mucosa (12–14), are highly virulent and have been linked with HUS, the most serious sequela of EHEC infection. The pathophysiologic importance of these subtypes was also confirmed by the finding that Stx2a and Stx2d are highly toxic when injected into mice (15, 16) or primates (17–19). Therefore, Stx neutralizers, particularly those customized to specifically neutralize Stx2a and Stx2d, would be highly valuable therapeutic agents for treating infections caused by various EHEC strains.

Stx molecules consist of a catalytic A subunit, which has RNA *N*-glycosidase activity and inhibits eukaryotic protein synthesis (20, 21), and a B-subunit pentamer. The B-subunit pentamer is responsible for high-affinity binding to the functional cell surface receptor Gb3 (Galα[1-4]-Galβ[1-4]-Glcβ-ceramide) (4, 22, 23) or Gb4 (GalNAcβ[1-3]-Galα[1-4]-Galβ[1-4]-Glcβ-ceramide), which is the receptor preferred by Stx2e (24). Each B subunit has three distinct binding sites for the trisaccharide moiety of Gb3 (i.e., sites 1, 2, and 3) (25, 26), enabling a multivalent interaction between the B-subunit pentamer and Gb3. This type of interaction contributes to the highly selective and potent binding of Stx to target cells, sometimes referred to as the "clustering effect." Accordingly, several compounds with clustered trisaccharides that can bind to the B subunit with high affinity have been developed and shown to effectively neutralize Stx both *in vitro* and *in vivo* (27–33). These compounds, however, cannot be customized to specific Stx subtypes, because all Stx subtypes recognize the trisaccharide as the natural binding unit.

Previously, we developed a library of multivalent peptides exhibiting the clustering effect, from which we identified Stx-neutralizing tetravalent peptides by screening the library for high-affinity binding to the specific receptor-binding sites (33–36). By targeting Stx2a receptor-binding site 3 or Stx1a site 1, we identified various tetravalent peptides demonstrating remarkable therapeutic potency in both a mouse model of EHEC infection (34, 36) and a nonhuman primate model (19). Recently, we established a novel technique to determine a wide range of binding

Received 22 February 2016 **Returned for modification** 11 April 2016
Accepted 24 June 2016
Accepted manuscript posted online 5 July 2016
Citation Mitsui T, Watanabe-Takahashi M, Shimizu E, Zhang B, Funamoto S, Yamasaki S, Nishikawa K. 2016. Affinity-based screening of tetravalent peptides identifies subtype-selective neutralizers of Shiga toxin 2d, a highly virulent subtype, by targeting a unique amino acid involved in its receptor recognition. Infect Immun 84:2653–2661. doi:10.1128/IAI.00149-16.
Editor: B. A. McCormick, The University of Massachusetts Medical School
Address correspondence to Kiyotaka Nishikawa, knishika@mail.doshisha.ac.jp.

motifs for the B subunit by directly screening hundreds of divalent peptides synthesized on a cellulose membrane. The amino acid sequences of these peptides were designed on the basis of information obtained from the multivalent peptide library (37). By targeting Stx1a receptor-binding site 2 of the B subunit, we identified 11 peptides that neutralize Stx1a (37). Thus, the combination of library screening and synthesis of peptides on a cellulose membrane enables the efficient design of customized neutralizing peptides targeting a specific region of the receptor-binding surface of the Stx B subunit.

The amino acid sequence of the Stx2d B subunit is highly homologous to that of the Stx2a B subunit, with a difference of only two amino acids (38), Asn16 and Ala24 of the Stx2d B subunit, corresponding to Asp16 and Asp24 of the Stx2a B subunit, respectively. Asp16 of the Stx2a B subunit constitutes functional receptor-binding site 1 (26, 32, 39). Although Asn16 of the Stx2d B subunit is predicted to form receptor-binding site 1, thus contributing to cytotoxic activity (16, 40), it is unclear whether Asn16 is directly involved in receptor binding.

Using a series of B-subunit receptor-binding site mutant forms, in the present study, we found that Asn16 of the Stx2d B subunit plays an essential role in receptor binding. We targeted Asn16 and screened a series of tetravalent peptides synthesized on a cellulose membrane, the sequences of which contained the B-subunit consensus binding motif (34, 36, 37). Using this approach, we identified two peptides that selectively neutralize Stx2d. We also investigated the molecular mechanism underlying the Stx2d-specific inhibitory effects of these neutralizing peptides.

MATERIALS AND METHODS

Materials. Gb3 polymer 1:0, which is a linear polymer of acrylamide with highly clustered trisaccharides, was obtained as described previously (31). AlphaScreen reagent and Amino-PEG_{500}-UC540 membranes (INTAVIS; Bioanalytical Instruments AG, Tübingen, Germany) used in the spot synthesis of peptides were purchased from PerkinElmer (Tokyo, Japan). Recombinant Stx2a, the histidine-tagged Stx2a B subunit (2aBH), and 2aBHs containing amino acid substitutions (2aBH-D16A, 2aBH-W29A, 2aBH-W33A, 2aBH-G61A, and 2aBH-W29A/G61A/W33A) were prepared as described previously (32). Stx2d was prepared from the culture supernatant of *E. coli* strain B2F1 (O91:H21) as described previously (41). The histidine-tagged Stx2d B subunit (2dBH) was prepared as follows. An NcoI-BamHI fragment was prepared from a lysate of *E. coli* strain B2F1 (O91:H21) by PCR with primers 5′-AGAGCCATGGATTGTGCTAAAG GTAAAATT-3′ and 5′-AGAGGGATCCGCGTCATTATTAAACTG-3′. The fragment was ligated into the vector pET-28a (Novagen, Merck, Germany). 2dBH was expressed in competent *E. coli* BL21DE (3) cells (Novagen) transformed with the vector, as described previously (31). To prepare 2dBHs containing amino acid substitutions (2dBH-N16A, 2dBH-W29A, 2dBH-G61A, 2dBH-W33A, and 2dBH-N16A/G61A/W33A), site-directed mutagenesis of pET28a-2dBH was performed with a QuikChange kit (Stratagene, CA, USA) with the following mutagenic oligonucleotides: 5′-TTTTACTGTGAATGTATCAGCCTCATTATACT TGGAAAA-3′ for N16A, 5′-CAGATTCCAGCGACTGGTAGCGTACT CTTTTCCGGCCAC-3′ for W29A, 5′-AAACTGCACTTCAGCAAAAG CGGA GCCTGATTCACAGGT-3′ for G61A, and 5′-CAGTAACGGTTG CAGATTAGCGCGACTGGTCCAGTACTC-3′ for W33A.

Kinetic analysis of binding between the Gb3 polymer and B subunits. Binding of the Gb3 polymer to 2dBH or 2dBH containing an amino acid substitution was quantified with a Biacore T100 system (GE Healthcare Sciences, USA) as described previously (34). After Ni^{2+} was fixed on a nitrilotriacetic acidic sensor chip (GE Healthcare Sciences), recombinant 2dBH or 2dBH with an amino acid substitution (10 μg/ml) was injected into the system and immobilized on the chip. Various concentrations of the Gb3 polymer were injected to reach a plateau at 25°C. Resonance was expressed in the arbitrary units (AU) used by the Biacore system. Binding kinetics were analyzed with BIAEVALUATION v1.1.1 (GE Healthcare Sciences).

Spot synthesis of tetravalent peptides on a cellulose membrane. Basic spot synthesis of peptides on a cellulose membrane was performed as described previously (37), with a ResPep SL SPOT synthesizer (INTAVIS Bioanalytical Instruments AG). Fmoc-βAla-OH (Watanabe Chemical Industries, Japan) was used in the first cycle, followed by aminohexanoic acid as a spacer. Fmoc-Lys(Fmoc)-OH (Watanabe Chemical Industries) was used in the next two cycles to create four branches in the peptide chain for subsequent motif synthesis. Prior to deprotection of the side chain residues, successful synthesis of each peptide was confirmed by staining the membrane with bromophenol blue (1% in *N*,*N*′-dimethylformamide), which reacts with the free amino residues produced only after completion of all of the reactions. After destaining with *N*,*N*′-dimethylformamide, the membrane was used in the binding assay.

Assay of 2dBH or 2dBH-N16A binding to tetravalent peptides. After blocking with 5% skim milk in phosphate-buffered saline, the membrane, prepared as described above, was blotted for 1 h at room temperature with ^{125}I-labeled 2dBH or ^{125}I-labeled 2dBH-N16A (1 μg/ml, 1×10^6 to 2×10^6 cpm/μg of protein) prepared as described previously (34). After extensive washing, the radioactivity bound to each peptide spot was quantified in terms of the number of pixels with a BAS 2500 bioimaging analyzer (GE Healthcare, Japan) as described previously (37).

Synthesis of tetravalent peptides. Tetravalent peptides were synthesized with *N*-α-9-fluorenylmethoxy carbonyl (Fmoc)-protected amino acids and standard (benzotriazol-1-yloxy)tris(dimethylamino)phosphonium hexafluorophosphate/1-hydroxybenzotriazole hydrate coupling chemistry as described previously (34). A Met-Ala sequence was included at the amino terminus of the tetravalent peptide so that its structure would be identical to that of MMA-tet, which was developed on the basis of the results of multivalent peptide library screening and found to effectively inhibit both Stx1a and Stx2a (36). The terminal amino groups of the tetravalent peptides were biotinylated with biotin (Sigma-Aldrich, USA) and 1-(bis[dimethylamino]methylene)-1*H*-benzotriazolium 3-oxide hexafluorophosphate (Peptide Institute Inc., Japan) in the last cycle of the peptide synthesis.

Cytotoxicity assay. Subconfluent Vero cells cultured in a 96-well plate in Dulbecco's modified Eagle's medium supplemented with 10% fetal calf serum were treated with Stx2a (10 pg/ml) or Stx2d (80 pg/ml) in the absence or presence of a given tetravalent peptide for 72 h at 37°C. The relative number of living cells remaining after treatment was determined with Cell Counting Kit-8 (Dojindo, Japan) as described previously (34).

Analysis of binding between tetravalent peptides and B subunits with the AlphaScreen assay. The AlphaScreen assay was used to assess binding between the tetravalent peptides and Stx B subunits as described previously (36). Various amounts of biotinylated tetravalent peptide and mutant 2aBH, 2dBH, or 2aBH/2dBH (10 μg/ml) were incubated in individual wells of an OptiPlate-384 (PerkinElmer) for 1 h at room temperature. The samples were then incubated with nickel chelate acceptor beads (20 μg/ml; PerkinElmer) for 30 min and then with streptavidin donor beads (20 μg/ml; PerkinElmer) for 1 h at room temperature in the dark. The plate was then subjected to excitation at 680 nm, and emission from the wells was monitored at 615 nm with an EnVision system (PerkinElmer). Data are expressed as the AU of signal intensity (counts per second) used by the EnVision system. The apparent K_D value for each tetravalent peptide was determined as the concentration yielding half of the maximum binding value.

RESULTS

Asn16 of the Stx2d B subunit plays an essential role in receptor binding. There is a difference of two amino acids between the sequences of the Stx2a B subunit and the Stx2d B subunit. Asn16, but not Ala24, of the Stx2d B subunit is located on the receptor-

TABLE 1 Kinetic analysis of Gb3 polymer 1:0 binding to a series of Stx2d B-subunit mutant forms[a]

Stx2d B subunit	Mutated site	Mean K_D (μM) ± SE	Mean RU_{max} ± SE (*n*)
2dBH		0.32 ± 0.03	438 ± 69.3 (8)
2dBH-N16A	1	58.7 ± 33[b]	19.6 ± 6.4[c] (3)
2dBH-W29A	1	34.5 ± 7.1	53.1 ± 2.4[d] (3)
2dBH-G61A	2	1.53 ± 0.05	246 ± 18.6 (3)
2dBH-W33A	3	16.5 ± 5.3	60.8 ± 13.3[d] (3)

[a] The kinetics of Gb3 polymer 1:0 binding to each immobilized Stx2d B-subunit mutant form were analyzed with the Biacore system. RU_{max}, maximum resonance unit. The concentration of Gb3 polymer 1:0 is shown as the trisaccharide moiety. The resonance unit is an AU used by the Biacore system.
[b] $P = 0.027$ (compared with 2dBH by ANOVA and Scheffe's test).
[c] $P < 0.01$ (compared with 2dBH by ANOVA and Scheffe's test).
[d] $P < 0.02$ (compared with 2dBH by ANOVA and Scheffe's test).

binding surface (38). Although Asn16 is predicted to form receptor-binding site 1 (16, 40), there is no direct evidence demonstrating that Asn16 is involved in Stx2d receptor binding. To elucidate the role of this residue in receptor binding, Asn16 was substituted with an Ala residue and the effect on receptor-binding activity was examined with Gb3 polymer 1:0, a linear polymer of acrylamide with highly clustered trisaccharides that functions as an excellent receptor mimic (31). The effects of Ala substitutions for other amino acids (i.e., Trp29, Gly61, and Trp33, which are predicted to form sites 1, 2, and 3, respectively) were also examined. Among the 2dBH mutant forms, the K_D values for binding to 2dBH-N16A, -W29A, and -W33A increased 183-, 108-, and 52-fold, respectively, whereas the K_D value for binding to 2dBH-G61A increased only slightly, by 4.8-fold (Table 1). The maximum binding (RU_{max}) values for 2dBH-N16A, -W29A, -G61A, and -W33A decreased to 4, 12, 56, and 14% of that for 2dBH, respectively. These results indicate that Asn16 contributes significantly to the receptor binding of 2dBH and suggest that Asn16 represents an ideal target for identifying Stx2d-selective neutralizers.

Screening of tetravalent peptides synthesized on a membrane to identify peptide motifs that specifically bind to 2dBH via Asn16. We recently developed a single cellulose membrane-based technique to synthesize divalent peptides with increased affinity for binding to the B subunit (37). Here, we established another novel membrane-based technique with Fmoc-Lys(Fmoc)-OH to synthesize tetravalent peptides for the subsequent synthesis of various motifs (Fig. 1A). The basic structure of the tetravalent peptide was designed to be exactly the same as that of the previously developed tetravalent peptide library (34) in order to satisfy all of the structural requirements critical for fully exerting the clustering effect for B-subunit binding (32, 34).

The tetravalent peptide motif was either XMA-RRRR or MMX-RRRR (where X denotes any amino acid except Cys), based on the motif of MMA-tet (MMA-RRRR), which markedly inhibits the cytotoxicity of both Stx1a and Stx2a (36). Previous reports have demonstrated the importance of the second Met residue for high-affinity binding to the B subunit (36), as well as the importance of the clustered Arg residues as a consensus Stx B-subunit binding motif (34, 36, 37). These results provided the rationale for the design and on-membrane synthesis of the tetravalent peptides examined in the present study (Fig. 1B).

The membrane was blotted with ^{125}I-2dBH or ^{125}I-2dBH-N16A (Fig. 1B), and the radioactivity bound to each peptide spot was quantified and analyzed (Fig. 1C). The ratio (2dBH/N16A) of ^{125}I-2dBH binding (2dBH-binding value) to ^{125}I-2dBH-N16A binding (N16A-binding value) was calculated and normalized to evaluate the specificity of binding through Asn16. The product of the 2dBH-binding value and the normalized 2dBH/N16A ratio (2dBH × ratio) was used to evaluate both binding intensity and specificity. Nine sequences with 2dBH-binding values of >1.20 (i.e., KMA-, LMA-, QMA-, IMA-, RMA-, MMK-, MMV-, MMS-, and MMM-RRRR) were identified as candidate motifs for high-affinity binding. Of these sequences, the LMA-RRRR and MMM-RRRR motifs were found to have the highest 2dBH × ratio product in each group, indicating that these motifs exhibit the highest Asn16-mediated binding intensity and selectivity. All nine of the above-mentioned motifs were assembled into tetramer forms with the same core structure and designated KMA-tet, LMA-tet, QMA-tet, IMA-tet, RMA-tet, MMK-tet, MMV-tet, MMS-tet, and MMM-tet, respectively.

LMA-tet and MMM-tet selectively inhibit Stx2d cytotoxicity. The effects of the nine tetravalent peptides described in the previous section on the cytotoxicity of Stx2a and Stx2d are illustrated in Fig. 2. At a concentration as low as 17 μM, LMA-tet, QMA-tet, IMA-tet, MMV-tet, and MMM-tet inhibited the cytotoxicity of Stx2a similarly to MMA-tet (the most effective peptide-based neutralizer of this subtype developed to date) (Fig. 2A and C). Notably, LMA-tet and MMM-tet inhibited the cytotoxicity of Stx2d with even more potency than MMA-tet, whereas QMA-tet, IMA-tet, and MMV-tet showed inhibitory efficacy similar to that of MMA-tet (Fig. 2B and D). The 50% inhibitory concentrations (IC_{50}s) of LMA-tet, MMM-tet, and MMA-tet for Stx2d were 2.9, 2.7, and 6.8 μM, respectively, and their IC_{50}s for Stx2a were 7.9, 6.8, and 5.5 μM, respectively. KMA-tet, RMA-tet, and MMK-tet showed no or limited inhibition of Stx2a and Stx2d cytotoxicity (Fig. 2A to D). In the absence of toxin, no cytotoxic activity was exhibited by any of the nine tetravalent peptides at concentrations of up to 17 μM (data not shown). Thus, five peptides (LMA-tet, QMA-tet, IMA-tet, MMV-tet, and MMM-tet) were identified as novel neutralizers of both Stx2a and Stx2d. LMA-tet and MMM-tet, in particular, exhibited clear selectivity for Stx2d.

LMA-tet and MMM-tet bind to the Stx2d B subunit via a relatively large region of the receptor-binding surface encompassing Asn16. To elucidate the mechanism by which LMA-tet and MMM-tet bind to the Stx2a or Stx2d B subunit, the binding to each B subunit or its receptor-binding site mutant forms was examined with the AlphaScreen assay. The results showed that LMA-tet and MMM-tet bound to 2aBH or 2dBH with high affinity (Fig. 3A). The patterns of binding to 2aBH and its mutant forms were quite similar, in that the maximum values of binding to 2aBH-D16A (a site 1 mutant form) and 2aBH-W29A/G61A/W33A (a site 1, 2, and 3 triple mutant form) were markedly reduced. The maximum values of LMA-tet and MMM-tet binding to 2aBH-W33A (a site 3 mutant form) were reduced to 66.4 and 74.3%, respectively, and the apparent K_D values were increased 5.1- and 4.2-fold, respectively (Fig. 3B). On the other hand, the maximum values of LMA-tet binding to 2aBH-W29A (a site 1 mutant form) and 2aBH-G61A (a site 2 mutant form) were not markedly affected, although the apparent K_D values were increased 4.8- and 1.7-fold, respectively (Fig. 3B). Similarly, the maximum values of MMM-tet binding to 2aBH-W29A and 2aBH-G61A were not affected, but the apparent K_D values were increased 3.8- and 1.5-fold, respectively (Fig. 3B). These results

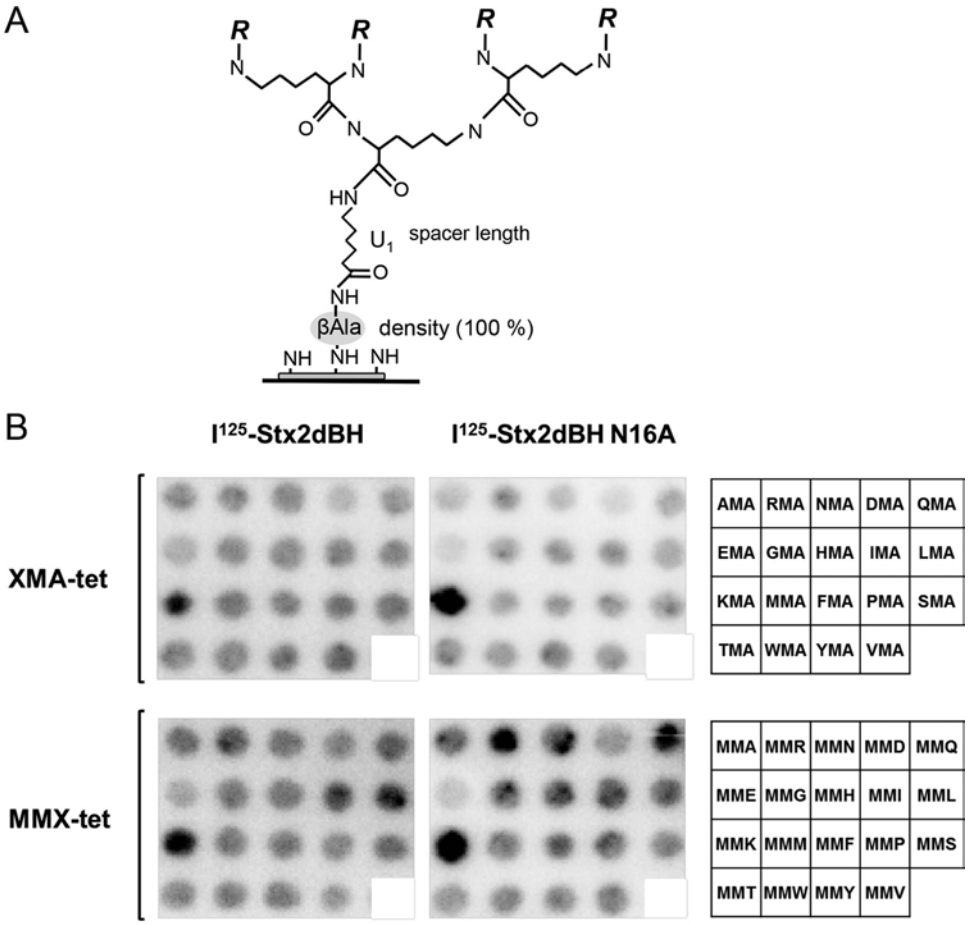

C

XMA-tet

XXX	2dBH-binding value	N16A-binding value	2dBH/N16A	2dBH X ratio
KMA	1.825	2.400	0.697	1.272
LMA	1.624	1.022	1.456	2.365
QMA	1.292	1.626	0.728	0.941
IMA	1.280	1.149	1.021	1.307
RMA	1.276	1.745	0.670	0.855
AMA	1.036	1.000	0.949	0.983
NMA	1.018	1.363	0.685	0.697
SMA	1.011	0.718	1.291	1.305
HMA	0.994	1.048	0.870	0.865
GMA	0.942	0.940	0.918	0.865
MMA	0.909	0.782	1.066	0.969
DMA	0.887	0.713	1.140	1.011
FMA	0.864	0.778	1.014	0.876
YMA	0.835	0.603	1.270	1.060
WMA	0.778	0.631	1.131	0.880
TMA	0.751	0.605	1.137	0.854
PMA	0.749	0.881	0.780	0.584
VMA	0.472	0.729	0.593	0.280
EMA	0.460	0.267	1.580	0.727

MMX-tet

XXX	2dBH-binding value	N16A-binding value	2dBH/N16A	2dBH X ratio
MMK	1.667	3.737	0.394	0.657
MMV	1.287	0.996	1.141	1.468
MMS	1.235	1.036	1.053	1.300
MMM	1.211	0.864	1.238	1.499
MMP	1.093	0.942	1.024	1.119
MMW	1.079	0.971	0.982	1.060
MMT	1.047	1.121	0.825	0.864
MMY	1.039	1.210	0.758	0.788
MMH	1.001	0.894	0.990	0.991
MMF	0.998	0.880	1.002	1.000
MMI	0.945	0.926	0.902	0.852
MMN	0.939	0.559	1.485	1.394
MMG	0.922	0.865	0.942	0.869
MML	0.919	0.845	0.961	0.883
MMA	0.871	0.667	1.154	1.005
MMR	0.854	0.914	0.825	0.705
MMQ	0.782	0.764	0.905	0.708
MME	0.637	0.463	1.215	0.774
MMD	0.472	0.347	1.204	0.568

FIG 1 Identification of Asn16-dependent 2dBH binding motifs by screening of tetravalent peptides synthesized on a cellulose membrane. (A) General structure of the tetravalent peptides synthesized on a cellulose membrane as described previously (37). The density of the tetravalent peptide was maximized by using Fmoc-β-Ala-OH without butoxycarbonyl-β-Ala-OH for the first peptide synthesis cycle. After the addition of one aminohexanoic acid (U) as a spacer following the first β-Ala, Fmoc-Lys(Fmoc)-OH was used for the next two cycles to form four branches in the peptide chain for subsequent synthesis of the various motifs examined in this study (*R* = Met-Ala-[indicated motif]-Ala-). (B) The tetravalent form of the XMA-RRRR or MMX-RRRR (X indicates any amino acid except Cys) motif was synthesized on a membrane (left and center). The first three amino acids present in the motif are indicated on the right. The membrane was blotted with ^{125}I-2dBH or ^{125}I-2dBH-N16A (1 μg/ml), and the radioactivity bound to each peptide spot was quantified as a pixel value. (C) The sum of the pixel values of all of the peptide spots was normalized to 19 (the number of tetravalent peptides synthesized on the membrane) so that each peptide would have a value of 1 in the absence of selectivity. The ratio of ^{125}I-2dBH binding (2dBH-binding value) to ^{125}I-2dBH-N16A binding (N16A-binding value) (2dBH/N16A) was calculated, and the sum of each ratio was also normalized to 19 to evaluate the specificity of binding through Asn16. The product of the 2dBH-binding value and the normalized 2dBH/N16A ratio (2dBH × ratio) was used to evaluate both binding intensity and specificity. The sequences were sorted in descending order on the basis of the 2dBH-binding values. 2dBH-binding values of >1.20 and the highest 2dBH × ratio products are shaded.

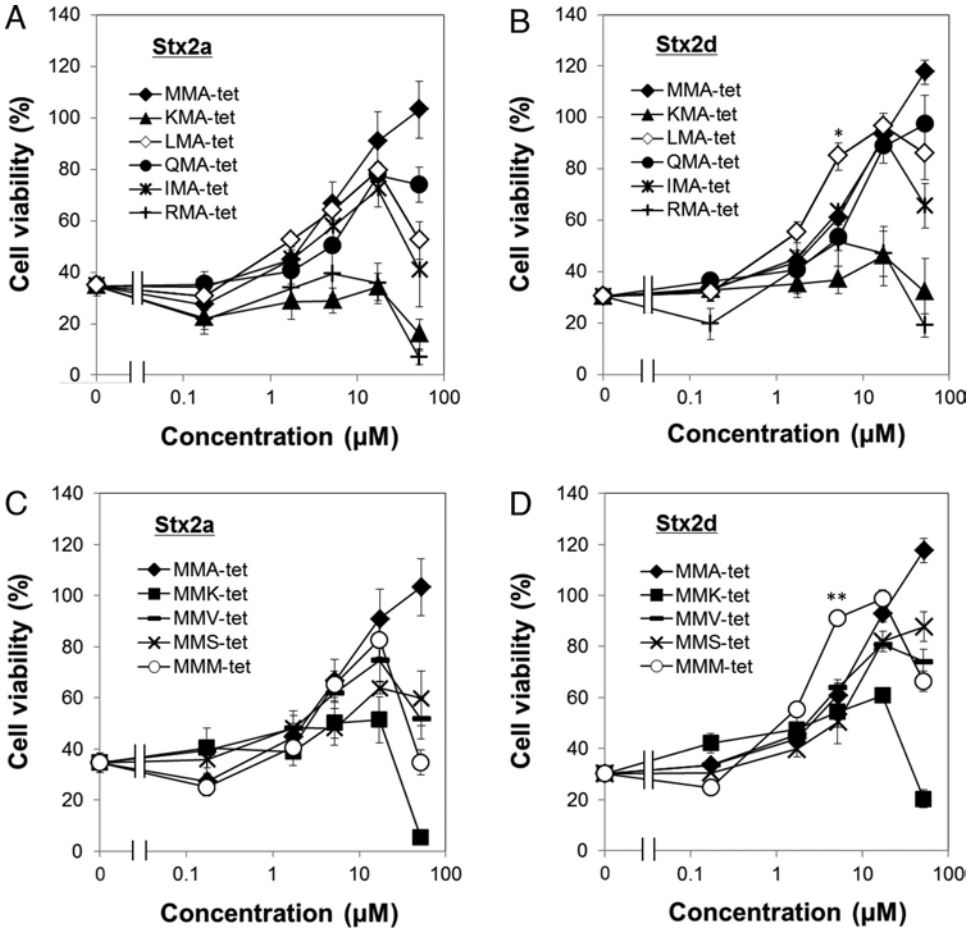

FIG 2 Inhibition of the cytotoxicity of Stx2a and Stx2d for Vero cells by the tetravalent peptides identified in this study. The effects of the tetravalent peptides indicated on the cytotoxicity of Stx2a (10 pg/ml; A and C) or Stx2d (80 pg/ml; B and D) for Vero cells were examined with a cytotoxicity assay. Data are presented as percentages of the control value (mean ± standard error, $n = 3$; *, $P < 0.05$; **, $P < 0.01$ [Tukey's test, compared with MMA-tet]).

suggest that Asp16, located at site 1 of the Stx2a B subunit, plays an essential role in the binding of LMA-tet and MMM-tet, whereas site 3 residue Trp33 (but not Trp29 at site 1 or Gly61 in site 2) plays a more limited role in binding.

In contrast, the maximum values of LMA-tet and MMM-tet binding to 2dBH-G61A (a site 2 mutant form), 2dBH-W33A (a site 3 mutant form), and 2aBH-W29A/G61A/W33A (a site 1, 2, and 3 triple mutant form) were markedly reduced, and the maximum values of binding to 2dBH-N16A (a site 1 mutant form) were substantially reduced (to 23.2 and 31.2% of the maximum binding to 2dBH, respectively) (Fig. 3B). The maximum values of LMA-tet and MMM-tet binding to 2dBH-W29A (a site 1 mutant form) were reduced to 62.1 and 57.0%, respectively, and their apparent K_D values increased 3.4- and 4.5-fold, respectively (Fig. 3B). Thus, in the case of the Stx2d B subunit, Asn16, Gly61, and Trp33, which constitute receptor-binding sites 1, 2, and 3, respectively, play significant roles in the binding of LMA-tet and MMM-tet, whereas Trp29 plays a more limited role. MA-tet, which has the same core structure as the other peptide but lacks a binding motif, did not bind to the B subunit (data not shown), providing further confirmation that the two motifs identified here mediate efficient binding to the Stx2d B subunit.

DISCUSSION

In this study, we found that Asn16 of the Stx2d B subunit, which is the only difference between the sequences of Stx2a and Stx2d on the receptor-binding surface, plays an essential role in the receptor binding of Stx2d. By Asn16-targeted screening of a series of tetravalent peptides synthesized on a cellulose membrane, we identified five novel Stx2d neutralizers: LMA-tet, QMA-tet, IMA-tet, MMV-tet, and MMM-tet. Each of these tetravalent peptides efficiently inhibited Stx2a as well. Interestingly, LMA-tet and MMM-tet exhibited clear selectivity for Stx2d.

The relative contributions of Asn16, Trp33, and Trp29 to receptor binding of the Stx2d B subunit were elucidated with Gb3 polymer 1:0, an excellent receptor mimic composed of highly clustered trisaccharides (31) (Table 1). In a previous study, we demonstrated that single substitution of Stx2a B-subunit residue Asp16, Trp29, or Trp33 with Ala has no effect on the binding kinetics of the Gb3 polymer, because in this case, the dysfunction in the corresponding receptor-binding site can be compensated for by the other sites (39). Conversely, an enzyme-linked immunosorbent assay-based study revealed that the binding of Stx2a and Stx2d B subunits to immobilized Gb3 exhibits essentially the same kinetics (42). Furthermore, the K_D value for binding of the

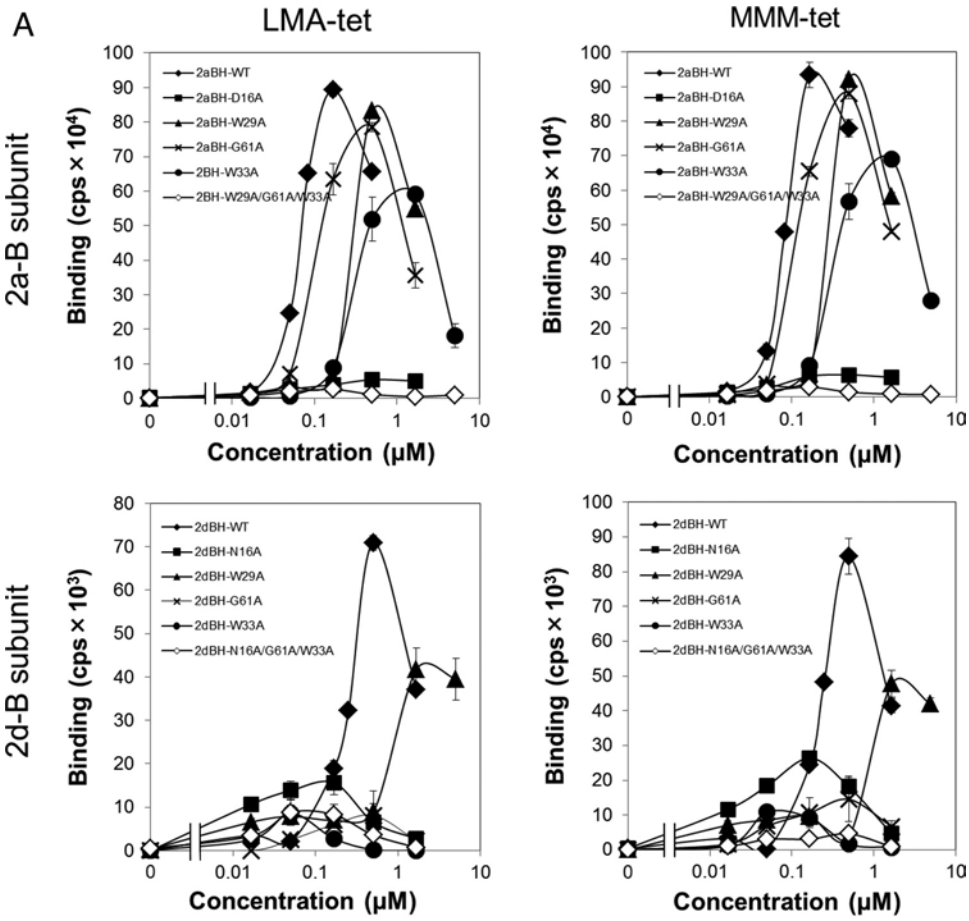

B

2BH	LMA-tet		MMM-tet	
	Apparent K_D (μM)	Maximun binding (%)	Apparent K_D (μM)	Maximun binding (%)
	mean ± se			
2aBH	0.069 ± 0.001	100	0.086 ± 0.006	100
2aBH-D16A	–	–	–	–
2aBH-W29A	0.33 ± 0.01***	93.3 ± 2.8	0.33 ± 0.01***	99.3 ± 7.7
2aBH-G61A	0.12 ± 0.01	88.1 ± 4.6	0.13 ± 0.01	95.0 ± 5.9
2aBH-W33A	0.35 ± 0.05***	66.4 ± 3.8***	0.36 ± 0.05***	74.3 ± 5.7*
2aBH-W29A/G61A/W33A	–	–	–	–
2dBH	0.28 ± 0.02	100	0.24 ± 0.02	100
2dBH-N16A	–	23.2 ± 6.0***	–	31.2 ± 1.0***
2dBH-W29A	0.96 ± 0.14**	62.1 ± 11***	1.07 ± 0.01**	57.0 ± 7.4***
2dBH-G61A	–	12.0 ± 5.9***	–	16.4 ± 9.9***
2dBH-W33A	–	12.8 ± 4.2***	–	13.2 ± 3.7***
2dBH-N16A/G61A/W33A	–	13.1 ± 6.7***	–	–

FIG 3 Analysis of the binding of LMA-tet and MMM-tet to 2aBH or 2dBH with the AlphaScreen assay. (A) The binding of biotinylated LMA-tet and MMM-tet to 2aBH, 2dBH, and their mutant forms (10 μg/ml) was examined with the AlphaScreen assay. Data are presented as signal intensity (mean number of counts per second ± standard error, $n = 3$). (B) The apparent K_D values of LMA-tet and MMM-tet for binding to 2aBH, 2dBH, and their mutant forms were determined as the concentration of the compound yielding half of the maximum binding value. The maximum values of LMA-tet and MMM-tet binding are presented as percentages of the values of their binding to 2aBH and 2dBH. —, not determined. *, $P < 0.05$; ***, $P < 0.005$ (Tukey's test); **, $P < 0.005$ (Student's t test, compared with 2aBH or 2dBH).

Gb3 polymer to the Stx2d B subunit (0.32 μM) (Table 1) was found to be even lower than that of binding to the Stx2a B subunit (0.68 μM) (39). These observations clearly indicate that the molecular interaction with the receptor differs for the Stx2a B subunit and Stx2d B subunit. Thus, Stx2d B-subunit Asn16 plays a physiologically more significant role in receptor binding than Stx2a B-subunit Asp16, further confirming the validity of selecting Asn16 as a target for the development of Stx2d-selective neutralizers.

In this study, we established a technique for cellulose membrane synthesis of tetravalent peptides with structures that satisfy all of the requirements for exerting the clustering effect for B-subunit binding (32, 34). Using a series of carbosilane dendrimers with clustered trisaccharides, referred to as SUPER TWIGs, we previously found that four trisaccharides, each of which is included in the structure separated by spacers of at least 11 Å, are sufficient for high-affinity binding to the B subunits of Stx1 and Stx2 (32). On the basis of our previous findings, our membrane peptide synthesis technique was optimized in the present study in order to synthesize tetravalent peptides containing an RRRR sequence motif. One of the four inhibitory motifs identified by targeting site 3 of the Stx2a B subunit by the peptide library technique contains a PPP-RRRR sequence (34). In addition, all of the inhibitory motifs identified by targeting site 1 (36) and site 2 (37) of the Stx1a B subunit have an RRRR motif. Replacing the RRRR motif with a DDDD motif completely abolishes binding to the Stx1a B subunit (37). In this study, screening of two series of tetravalent peptides synthesized on a membrane with XMA-RRRR or MMX-RRRR motifs led to the identification of nine candidate Stx2d B-subunit binding motifs. However, as shown in Fig. 1C, the addition of an Asp or Glu residue next to the RRRR motif yielded the lowest value of binding to the Stx2d B subunit, further confirming the importance of the cluster of basic amino acids for binding to the Stx2d B subunit.

To date, a variety of Stx neutralizers containing a cluster of trisaccharides as an Stx binding unit have been developed (27–32). However, it is difficult to develop subtype-selective neutralizers based on these neutralizers, because all of the Stx subtypes recognize Gb3 as a common receptor (4, 22–24). The B subunits of Stx2a, Stx2c, and Stx2d, in particular, display similar glycolipid-binding affinities (42). In this study, by targeting Asn16 of the Stx2d B subunit, we identified two Stx2d-selective neutralizers, LMA-tet and MMM-tet. Interestingly, Asn16, Gly61, and Trp33 of the Stx2d B subunit (which constitute receptor-binding sites 1, 2, and 3, respectively) were found to contribute equally to the efficient binding of LMA-tet and MMM-tet, whereas the corresponding Stx2a B-subunit amino acid Asp16 in site 1 (but not Gly61 or Trp33) was essential for neutralizer binding (Fig. 3). These observations clearly demonstrate that the mechanism by which the neutralizers bind to the B-subunit receptor-binding surface differs for Stx2d and Stx2a, even though both Asn16 of the Stx2d B subunit and Asp16 of the Stx2a B subunit are involved. This unique binding mechanism may contribute to the Stx2d-selective inhibitory activity of the neutralizers we identified. Of note, G61 of the Stx2d B subunit was found to be essential for the binding of LMA-tet and MMM-tet (Fig. 3), whereas this amino acid was not involved in the binding of Gb3 polymer 1:0 (Table 1), indicating that the peptide neutralizers and the Gb3 polymer bind to the Stx2d B subunit via different molecular mechanisms. Thus, the best region to target for developing a subtype-selective Stx neutralizer may not necessarily be consistent with the functional receptor-binding regions, further demonstrating the difficulty of using trisaccharides as Stx-binding units in the development of subtype-selective neutralizers.

Of the various Stx subtypes, Stx2a (10, 11) and Stx2d (12–14) are highly toxic and have been linked with HUS. Another Stx2 subtype, Stx2c, is also commonly associated with HUS (43, 44). Although Stx2c is much less toxic than Stx2a and Stx2d *in vivo* because of the instability of its A subunit (16, 45), the amino acid sequence of its B subunit is the same as that of the Stx2d B subunit (8, 43). Interestingly, we found that LMA-tet and MMM-tet also efficiently inhibited the cytotoxicity of Stx2c for Vero cells, with IC_{50}s of 2.2 and 1.6 μM, respectively, compared with 3.3 μM for MMA-tet (data not shown). As shown here, LMA-tet and MMM-tet clearly exhibited Stx2d inhibitory effects superior to those of MMA-tet (Fig. 2). MMA-tet, which was originally developed for Stx1a (36), is a universal neutralizer that efficiently inhibits various Stx subtypes, including Stx1a, Stx2a (36, 37), and Stx2d (Fig. 2). These observations clearly demonstrate the usefulness of developing subtype-selective neutralizers in addition to a universal neutralizer such as MMA-tet. LMA-tet and MMM-tet also exhibited potent inhibition of the cytotoxicity of Stx2a, with IC_{50}s (7.9 and 6.8 μM, respectively) similar to that of MMA-tet (5.5 μM) (Fig. 2). Thus, the use of these compounds alone or in combination with MMA-tet is predicted to be a more effective treatment for infections with EHEC producing these highly virulent Stx subtypes.

ACKNOWLEDGMENTS

We thank Mika Fukumoto (Doshisha University) for technical assistance.

This work was supported by a grant from the MEXT-Supported Program for the Strategic Research Foundation at Private Universities; JSPS KAKENHI grants 24390035 and 15K08480; the Research Program on Emerging and Re-emerging Infectious Diseases of the Japan Agency for Medical Research and Development, AMED; the Research Program on Development of New Drugs, AMED; the Mochida Memorial Foundation for Medical and Pharmaceutical Research; and a grant from the Asahi Glass Foundation, Japan.

FUNDING INFORMATION

This work, including the efforts of Kiyotaka Nishikawa, was funded by Japan Society for the Promotion of Science (JSPS) KAKENHI (24390035). This work, including the efforts of Miho Watanabe-Takahashi, was funded by Japan Society for the Promotion of Science (JSPS) KAKENHI (15K08480). This work, including the efforts of Kiyotaka Nishikawa, was funded by The Research Program on Emerging and Re-emerging Infectious Diseases From Japan Agency for Medical Research and Development. This work, including the efforts of Kiyotaka Nishikawa, was funded by The Research Program on Development of New Drugs From Japan Agency for Medical Research and Development. This work, including the efforts of Kiyotaka Nishikawa, was funded by Ministry of Education, Culture, Sports, Science, and Technology (MEXT) for the Strategic Research Foundation at Private Universities. This work, including the efforts of Miho Watanabe-Takahashi, was funded by The Mochida Memorial Foundation for Medical and Pharmaceutical Research. This work, including the efforts of Miho Watanabe-Takahashi, was funded by Asahi Glass Foundation, Japan.

REFERENCES

1. **Karmali MA, Steele BT, Petric M, Lim C.** 1983. Sporadic cases of hemolytic uremic syndrome associated with fecal cytotoxin and cytotoxin-producing *Escherichia coli*. Lancet **i**:619–620.
2. **Riley LW, Remis RS, Helgerson SD, McGee HB, Wells JG, Davis BR, Hebert RJ, Olcott ES, Johnson LM, Hargrett NT, Blake PA, Cohen ML.** 1983. Hemorrhagic colitis associated with a rare *Escherichia coli* serotype. N Engl J Med **308**:681–685. http://dx.doi.org/10.1056/NEJM198303243081203.
3. **O'Brien AD, Holmes RK.** 1987. Shiga and Shiga-like toxins. Microbiol Rev **51**:206–220.
4. **Paton JC, Paton AW.** 1998. Pathogenesis and diagnosis of Shiga toxin-producing *Escherichia coli* infections. Clin Microbiol Rev **11**:450–479.
5. **Tarr PI, Gordon CA, Chandler WL.** 2005. Shiga-toxin-producing Escherichia coli and haemolytic uraemic syndrome. Lancet **365**:1073–1086.
6. **Trachtman H, Austin C, Lewinski M, Stahl RA.** 2012. Renal and neu-

rological involvement in typical Shiga toxin-associated HUS. Nat Rev Nephrol **8:**658–669. http://dx.doi.org/10.1038/nrneph.2012.196.
7. **Gyles CL.** 2007. Shiga toxin-producing *Escherichia coli*: an overview. J Anim Sci **85:**E45–E62. http://dx.doi.org/10.2527/jas.2006-508.
8. **Scheutz F, Teel LD, Beutin L, Pierard Dpdote Buvens G, Karch H, Mellmann A, Caprioli A, Tozzoli R, Morabito S, Strockbine NA, Melton-Celsa AR, Sanchez M, Persson S, O'Brien AD.** 2012. Multicenter evaluation of a sequence-based protocol for subtyping Shiga toxins and standardizing Stx nomenclature. J Clin Microbiol **50:**2951–2963. http://dx.doi.org/10.1128/JCM.00860-12.
9. **Melton-Celsa AR.** 2014. Shiga toxin (Stx) classification, structure, and function. Microbiol Spectr **2:**EHEC-0024-2013.
10. **Ostroff SM, Tarr PI, Neill MA, Lewis JH, Hargrett-Bean N, Kobayashi JM.** 1989. Toxin genotypes and plasmid profiles as determinants of systemic sequelae in *Escherichia coli* O157:H7 infections. J Infect Dis **160:**994–998. http://dx.doi.org/10.1093/infdis/160.6.994.
11. **Tesh VL, Burris JA, Owens JW, Gordon VM, Wadolkowski EA, O'Brien AD, Samuel JE.** 1993. Comparison of the relative toxicities of Shiga-like toxins type I and type II for mice. Infect Immun **61:**3392–3402.
12. **Melton-Celsa AR, Darnell SC, O'Brien AD.** 1996. Activation of Shiga-like toxins by mouse and human intestinal mucus correlates with virulence of enterohemorrhagic *Escherichia coli* O91:H21 isolates in orally infected, streptomycin-treated mice. Infect Immun **64:**1569–1576.
13. **Kokai-Kun JF, Melton-Celsa AR, O'Brien AD.** 2000. Elastase in intestinal mucus enhances the cytotoxicity of Shiga toxin type 2d. J Biol Chem **275:**3713–3721. http://dx.doi.org/10.1074/jbc.275.5.3713.
14. **Bielaszewska M, Friedrich AW, Aldick T, Schurk-Bulgrin R, Karch H.** 2006. Shiga toxin activatable by intestinal mucus in Escherichia coli isolated from humans: predictor for a severe clinical outcome. Clin Infect Dis **43:**1160–1167. http://dx.doi.org/10.1086/508195.
15. **Bunger JC, Melton-Celsa AR, O'Brien AD.** 2013. Shiga toxin type 2dact displays increased binding to globotriaosylceramide in vitro and increased lethality in mice after activation by elastase. Toxins (Basel) **5:**2074–2092. http://dx.doi.org/10.3390/toxins5112074.
16. **Fuller CA, Pellino CA, Flagler MJ, Strasser JE, Weiss AA.** 2011. Shiga toxin subtypes display dramatic differences in potency. Infect Immun **79:**1329–1337. http://dx.doi.org/10.1128/IAI.01182-10.
17. **Siegler RL, Obrig TG, Pysher T, Tesh JVL, Denkers ND, Taylor FB.** 2003. Response to Shiga toxin 1 and 2 in a baboon model of hemolytic uremic syndrome. Pediatr Nephrol **18:**92–96.
18. **Stearns-Kurosawa DJ, Collins V, Freeman S, Tesh VL, Kurosawa S.** 2010. Distinct physiologic and inflammatory responses elicited in baboons after challenge with Shiga toxin type 1 or 2 from enterohemorrhagic *Escherichia coli*. Infect Immun **78:**2497–2504. http://dx.doi.org/10.1128/IAI.01435-09.
19. **Stearns-Kurosawa DJ, Collins V, Freeman S, Debord D, Nishikawa K, Oh SY, Leibowitz CS, Kurosawa S.** 2011. Rescue from lethal Shiga toxin 2-induced renal failure with a cell-permeable peptide. Pediatr Nephrol **26:**2031–2039. http://dx.doi.org/10.1007/s00467-011-1913-y.
20. **Endo Y, Tsurugi K, Yutsudo T, Takeda Y, Ogasawara T, Igarashi K.** 1988. Site of action of a Vero toxin (VT2) from Escherichia coli O157:H7 and of Shiga toxin on eukaryotic ribosomes. RNA *N*-glycosidase activity of the toxins. Eur J Biochem **171:**45–50.
21. **Saxena SK, O'Brien AD, Ackerman EJ.** 1989. Shiga toxin, Shiga-like toxin II variant, and ricin are all single-site RNA N-glycosidases of 28 S RNA when microinjected into *Xenopus* oocytes. J Biol Chem **264:**596–601.
22. **Karmali MA, Petric M, Lim C, Fleming PC, Arbus GS, Lior H.** 1985. The association between idiopathic hemolytic uremic syndrome and infection by verotoxin-producing *Escherichia coli*. J Infect Dis **151:**775–782. http://dx.doi.org/10.1093/infdis/151.5.775.
23. **Melton-Celsa AR, O'Brien AD.** 1998. Structure, biology, and relative toxicity of Shiga toxin family members for cells and animals, p 121–128. *In* Kaper JB, O'Brien AD (ed), *Escherichia coli* O157:H7 and other Shiga toxin-producing *E. coli* strains. ASM Press, Washington, DC.
24. **DeGrandis S, Law H, Brunton J, Gyles C, Lingwood CA.** 1989. Globotetraosylceramide is recognized by the pig edema disease toxin. J Biol Chem **264:**12520–12525.
25. **Ling H, Boodhoo A, Hazes B, Cummings MD, Armstrong GD, Brunton JL, Read RJ.** 1998. Structure of the Shiga-like toxin I B-pentamer complexed with an analogue of its receptor Gb3. Biochemistry **37:**1777–1788. http://dx.doi.org/10.1021/bi971806n.
26. **Fraser ME, Fujinaga M, Cherney MM, Melton-Celsa AR, Twiddy EM, O'Brien AD, James MN.** 2004. Structure of Shiga toxin type 2 (Stx2) from *Escherichia coli* O157:H7. J Biol Chem **279:**27511–27517. http://dx.doi.org/10.1074/jbc.M401939200.
27. **Kitov PI, Sadowska JM, Mulvey G, Armstrong GD, Ling H, Pannu NS, Read RJ, Bundle DR.** 2000. Shiga-like toxins are neutralized by tailored multivalent carbohydrate ligands. Nature **403:**669–672. http://dx.doi.org/10.1038/35001095.
28. **Paton AW, Morona R, Paton JC.** 2000. A new biological agent for treatment of Shiga toxigenic *Escherichia coli* infections and dysentery in humans. Nat Med **6:**265–270. http://dx.doi.org/10.1038/73111.
29. **Nishikawa K, Matsuoka K, Kita E, Okabe N, Mizuguchi M, Hino K, Miyazawa S, Yamasaki C, Aoki J, Takashima S, Yamakawa Y, Nishijima M, Terunuma D, Kuzuhara H, Natori Y.** 2002. A therapeutic agent with oriented carbohydrates for treatment of infections by Shiga toxin-producing *Escherichia coli* O157:H7. Proc Natl Acad Sci U S A **99:**7669–7674. http://dx.doi.org/10.1073/pnas.112058999.
30. **Mulvey GL, Marcato P, Kitov PI, Sadowska J, Bundle DR, Armstrong GD.** 2003. Assessment in mice of the therapeutic potential of tailored, multivalent Shiga toxin carbohydrate ligands. J Infect Dis **187:**640–649. http://dx.doi.org/10.1086/373996.
31. **Watanabe M, Matsuoka K, Kita E, Igai K, Higashi N, Miyagawa A, Watanabe T, Yanoshita R, Samejima Y, Terunuma D, Natori Y, Nishikawa K.** 2004. Oral therapeutic agents with highly clustered globotriose for treatment of Shiga toxigenic *Escherichia coli* infections. J Infect Dis **189:**360–368. http://dx.doi.org/10.1086/381124.
32. **Nishikawa K, Matsuoka K, Watanabe M, Igai K, Hino K, Terunuma D, Kuzuhara H, Natori Y.** 2005. Identification of the optimal structure for a Shiga toxin neutralizer with oriented carbohydrates to function in the circulation. J Infect Dis **191:**2097–2105. http://dx.doi.org/10.1086/430388.
33. **Nishikawa K.** 2011. Recent progress of Shiga toxin neutralizer for treatment of infections by Shiga toxin-producing Escherichia coli. Arch Immunol Ther Exp (Warsz) **59:**239–247. http://dx.doi.org/10.1007/s00005-011-0130-5.
34. **Nishikawa K, Watanabe M, Kita E, Igai K, Omata K, Yaffe MB, Natori Y.** 2006. A multivalent peptide-library approach identifies a novel Shiga toxin-inhibitor that induces aberrant cellular transport of the toxin. FASEB J **20:**2597–2599. http://dx.doi.org/10.1096/fj.06-6572fje.
35. **Watanabe-Takahashi M, Sato T, Dohi T, Noguchi N, Kano F, Murata M, Hamabata T, Natori Y, Nishikawa K.** 2010. An orally applicable Shiga toxin neutralizer functions in the intestine to inhibit the intracellular transport of the toxin. Infect Immun **78:**177–183. http://dx.doi.org/10.1128/IAI.01022-09.
36. **Tsutsuki K, Watanabe-Takahashi M, Takenaka Y, Kita E, Nishikawa K.** 2013. Identification of a peptide-based neutralizer that potently inhibits both Shiga toxins 1 and 2 by targeting specific receptor-binding regions. Infect Immun **81:**2133–2138. http://dx.doi.org/10.1128/IAI.01256-12.
37. **Kato M, Watanabe-Takahashi M, Shimizu E, Nishikawa K.** 2015. Identification of a wide range of motifs inhibitory to Shiga toxin by affinity-driven screening of customized divalent peptides synthesized on a membrane. Appl Environ Microbiol **81:**1092–1100. http://dx.doi.org/10.1128/AEM.03517-14.
38. **Ito H, Terai A, Kurazono H, Takeda Y, Nishibuchi M.** 1990. Cloning and nucleotide sequencing of Vero toxin 2 variant genes from Escherichia coli O91:H21 isolated from a patient with the hemolytic uremic syndrome. Microb Pathog **8:**47–60. http://dx.doi.org/10.1016/0882-4010(90)90007-D.
39. **Watanabe M, Igai K, Matsuoka K, Miyagawa A, Watanabe T, Yanoshita R, Samejima Y, Terunuma D, Natori Y, Nishikawa K.** 2006. Structural analysis of the interaction between Shiga toxin B-subunits and linear polymers bearing clustered globotriose residues. Infect Immun **74:**1984–1988. http://dx.doi.org/10.1128/IAI.74.3.1984-1988.2006.
40. **Lindgren SW, Samuel JE, Schmitt CK, O'Brien AD.** 1994. The specific activities of Shiga-like toxin type II (SLT-II) and SLT-II-related toxins of enterohemorrhagic *Escherichia coli* differ when measured by Vero cell cytotoxicity but not by mouse lethality. Infect Immun **62:**623–631.
41. **Oku Y, Yutsudo T, Hirayama T, O'Brien AD, Takeda Y.** 1989. Purification and some properties of a Vero toxin from a human strain of Escherichia coli that is immunologically related to Shiga-like toxin II (VT2). Microb Pathog **6:**113–122. http://dx.doi.org/10.1016/0882-4010(89)90014-4.
42. **Karve SS, Weiss AA.** 2014. Glycolipid binding preferences of Shiga toxin variants. PLoS One **9:**e101173. http://dx.doi.org/10.1371/journal.pone.0101173.

43. **O'Brien AD, Tesh VL, Donohue-Rolfe A, Jackson MP, Olsnes S, Sandvig K, Lindberg AA, Keusch GT.** 1992. Shiga toxin: biochemistry, genetics, mode of action, and role in pathogenesis. Curr Top Microbiol Immunol **180:**65–94.
44. **Persson S, Olsen KE, Ethelberg S, Scheutz F.** 2007. Subtyping method for *Escherichia coli* Shiga toxin (verocytotoxin) 2 variants and correlations to clinical manifestations. J Clin Microbiol **45:**2020–2024. http://dx.doi.org/10.1128/JCM.02591-06.
45. **Bunger JC, Melton-Celsa AR, Maynard EL, O'Brien AD.** 2015. Reduced toxicity of Shiga toxin (Stx) type 2c in mice compared to Stx2d is associated with instability of Stx2c holotoxin. Toxins (Basel) **7:**2306–2320. http://dx.doi.org/10.3390/toxins7062306.

神経細胞のタンパク質恒常性維持に関わる
プロテアソームの発現機構と神経変性疾患治療戦略

同志社大学大学院生命医科学研究科　　小林　聡
同志社大学生命医科学部　　和久　剛

１．はじめに

アルツハイマー病やパーキンソン病をはじめとする高次神経機能障害の発症要因のひとつは、神経細胞のタンパク質恒常性（Proteostasis）の破綻と捉えることができる（図１）。通常、細胞内ではタンパク質の品質管理がされており、変性タンパク質が生じた場合はユビキチン-プロテアソーム系とオートファジー系という２つのタンパク質分解システムにより積極的に分解除去されている。これらのタンパク質恒常性の維持システムは加齢に応じて機能低下することから、神経細胞内での変性タンパク質の蓄積が亢進する。本研究では、近年プロテアソームの誘導的発現を制御することが明らかにされた転写因子 Nrf1 に着目し、Nrf1 による遺伝子発現制御機構を解明することを目的とする。これら知見を、Nrf1 をターゲットにしたプロテアソーム誘導による神経変性疾患の新規治療法につなげることが本研究の最終目標である。

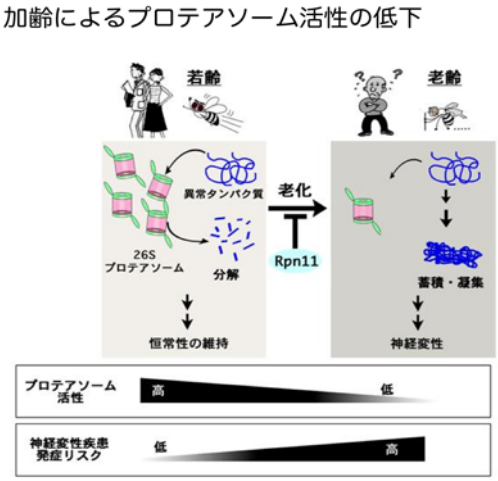

図１　プロテアソーム誘導は神経変性疾患の治療法につながるか？
(殿城亜矢子 東京大学ＨＰより)

２．研究の背景

ストレス応答型転写因子群　CNC ファミリー

Nrf1 は、bZip 型転写因子から構成される CNC ファミリーに属している。同ファミリーは、p45/NF-E2、Nrf1、Nrf2、Nrf3 と Bach1、Bach2 の 6 つの転写因子から構成

されている（図１）。前者は転写活性化因子であり、一方後者は転写抑制因子として機能する。これらファミリー因子は、やはり bZip 型転写因子である小 Maf 因子群とヘテロ二量体を形成し、抗酸化剤応答配列（ARE: antioxidant response element）あるいは MARE 配列（Maf recognition element）を介して、遺伝子発現を正ないし負に制御する。すなわち１つの調節配列に対して、複数の転写因子が関与する複雑な遺伝子発現制御システムが存在することになる。

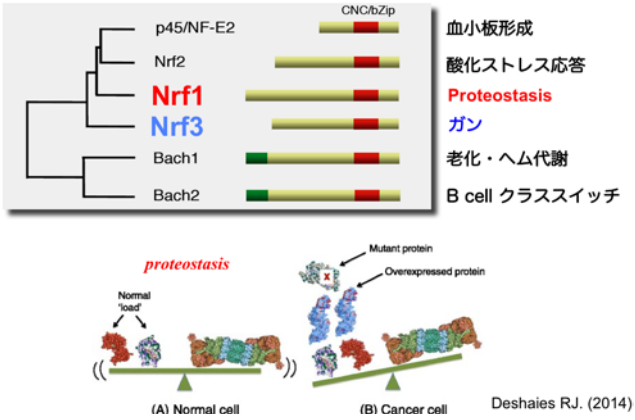

図２　CNC ファミリー転写因子の構造と生理機能

３．研究成果

（１）Nrf1 によるプロテアソーム遺伝子発現を介したタンパク質恒常性維持作用

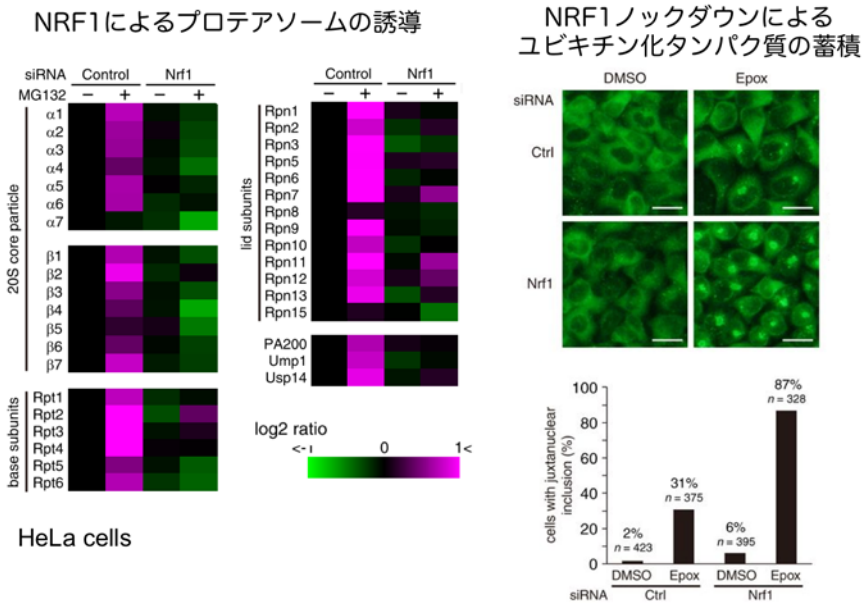

図３　Nrf1 によるプロテアソームリカバリー制御

これまで機能未知であった Nrf1 に関して、近年プロテアソームリカバリーとよばれるタンパク質恒常性維持機構の１つを Nrf1 が制御することが報告された（Steffen J. (2010) Mol Cell, Radhakrishnan S. (2010) Mol Cell）。プロテアソームリカバリーとはプロテアソーム活性が加齢や薬剤などで低下した場合に、同遺伝子を発現誘導することでそれを相補する生体応答機構である。実際、我々も HeLa 細胞においてプロテアソーム阻害剤 MG132 処理に対するプロテソームリカバリーは Nrf1 が中心的に制御していること、さらには Nrf1 ノックダウンにより細胞内へのユビキチン陽性タンパク質の蓄積が亢進することを見出した（図３、Tsuchiya Y. (2013) Mol Cell Biol）。

（２）Nrf1 欠失により発症する神経変性疾患はプロテアソームの低下が原因ではない

ユビキチン鎖の着脱によるタンパク質恒常性の維持機構

上述したようなタンパク質品質管理に関わる Nrf1 であるが、その生理機能解明のためにこれまで様々な組織での条件付きノックアウトマウスの報告がなされている（Bugno M. (2015) Biochem Biophys Acta 1849, 1260-1276）。その中で、申請者らは神

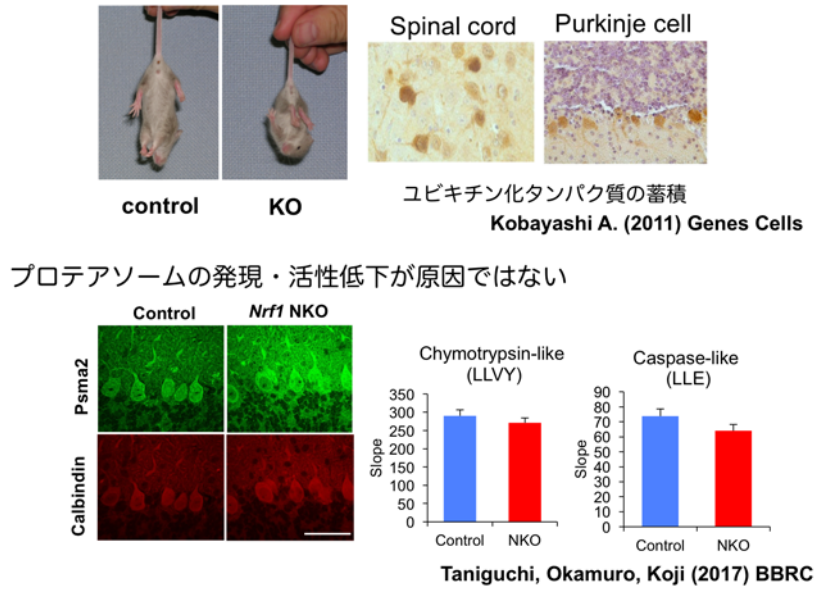

図４　神経特異的 Nrf1KO マウスは早期の神経変性疾患を発症する

経幹細胞・前駆細胞特異的な Nrf1 ノックアウトマウス（Nrf1NKO マウス）の作製に成功している（Kobayashi A. (2011) Genes Cells）。興味深いことに、同マウスは生後まもなく進行性の運動失調をともなう神経変性疾患を呈する。さらに、小脳プルキンエ細胞や海馬・脊髄のニューロンにおいてユビキチン陽性タンパク質の蓄積を伴う神経変性を起こすことを見出した。一方、米国 Chan 博士らは、成熟した神経で Nrf1 をノック

アウトさせたマウスを構築し、同様に神経変性疾患を後期に発症すること、これらはプロテアソーム遺伝子の発現低下が原因である可能性が高いことを報告している（Lee CS. (2010) Proc Natl Acad Sci USA）。したがって Nrf1NKO マウスの神経変性もまたプロテアソームの発現低下が原因であることが強く予想された。しかしながら予想外にプロテアソームの発現ならびに活性は不変であることがわかった（図４, Taniguchi H. (2016) Biochem Biophys Res Commun）。

そこで神経変性疾患を引き起こす Nrf1 標的遺伝子をマイクロアレイ解析で探索した結果、多くの脱ユビキチン化酵素群が発現低下していることを見出した。そのいくつかの遺伝子の制御領域には、Nrf1 結合配列である ARE 配列（antioxidant response element）が存在することをゲノムデータ解析で確認した。次に、脱ユビキチン化酵素群の中で神経変性疾患に関わる *Usp9x* 遺伝子に着目し、実際 Nrf1 が直接的に発現制御していることを siRNA ノックダウン実験ならびにルシフェラーゼ解析で示した。以上の結果から、*Nrf1* NKO マウスが示す神経変性疾患は、神経細胞内のユビキチン鎖の着脱機構の破綻によるタンパク質恒常性の低下である可能性を示した。

（３）Nrf1 によるプロテアソーム遺伝子発現機構の解明

Nrf1 が発現制御する２６Ｓプロテアソームは、３３サブユニットから構成される巨大タンパク質複合体であり、これらは３３遺伝子座からそれぞれ転写・翻訳されるというきわめて特徴的な性状をもつ（図５）。これだけの多数の遺伝子群を同時に過不足なく発現するためには、一般的な転写制御機構とは異なるメカニズムの存在が想起される。

そのような観点からも、Nrf1 によるプロテアソーム発現機構を解明するために、Nrf1 の転写共役因子を同定行った。具体的には、Nrf1 結合因子を網羅的に同定するプロテオーム解析を行い、エピジェネティック制御因子 HCF1 を同定した。さらに HCF1 が Nrf1 によるプロテアソームの発現に関わることを、RNA 干渉法のノックダウン実験で確認した（図６）。今後さらに詳細に Nrf1 と HCF-1 の機能連関を解析する必要性がある。

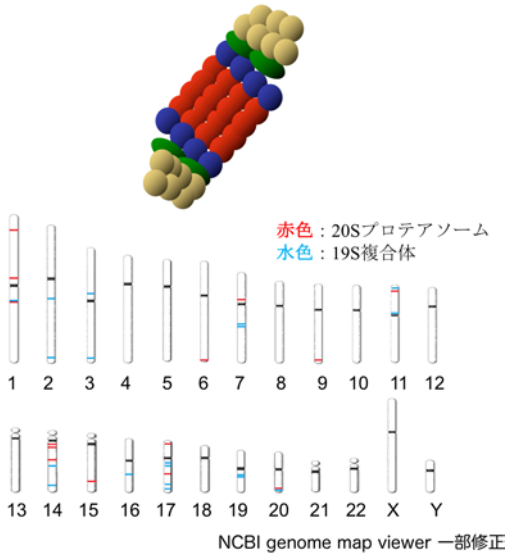

図５　プロテアソーム遺伝子座

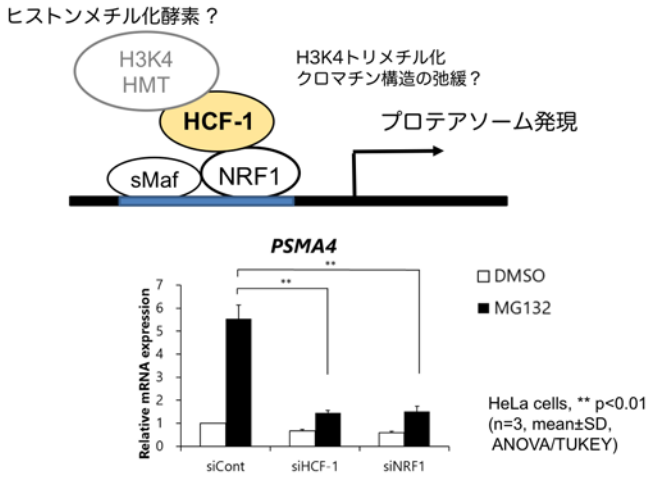

図６　Nrf1 のプロテアソーム誘導にエピジェネティック制御因子 HCF-1 が関与する

（４）Nrf1 活性制御機構の解明

１）脱ユビキチン化による NRF1 の活性化機構

NRF1 は通常、N 末端の NHB1 ドメインを介して小胞体にアンカーされ、さらには ERAD ユビキチン結合酵素 HRD1 によるユビキチン依存的なタンパク質分解を受けて、機能抑制されていることを我々は明らかにしてきた（Tsuchiya Y. (2011) Mol Cell Biol）。しかし、これら抑制機構からの NRF1 活性化メカニズムについては不明なままであった。我々は NRF1 活性化メカニズムを解明する目的で、NRF1 結合因子を網羅的に単離同定するプロテオーム解析を行い、脱ユビキチン化酵素 USP15 を同定に成功した(Fukagai K. (2016) Biochem Biophys Res Commun)。USP15 は、核において NRF1 を脱ユビキチン化し安定化させることを見出した。したがって NRF1 タンパク質の安定性は、USP15 による脱ユビキチン化機構と、すでに我々が解明した β-TRCP によるユビキチン化機構の拮抗作用により制御されていることになる。一方、残

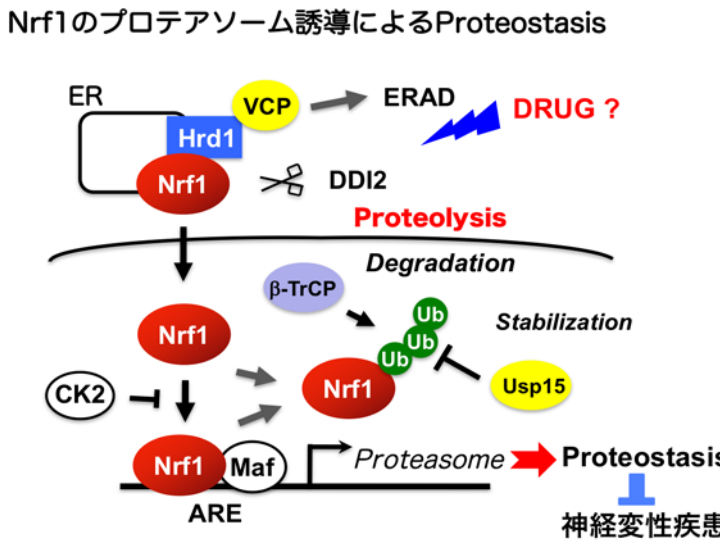

図７　Nrf1 活性制御によるタンパク質品質管理機構

念ながら、NRF1 によるプロテアソーム遺伝子の発現機構に USP15 が関わることを証明することはできなかった、なぜなら *USP15* ノックダウンにより NRF1 遺伝子自体が強く誘導されるためである。しかし、この結果はむしろ *USP15* ノックダウンに対するネガティブフィードバックループ機構の存在を意味するため、USP15 は NRF1 の活性制御していることを強く支持する。さらに、このように様々な活性制御機構が存在する NRF1 はプロテアソーム遺伝子群の発現を微細に制御する重要な転写因子であることを示唆しているものと考える。

今後の展望

本研究において、Nrf1 の活性化はプロテアソームを誘導することでタンパク質品質管理機構を亢進させ、ひいては神経変性疾患の治療につながる可能性を示した。したがって本研究で解明した Nrf1 活性制御機構をターゲットとした Nrf1 活性化剤の創薬研究を行える状況になった。その観点から、近年 Nrf1 の小胞体からの解離に関わるタンパク質切断酵素 DDI2 の発見は、Nrf1 研究においてきわめて重要な報告となった（図８，Lehrbach N. (2016) eLife, Koizumi S. (2016) eLife）。今後は DDI2 による Nrf1 切断機構の解明を通じて、Nrf1 活性化剤のスクリーニングを行うことは大変魅力的な研究課題となる。

さらには本研究を展開する中で、Nrf1 関連遺伝子である Nrf3 がプロテアソームの発現を介してガン発生に重要な機能をもっていることを発見した（和久ら、特許出願中）。今後は、神経変性疾患だけではなく、ガンにおけるプロテアソームの生理機能についても研究を進める予定である。

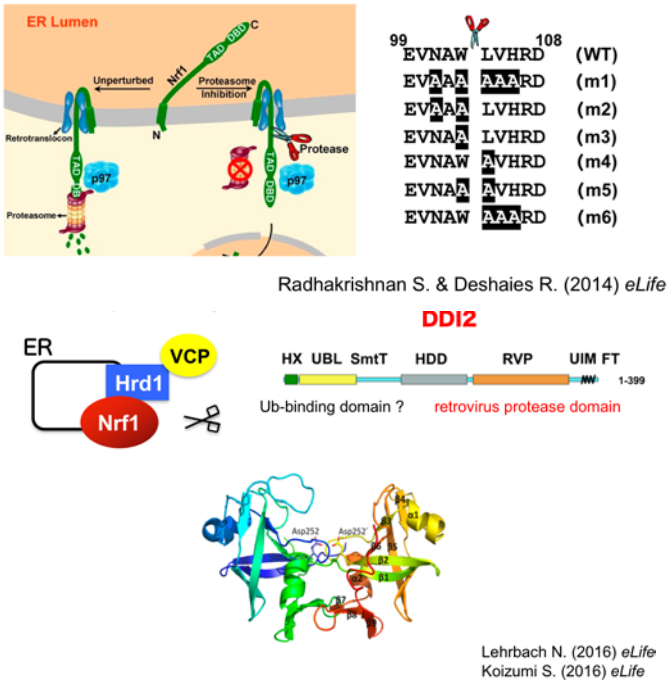

図８ Nrf1 切断酵素 DDI2 の発見

５．論文・実績リスト

原著論文

１）Yamagata K, and Kobayashi A. (2017) The cysteine-rich domain of TET2 binds preferentially to mono- and dimethylated histone H3K36. ***J Biochem***. pii: mvx004

２）Taniguchi, H., Okamuro, S., Kohji, M., Waku, T., Kubo, K., Hatanaka, A., Sun, Y., A M Chowdhury, AM A., Fukamizu, A., Kobayashi, A. (2017) Possible roles of the transcription factor Nrf1 (NFE2L1) in neural homeostasis by regulating the gene expression of deubiquitinating enzymes. ***Biochem Biophys Res Commun.*** 484, 176-183.

３）Fukagai, K., Waku, T., Chowdhury, AM., Kubo, K., Matsumoto, M., Kato, H., Natsume, T., Tsuruta, F., Chiba, T., Taniguchi, H., Kobayashi, A. (2016) USP15 stabilizes the transcription factor Nrf1 in the nucleus, promoting the proteasome gene expression. ***Biochem Biophys Res Commun.*** 2016 478, 363-370.

４）Waku, T., Nakajima, Y., Yokoyama, W., Nomura, N., Kako, K., Kobayashi, A., Shimizu, T., Fukamizu, A. (2016) NML-mediated rRNA base methylation links ribosomal subunit formation to cell proliferation in a p53-dependent manner. ***J Cell Sci.*** 129, 2382-2893.

５）Karim, MR., Taniguchi, H., Kobayashi, A. (2015) Constitutive activation of Drosophila CncC transcription factor reduces lipid formation in the fat body. ***Biochem. Biophys. Res. Com.*** 463, 693-698.

６）Ito, T., Taniguchi, H., Fukagai, K., Okamuro, S. and Kobayashi, A. (2015) Inhibitory mechanism of FAT4 gene expression in response to actin dynamics during Src-induced carcinogenesis. ***PLOS ONE***, 10, e0118336.

７）Tsuchiya, Y., Taniguchi, H., Ito, Y., Morita, T., Karim, MR., Ohtake, N., Fukagai, K., Ito, T., Okamuro, S., Iemura, S., Natsume, T., Nishida, E. and Kobayashi, A. (2013) The CK2-Nrf1 axis controls the clearance of ubiquitinated proteins by regulating proteasome gene expression. Mol. Cell. Biol. 33, 3461-3472.

学会発表

招待講演

１）小林　聡「転写因子 Nrf1 による代謝制御」BMB2015，神戸，ワークショップ 2015 年 12 月 3 日

２）小林　聡「ストレス応答における恒常性維持の遺伝子発現機構」平成 26 年度 京都大学大学院生命科学研究科リトリート．同志社大学びわこリトリートセンター，2014 年 10 月 30-31 日

３）Akira Kobayashi "Multiple regulation of the Nrf2-related factor Nrf1 for proteostasis" The Environmental Response IV, Sendai, February 28-March 2, 2014.

国際学会

１） The HRD1-NRF3 axis regulates the proliferation of colon cancer cells by inducing the UHMK1 gene expression. AM Masudul Azad Chowdhury, Hiroki Kato, Tsuyoshi Waku, Akira Kobayashi, Targeting Cancer: 81st Cold Spring Harbor Symposium. Cold Spring harbor, Jun 1-6, 2016.

２） Functional analyses of the transcription factor Nrf1 isoforms by using CRISPR/Cas9 system. Kubo, K., Waku, T., Kobayashi, A. The Conference on Transposition and Genome Engineering 2015, Nara, Japan, Nov. 17-20, 2015.

３） USP15 stabilizes and activates the transcription factor Nrf1 by deubiquitination. Fukagai, K., Taniguchi, H., Natsume, T., Tsuruta, F., Chiba, T., Kobayashi, A. ZOMESVIII, Xiamen, China, Nov.18-21, 2014.

４） Inhibitory mechanism of FAT4 gene expression in response to actin dynamics during Src-induced carcinogenesis. Ito, T., Taniguchi, H., Kobayashi, A. Keystone Symposia, Stem Cells and Cancer, Banff, Alberta Canada, February 2-7, 2014

５）Identification of NRF3 (NFE2L3) as a new colorectal cancer-related transcription factor. Hori, M., Taniguchi, H., Karim, MR. and Kobayashi, A. Gordon conference. Stem cells & Cancer. Les Diablerets, Switzerland, April 21-26, 2013.

６） Dual regulation of the transcription factor Nrf1(Nfe2l1) by β-TrCP- and Hrd1-dependent degradation mechanisms. Tsuchiya, Y., Morita, T., Iemura, S., Natsume, T. and Kobayashi, A. The 35th Naito conference, “The Ubiquitin-Proteasome System: From Basic Mechanisms to Pathophysiological Roles”, Hokkaido, Japan, July 9-12, 2013.

７） The antioxidant response and longevity-promoting transcription factor, nrf/cncc, regulates lipid storage in drosophila fat body cells. Karim MR., Taniguchi, H., Kobayashi, A. The 23rd European Drosophila Research Conference 2013, Barcelona, Spain, Oct. 16-19, 2013.

８） Dual regulation of the transcription factor Nrf1(Nfe2l1) by β-TrCP- and Hrd1-dependent degradation mechanisms. Tsuchiya, Y., Morita, T., Kim, M., Iemura, S., Natsume, T., Yamamoto, M., and Kobayashi, A. The 33rd Naito Conference on “Oxygen Biology: Hypoxia, Oxidative Stress and Diseases”, Hokkaido, Japan, June 26-29, 2012.

国内学会

１）遺伝子発現の変調によるガン進展メカニズム解明．和久　剛．第五回　四私大合同生命科学シンポジウム ”数理・情報による生命科学の新たな潮流”

関西学院　2017 年 3 月 7 日

2）トランスクリプトームデータを用いた相関解析によるガン関連遺伝子群の同定. 孫宣蒙. 第五回　四私大合同生命科学シンポジウム ”数理・情報による生命科学の新たな潮流”　関西学院　2017 年 3 月 7 日

3）転写因子 NRF3 はプロテアソーム発現亢進を介して p53 依存的なガン抑制シグナルを阻害する. 和久　剛、小林　聡. 転写研究会・新学術領域「転写サイクル」共催　冬の若手ワークショップ 2017. 一宮シーサイドオーツカ　2017 年 1 月 30 日-2 月 1 日

4）エピジェネティック制御因子 HCF-1 を介した転写因子 NRF1 のプロテアソーム発現機構の解析. 松本麻莉子、山形一行、北川大祐、谷口浩章、土谷佳樹小林聡. 第 39 回日本分子生物学会年会 横浜 2016 年 11 月 30 日-12 月 2 日 (ポスター)

5）転写因子 NRF3 はガン細胞の 20S プロテアソーム発現を制御する. 鎌田七海、畠中惇至、糀美早紀、和久剛、小林聡. 第 39 回日本分子生物学会年会 横浜 2016 年 11 月 30 日-12 月 2 日 (ポスター)

6）転写因子 NRF3 によるガン細胞におけるプロテアソーム発現機構. 田中裕也、○鎌田七海、和久剛、小林聡. 第 89 回日本生化学会大会　仙台　2016 年 9 月 25–27 日

7）転写因子 NRF1 の活性化メカニズムにおけるシグナルペプチダーゼ SEC11A の機能解析. 畠中惇至、和久剛、谷口浩章、小林聡. 第 89 回日本生化学会大会　仙台　2016 年 9 月 25–27 日

8）転写因子 NRF3 は p53 依存的なガン細胞の増殖抑制を阻害する. 和久剛、加藤裕紀、渡辺秀教、岩成宏子、辰巳千夏、畠中惇至、浜窪隆雄、小林聡. 第 89 回日本生化学会大会　仙台　2016 年 9 月 25–27 日

9）転写因子 NRF1 の OGT-HCF-1 複合体を介した分解制御機構. 関根弘樹, 加藤幸一郎, 福田愛菜, 鈴木教郎, 岡崎慶斗, Md. Morshedul Alam, 辻田忠志, 小林聡, 山本雅之, 本橋ほづみ. 第 89 回日本生化学会大会　仙台　2016 年 9 月 25–27 日

10）Cysteine rich domain of TET2 protein as a reader of histone H3 K36 mono and di methylation. Kazuyuki Yamagata, Hiroshi Kimura, Akira Kobayashi and Yang Shi.　第 89 回日本生化学会大会　仙台　2016 年 9 月 25–27 日

11）白血病で高頻度に変異の起こる TET2 の CR ドメインはヒストン修飾を認識する. 山形一行、木村宏、小林聡、Yang Shi. 第 4 回がんと代謝研究会　2016 年 7 月 7-8 日 鹿児島

12）白血病で高頻度に変異の起こる TET2 の CR ドメインはヒストン修飾を認識する

山形一行、木村宏、小林聡、Yang Shi. 平成 28 年度新学術領域研究「学術研究支援基盤形成 【先端モデル動物支援プラットフォーム】若手支援技術講習会 蓼科 平成 28 年 9 月 14-17 日

13) 転写因子 NRF3 のガン細胞における機能解析. 和久 剛. 冬の若手ワークショップ 2016. 山中湖 2016 年 2 月 4-6 日（口頭発表）

14）転写因子 NRF3 は細胞周期を調節することで大腸ガン細胞の増殖に関与する. 加藤裕紀、和久 剛、辰巳千夏、小林 聡. 新学術領域「転写代謝システム」領域班会議 熊本市 2015 年 6 月 14-16 日（ポスター）

15）CNC ファミリー転写因子による転写代謝システムの解析. 小林 聡、M Rezaul Karim、谷口浩章. 新学術領域「転写代謝システム」領域班会議 熊本市 2015 年 6 月 14-16 日

16）神経特異的 Nrf1KO マウスの神経変性に対する還元型グルタチオン経口投与の効果. 久保 花織、谷口 浩章、森田 匡彦、小林 聡

17) 転写研究会・転写サイクル・転写代謝システム共催「冬の若手ワークショップ 2015 @伊香保」2015 年 2 月 5-7 日（ポスター）

18） Neural stem cell-specific disruption of the transcription factor Nrf1 (NFE2L1) gene leads to aberrant accumulation of phosphorylated α-synuclein in cerebellar Purkinje cells. Taniguchi, H., Okamuro, S., Miyasaka, T., Kanazawa, Y., Matsumoto, M., Kubo, K., Katahira, T., Motoyama, J., Kobayashi, A. 第 37 回 日本分子生物学会年会. 横浜. 2014 年 11 月 25-27 日（ポスター）

19） Homeostatic maintenance of neuronal activity by the transcription factor Nrf1 (NFE2L1). Okamuro, S., Taniguchi, H., Kanazawa, Y., Katahira, T., Motoyama, J., Yamamoto, M., Kobayashi, A. 第 37 回 日本神経科学会. 横浜. 2014 年 9 月 11-13 日 (ポスター)

20） The Antioxidant Response and Longevity-Promoting Transcription Factor, NRF/CNCC, Regulates Lipid Storage in Drosophila Fat Body Cells. M. Rezaul Karim, Hiroaki Taniguchi, Akira Kobayashi. 第 36 回 日本分子生物学会年会. 神戸ポートアイランド. 2013 年 12 月 3-6 日（ポスター）

21) ストレス応答型転写因子 Nrf1 の活性化メカニズムの解析. 深谷 恒介, 谷口 浩章, 夏目 徹, 鶴田 文憲, 千葉 智樹, 小林 聡. 第 36 回 日本分子生物学会年会. 神戸ポートアイランド. 2013 年 12 月 3-6 日（ポスター）

22）中枢神経系における転写因子 Nrf1 欠損による神経変性発症メカニズムの解析. 岡室 翔太, 谷口 浩章, 金澤 唯, 片平 立矢, 元山 純, 山本 雅之, 小林 聡. 第 36 回

日本分子生物学会年会. 神戸ポートアイランド. 2013 年 12 月 3-6 日（ポスター）

23）マクロファージを介した免疫応答における Nrf1 の機能解析. 森田 智子, 谷口 浩章, 三浦 尚, 小林 聡. 第 36 回 日本分子生物学会年会. 神戸ポートアイランド. 2013 年 12 月 3-6 日（ポスター）

24）Actin 細胞骨格ダイナミクスによる膜タンパク FAT4 の発現調節機構. 井藤 喬夫, 谷口 浩章, 小林 聡. 第 36 回 日本分子生物学会年会. 神戸ポートアイランド. 2013 年 12 月 3-6 日（ポスター）

25）転写因子 Nrf1 の免疫細胞における生理機能の解析. 森田智子, 谷口浩章, 小林聡. 第 60 回 日本生化学会 近畿支部例会. 大阪大学. 2013 年 5 月 18 日 (口頭発表・ポスター)

26）ストレス応答型転写因子 Nrf1 の活性化メカニズムの解析. 深谷恒介, 谷口浩章, 夏目 徹, 小林 聡. 第 60 回 日本生化学会 近畿支部 例会. 大阪大学. 2013 年 5 月 18 日(口頭発表・ポスター)

27）転写因子 Nrf1 欠損による神経変性発症メカニズムの解析. 岡室翔太, 谷口浩章, 小林 聡. 第 60 回 日本生化学会 近畿支部例会. 大阪大学. 2013 年 5 月 18 日 (口頭発表・ポスター).

28）Epigenetics と力学的環境因子による EMT 制御機構への影響の解析. 大竹規仁, 谷口浩章, 小林 聡. 第 60 回 日本生化学会 近畿支部 例会. 大阪大学. 2013 年 5 月 18 日 (口頭発表・ポスター)

29) USP15 activates the transcription factor Nrf1 through inhibiting its proteasomal degradation. Kosuke Fukagai, Hiroaki Taniguchi, Natsume Toru, Akira Kobayashi. 第 86 回日本生化学会大会. 横浜. 2013 年 9 月 11-13 日 (ポスター)

30）転写因子 Nrf1 の神経特異的欠損による神経変性発症メカニズムの解析. 岡室 翔太, 谷口 浩章, 片平 立矢, 元山 純, 山本 雅之, 小林 聡第 86 回日本生化学会大会. 横浜. 2013 年 9 月 11-13 日 (ポスター)

31 ） Identification of NRF3 (NFE2L3) as a new colorectal cancer-related transcription factor. Kobayashi, A. 第 72 回日本癌学会学術総会. 横浜. 2013 年 10 月 3-5 日 (ポスター)

32）癌遺伝子 Src による細胞骨格を介した FAT4 の発現抑制機構. 井藤喬夫, 谷口浩章, 小林 聡. 第 1 回 がんと代謝研究会 (鶴岡). 2013 年 10 月 30 日-11 月 1 日（ポスター）

33）新たな大腸がん関連転写因子 NRF3 の同定. 堀 美久, 竹内沙織, 井岡理絵, 谷口浩章, ○小林 聡. 第 1 回 がんと代謝研究会 (鶴岡). 2013 年 10 月 30 日-11 月 1

日（ポスター）

34）ウイルス感染による転写因子 Nrf1 の発現誘導機構の解析．森田智子，土谷佳樹，小林 聡．日本分子生物学会春季シンポジウム．山梨．2012 年 4 月 25-26 日 (ポスター)

著書

小林 聡、土谷佳樹、「プロテアソームリカバリーにおける転写因子 Nrf1 (NFE2L1) 遺伝子発現機構」生化学第 65 巻(2014) 265-268.

特許出願

・国内

「抗がん剤」 和久剛、小林聡、加藤裕紀、渡辺秀教、特願 2016-230449、2016 年 11 月 28 日

・海外

「抗がん剤」 和久剛、小林聡、加藤裕紀、糀美早紀、渡辺秀教、PCT/JP2017/010445 2017 年 3 月 15 日

アウトリーチ活動

1）和久　剛、畠中淳至、小林 聡 「転写因子 NRF3 を標的としたプロテアソーム阻害による抗がん剤創薬」 同志社大学リエゾンフェア　2016 年 12 月 2 日 京都

2）和久　剛「転写因子 NRF3 を標的としたプロテアソーム阻害による抗がん剤創薬」第 3 回 同志社大学「新ビジネス」フォーラム 2016 年 12 月 8 日 東京

MCB
Journals.ASM.org

The Casein Kinase 2-Nrf1 Axis Controls the Clearance of Ubiquitinated Proteins by Regulating Proteasome Gene Expression

Yoshiki Tsuchiya,[a] Hiroaki Taniguchi,[a] Yoshiyuki Ito,[a] Tomoko Morita,[a] M. Rezaul Karim,[a] Norihito Ohtake,[a] Kousuke Fukagai,[a] Takao Ito,[a] Shota Okamuro,[a] Shun-ichiro Iemura,[b] Tohru Natsume,[b] Eisuke Nishida,[c] Akira Kobayashi[a]

Laboratory for Genetic Code, Graduate School of Life and Medical Sciences, Doshisha University, Kyotanabe, Japan[a]; National Institutes of Advanced Industrial Science and Technology, Biological Information Research Center (JBIRC), Kohtoh-ku, Tokyo, Japan[b]; Department of Cell and Developmental Biology, Graduate School of Biostudies, Kyoto University, Kyoto, Japan[c]

Impairment of the ubiquitin-proteasome system (UPS) has been implicated in the pathogenesis of human diseases, including neurodegenerative disorders. Thus, stimulating proteasome activity is a promising strategy to ameliorate these age-related diseases. Here we show that the protein kinase casein kinase 2 (CK2) regulates the transcriptional activity of Nrf1 to control the expression of the proteasome genes and thus the clearance of ubiquitinated proteins. We identify CK2 as an Nrf1-binding protein and find that the knockdown of CK2 enhances the Nrf1-dependent expression of the proteasome subunit genes. Real-time monitoring of proteasome activity reveals that CK2 knockdown alleviates the accumulation of ubiquitinated proteins upon proteasome inhibition. Furthermore, we identify Ser 497 of Nrf1 as the CK2 phosphorylation site and demonstrate that its alanine substitution (S497A) augments the transcriptional activity of Nrf1 and mitigates proteasome dysfunction and the formation of p62-positive juxtanuclear inclusion bodies upon proteasome inhibition. These results indicate that the CK2-mediated phosphorylation of Nrf1 suppresses the proteasome gene expression and activity and thus suggest that the CK2-Nrf1 axis is a potential therapeutic target for diseases associated with UPS impairment.

Accumulation of misfolded and ubiquitinated proteins is a common pathological feature of various human diseases, such as amyotrophic lateral sclerosis (ALS), inclusion body myopathies, alcoholic and nonalcoholic steatohepatitis, and neurodegenerative disorders, including Alzheimer's, Parkinson's, and Huntington's disease (1–3). Multiple lines of evidence suggest that both the ubiquitin-proteasome system (UPS) and autophagy are responsible for the clearance of ubiquitinated proteins that would accumulate in these age-related diseases. It has been demonstrated that the 26S proteasome can degrade soluble ubiquitinated proteins but not the insoluble aggregates, which are targeted by the autophagy-lysosome pathway (4–7). Impairment of proteasome activity is known to cause proteins that are normally turned over by the UPS to aggregate and form inclusion bodies. Thus, it is expected that the upregulation of proteasome activity could prevent inclusion body formation and mitigate the progression of neurodegenerative and related diseases that are caused by the accumulation of abnormal proteins.

Nrf1 (nuclear factor E2-related factor 1 or Nfe2l1) is a member of the Cap'n'Collar (CNC) family of basic leucine zipper (bZip) transcription factors, which also includes p45 NF-E2, Nrf2, and Nrf3 (8, 9). Nrf1 regulates its target gene expression through either the antioxidant response element (ARE) or the Maf recognition element (MARE) by heterodimerizing with small Maf proteins (8, 9). Several gene targeting studies have implicated Nrf1 in the regulation of cellular homeostasis in embryos, hepatocytes, and osteoclasts (10–14). Recent studies have revealed that Nrf1 also plays an essential role in maintaining neuronal cells and that the loss of Nrf1 induces neurodegeneration and abnormal accumulation of ubiquitinated protein aggregates in neurons (15, 16). The impairment of protein homeostasis that is induced by Nrf1 deficiency may be due to the decreased expression of proteasome subunits in these neurons (16). Indeed, Nrf1 controls the expression of proteasome subunit genes in mammalian cells under proteasome dysfunction (17, 18). Therefore, it is critically important to reveal the role of Nrf1 in the regulation of proteasome gene expression and to elucidate the molecular mechanisms underlying the regulation of Nrf1 activity.

In this study, we reveal that the vast majority of proteasome subunit genes and some proteasome-associated genes are under the transcriptional control of Nrf1. We identify the protein kinase casein kinase 2 (CK2) as an Nrf1-interacting protein and demonstrate that CK2 controls proteasome gene expression and activity by suppressing the transcriptional activity of Nrf1. A mutation of the CK2 phosphorylation site of Nrf1 enhances the proteasome activity and reduces the formation of juxtanuclear inclusion bodies. Thus, our work proposes that the CK2-Nrf1 axis could be a new regulatory target for the efficient clearance of ubiquitinated proteins.

MATERIALS AND METHODS

Antibodies. The antibodies utilized in this study were normal rabbit IgG (Santa Cruz), anti-Flag (M2; Sigma), anti-α-tubulin (DM1A; Sigma), antihemagglutinin (anti-HA) (Y-11; Santa Cruz), anti-green fluorescent protein (anti-GFP) (B-2; Santa Cruz), anti-Nrf1 (H-285; Santa Cruz), anti-MafK (C-16; Santa Cruz), anti-CK2α (1AD9; Santa Cruz), anti-CK2α′ (ab10474; Abcam), anti-CK2β (6D5; Santa Cruz), anti-p62/

Received 15 September 2012 Returned for modification 10 October 2012
Accepted 6 June 2013
Published ahead of print 1 July 2013
Address correspondence to Akira Kobayashi, akobayas@mail.doshisha.ac.jp.
M.R.K., N.O., K.F., T.I., and S.O. contributed equally to this work.
Supplemental material for this article may be found at http://dx.doi.org/10.1128/MCB.01271-12.

doi:10.1128/MCB.01271-12

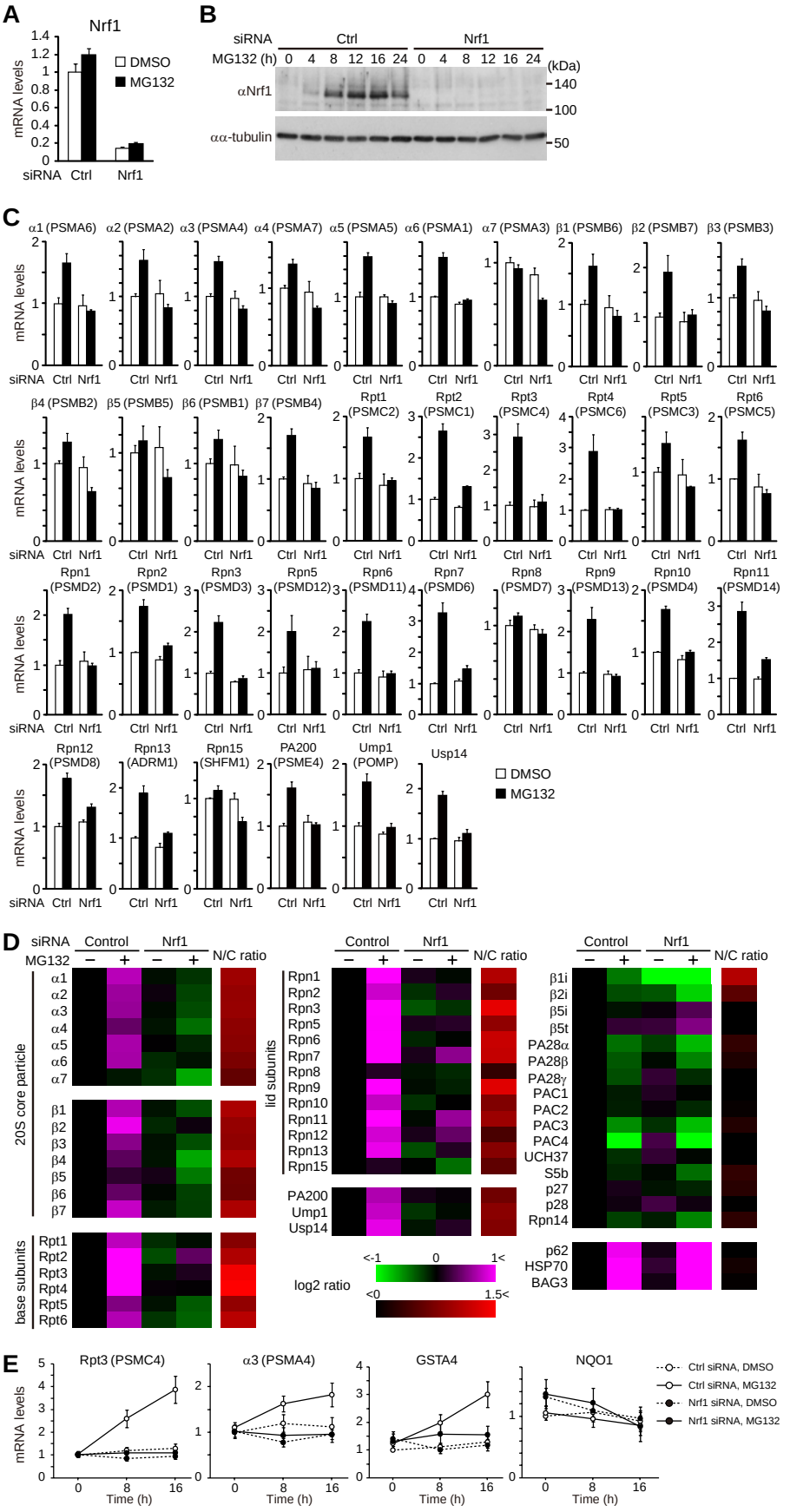

SQSTM1 (PM045; MBL), antiubiquitin (P4D1; Santa Cruz), and anti-LC3 (PD014; MBL). The rabbit polyclonal antibodies directed against mouse Nrf1 that were used in chromatin immunoprecipitation (ChIP) experiments were raised by immunizing rabbits with a purified recombinant six-histidine (6×His)-tagged Nrf1 protein (residues 292 to 741) that was expressed in *Escherichia coli*. The resultant antibodies were subjected to affinity purification.

Plasmids and recombinant proteins. The 3×Flag mouse Nrf1 expression plasmid was described previously (19). Human CK2α (hCK2α) and hCK2β cDNAs were subcloned into pcDNA3 (HA). The ubiquitin-fused luciferase reporter (Ub-FL) reporter plasmid was kindly provided by David Piwnica-Worms (20). The 3xPSMA4-ARE-Luc (Luc stands for luciferase) plasmid was kindly provided by Raymond J. Deshaies (17). The pRBGP2-Luciferase plasmid was described previously (21). The MafK expression plasmid was described previously (22). PCR-amplified Nrf1 fragments were subcloned into pET-15b. Recombinant 6× histidine-tagged Nrf1 fragments were expressed in *E. coli* and purified with nickel-nitrilotriacetic acid (Ni-NTA)−agarose (Qiagen). Recombinant CK2α was described previously (23).

Cell culture and transfection. HeLa cells, COS7 cells, and MCF10A cells were cultured in Dulbecco's modified Eagle's medium (DMEM) (Wako) that was supplemented with 10% fetal calf serum (FCS) (Invitrogen), 4,500 mg/liter glucose, 40 μg/ml streptomycin, and 40 units/ml penicillin. Mouse embryonic fibroblasts (MEFs) were cultured in Iscove's modified Dulbecco's medium (IMDM) (Wako) that was supplemented with 10% FCS, 2 mM glutamine (Invitrogen), 40 μg/ml streptomycin, and 40 units/ml penicillin. The transfection of plasmid DNA and small interfering RNA (siRNA) was achieved using Lipofectamine Plus and Lipofectamine 2000 (Invitrogen), respectively.

siRNA knockdown experiment. The cells were cultured for 24 h in medium without antibiotics. The cells were transfected twice with 40 nM siRNA (at 24 and 48 h after plating) using Lipofectamine 2000. The sequences of the siRNAs employed in the present study are listed in Table S3 in the supplemental material. Twenty-four hours after the last transfection, the cells were utilized for each experiment. For immunoblot analysis, the cells were lysed with an SDS sample buffer (50 mM Tris-HCl [pH 6.8], 10% glycerol, and 1% SDS), and the resultant whole-cell extracts were subjected to immunoblotting with the antibodies indicated in Fig. 1B, 2A and C, 5C, and 6C.

RNA extraction and real-time quantitative PCR. Total RNA was extracted from cells with the RNeasy minikit (Qiagen) and subjected to cDNA synthesis with random hexamer primers and Moloney murine leukemia virus (M-MLV) reverse transcriptase (Invitrogen) according to the manufacturer's instructions. Real-time quantitative PCR was performed with FastStart Universal SYBR (Roche) and ABI Prism 7900 (Life Technologies). The PCR primers employed in the present study are listed in Table S4 in the supplemental material.

Immunoprecipitation and immunoblot analysis. COS7 cells were treated with the proteasome inhibitor MG132 (Peptide Institute) at a concentration of 10 μM for 4 h and subjected to preparation as whole-cell extracts with lysis buffer (50 mM Tris-HCl [pH 8.0], 10% glycerol, 100 mM NaF, 50 mM NaCl, 2 mM EDTA, 2 mM sodium orthovanadate, 10 mM sodium pyrophosphate, 10 mM β-glycerophosphate, 0.1% NP-40, 1 mM phenylmethylsulfonyl fluoride (PMSF), and 1× protease inhibitor cocktail [Roche]). The whole-cell extracts were subjected to immunoprecipitation with anti-Flag M2 affinity gels (Sigma) at 4°C for 2 h. After the anti-Flag M2 affinity gels were washed with wash buffer (50 mM Tris-HCl [pH 7.4], 150 mM NaCl, and 0.1% NP-40) three times, the immunocomplexes were eluted by boiling in SDS sample buffer and subjected to immunoblot analysis using the antibodies indicated in the figures. The blots were treated with a horseradish peroxidase-conjugated secondary antibody (Invitrogen) and were developed with an enhanced chemiluminescence (ECL) kit (GE Healthcare).

Chromatin immunoprecipitation. HeLa cells grown in a 100-mm dish were cross-linked in 1% formaldehyde for 10 min, followed by quenching with 1/10 volume of 1.25 M glycine solution and two washes with phosphate-buffered saline (PBS). The cells were lysed in cell lysis buffer (5 mM Tris-HCl [pH 8.0], 85 mM KCl, 0.5% NP-40, 1 mM PMSF, and 1× protease inhibitor cocktail). Nuclear extracts were prepared by treating the nuclear pellets with ChIP SDS lysis buffer (50 mM Tris-HCl [pH 8.0], 10 mM EDTA, 1% SDS, 1 mM PMSF, and 1× protease inhibitor cocktail), followed by sonication using a Bioruptor (Tosho Electric Co., Ltd.). Proteins were immunoprecipitated in ChIP dilution buffer (16.7 mM Tris-HCl [pH 8.0], 167 mM NaCl, 1.2 mM EDTA, 0.01% SDS, 1.1% Triton X-100, 1 mM PMSF, and 1× protease inhibitor cocktail) using the antibodies indicated in the figures and Dynabeads protein G (Invitrogen). The beads were washed with low-salt wash buffer (20 mM Tris-HCl [pH 8.0], 150 mM NaCl, 2 mM EDTA, 0.1% SDS, and 1% Triton X-100), high-salt wash buffer (20 mM Tris-HCl [pH 8.0], 500 mM NaCl, 2 mM EDTA, 0.1% SDS, and 1% Triton X-100), lithium wash buffer (10 mM Tris-HCl [pH 8.0], 250 mM LiCl, 1% deoxycholate, 1 mM EDTA, and 1% NP-40), and Tris-EDTA (TE) buffer. Cross-linking was reversed overnight at 65°C in ChIP elution buffer (1% SDS and 50 mM $NaHCO_3$). ChIPed DNA was then treated with RNase A and proteinase K, purified with a QIAquick PCR purification kit (Qiagen), and analyzed by real-time quantitative PCR.

Bioluminescence recordings. HeLa cells were transfected with a Ub-FL reporter in combination with the indicated siRNAs or 3× Flag Nrf1 (wild-type or S497A mutant) vectors using Lipofectamine 2000. Forty-eight hours after transfection, the cells were treated with 0.1 mM D-luciferin (Toyobo), and bioluminescence was measured and integrated for 1 min at 10-min intervals with a luminometer (AB-2550 Kronos Dio; Atto). Epoxomicin was added to the culture medium 1 to 2 h after the start of the measurement.

Luciferase reporter assay. Cells expressing the reporters indicated in the legends for Fig. 3A and B, 5A and D to F, and 6 were lysed, and the luciferase activities were measured with the PicaGene luciferase assay system (Toyo Ink) and a Berthold Lumat LB9507 luminometer.

Measurement of proteasome activity. HeLa cells transfected with the siRNAs indicated in the figures were treated with 10 nM epoxomicin for 24 h. The proteasome activity was determined by measuring chymotrypsin activity with Proteasome-Glo chymotrypsin-like cell-based assay (Promega) according to the manufacturer's instructions.

FIG 1 Nrf1 regulates the expression of proteasome subunit genes that are induced by proteasome inhibition in HeLa cells. (A) siRNA-mediated knockdown of Nrf1. HeLa cells transfected with control (Ctrl) siRNA or Nrf1 siRNA were treated with DMSO or 1 μM MG132 for 16 h. mRNA expression levels of Nrf1 were determined by real-time quantitative PCR analysis. The values were normalized to 18S rRNA values and presented as the means plus standard deviations (SD) (error bars) ($n = 3$). (B) MG132 induces the accumulation of Nrf1 proteins. HeLa cell extracts were prepared at the indicated time points after 1 μM MG132 treatment and subjected to immunoblot analysis with anti-Nrf1 (αNrf1) (H-285) antibody. αα-tubulin, anti-α-tubulin antibody. (C) Nrf1-dependent induction of proteasome genes. The mRNA expression levels of the indicated genes were determined by real-time quantitative PCR. The expression level in the cells transfected with the control siRNA and treated with DMSO was set at 1. The values were normalized to 18S rRNA values and presented as the means plus SD ($n = 3$). (D) The heat map shows the mRNA expression levels of the indicated genes that correspond to the graphs in Fig. 1C and data not shown. The values were normalized to 18S rRNA values and presented as the means of at least three replicates. The N/C ratio is the ratio of the expression level in Nrf1 siRNA-treated cells to the expression level in control siRNA-treated cells with MG132 treatment. The color bar indicates the range of the expression ratios in log space. (E) Time course of expression of PSMC4, PSMA4, GSTA4, and NQO1 upon MG132 treatment. The values were normalized to 18S rRNA values and presented as the means ± SD ($n = 5$).

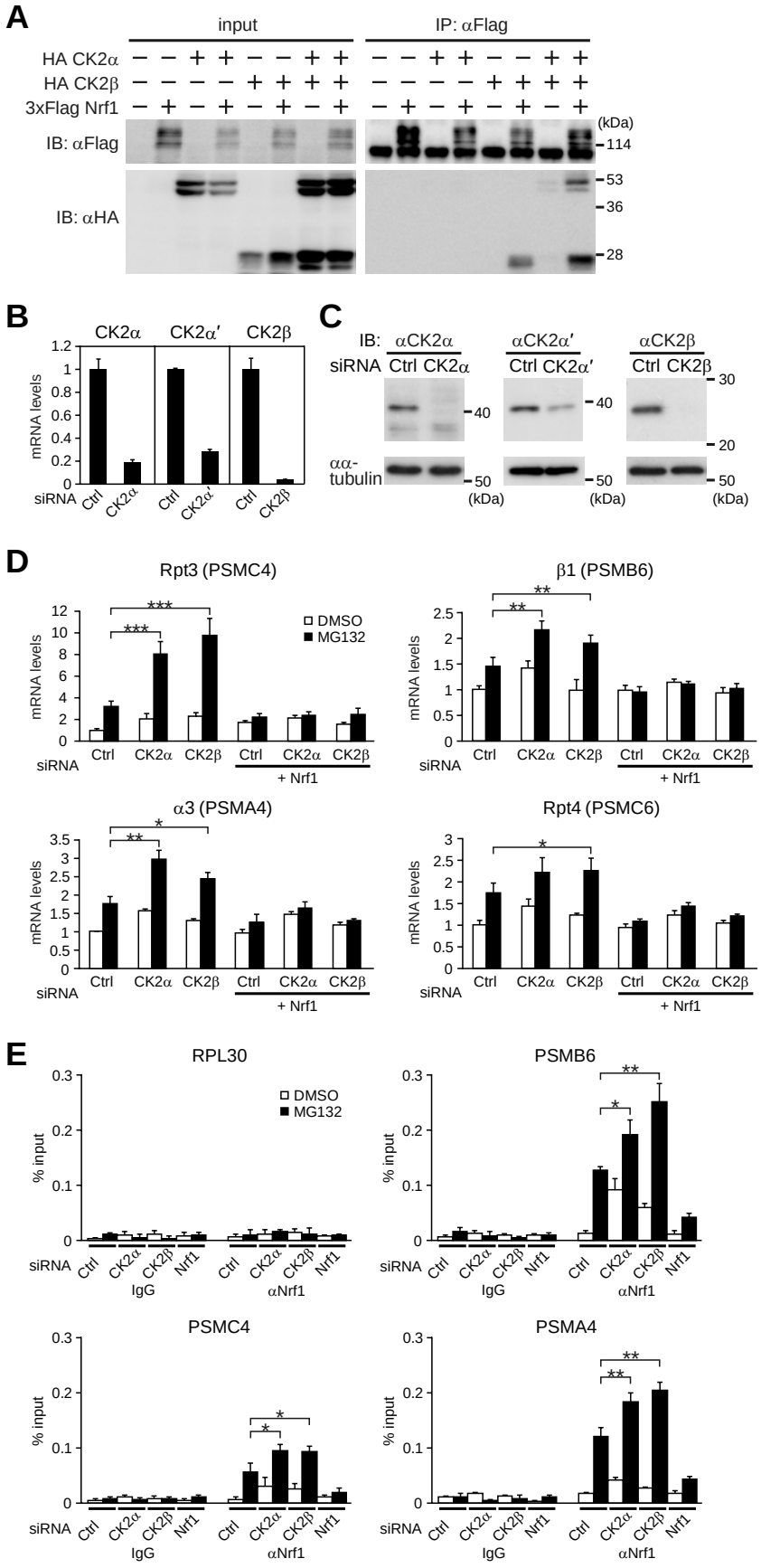

***In vitro* kinase assay.** Purified Nrf1 fragments were incubated with or without 100 ng of recombinant CK2α in kinase reaction buffer (50 mM Tris-HCl [pH 7.5], 200 mM NaCl, 10 mM $MgCl_2$, 15 mM β-glycerophosphate, 2 mM EGTA, 1 mM dithiothreitol [DTT], and 50 μM ATP) supplemented with 0.1 MBq of [γ-^{32}P]ATP for 15 min at 37°C. The reaction was stopped by the addition of SDS sample buffer. After resolution by SDS-PAGE, substrate phosphorylation was detected with a bioimaging analyzer (BAS-2500; Fujifilm).

Cycloheximide chase experiment. COS7 cells that were transfected with the plasmids indicated in the figures were treated with 20 μg/ml of cycloheximide, and the whole-cell extracts were prepared at the time points indicated in the figures and subjected to immunoblot analysis with the antibodies indicated in the figures.

Immunocytochemical staining. The cells were fixed with 4% formaldehyde for 10 min, washed twice with PBS, and permeabilized with 0.5% Triton X-100 in PBS for 5 min. The cells were washed twice with PBS and treated with the antibodies indicated in the figures for 1 h at room temperature. After the cells were washed three times with PBS, they were incubated with Alexa Fluor 488- or Alexa Fluor 546-conjugated secondary antibodies (Invitrogen) for 30 min at room temperature. The nuclei were stained with 4′,6′-diamidino-2-phenylindole (DAPI). After the cells were washed three times with PBS, they were sealed with a drop of fluorescence mounting medium (Dako). Fluorescent images were captured with an Olympus LX71 fluorescence microscope.

RESULTS

Nrf1 regulates the expression of almost all proteasome subunits and several proteasome-related genes. We first evaluated the importance of Nrf1 in the transcriptional induction of proteasome subunits and proteasome-related genes upon inhibition of the proteasome in HeLa cells. To this end, HeLa cells were treated with the proteasome inhibitor MG132 for 16 h in the presence or absence of siRNA that targets Nrf1. The Nrf1 mRNA expression level was significantly repressed by the Nrf1-specific siRNA (Fig. 1A). MG132 stabilized the Nrf1 protein as previously reported (17–19), and the siRNA-mediated knockdown of Nrf1 efficiently suppressed the accumulation of Nrf1 protein (Fig. 1B). Upon inhibition of the proteasome, Nrf1 is reported to stimulate the expression of a large set of proteasome subunit genes and the proteasome maturation factor POMP (18). Thus, we first examined the mRNA expression profiles of all the proteasome subunits and well-characterized proteasome-related genes. We found that most of the proteasome subunit genes were upregulated by MG132 in an Nrf1-dependent manner (Fig. 1C and D) and that the expression of almost all the base and lid subunit genes was significantly induced by proteasome inhibition in HeLa cells. In addition, among the many proteasome-related genes, the proteasome activator PA200, the proteasome-associated deubiquitinating enzyme Usp14, and POMP were markedly upregulated by MG132 in an Nrf1-dependent manner (Fig. 1C and D). These results reemphasize the importance of Nrf1 in the strong coordination of proteasome biogenesis. A time profile of proteasome subunit gene expression was correlated with that of Nrf1 accumulation in cells that were treated with MG132 (Fig. 1B and E).

It has been reported that dysfunction of the proteasome leads to the induction of molecular chaperones and several autophagy-related genes, including Hsp70, p62/SQSTM1, and Bag3 (24–26). These genes contribute to protein quality control and the activation of selective autophagy, another degradation pathway for ubiquitinated proteins (27, 28). We examined whether Nrf1 is involved in the expression of autophagy-related genes that are induced by proteasome inhibition. Treatment of the cells with MG132 significantly induced these genes, and knockdown of Nrf1 had little impact on this induction (Fig. 1D and data not shown). We also examined the expression of other candidate genes for Nrf1 targets, GSTA4 and NQO1, which are well-known ARE-regulated genes. As a result, expression of GSTA4 but not NQO1 was induced by MG132 in an Nrf1-dependent manner (Fig. 1E). These results indicate that, upon proteasome inhibition, Nrf1 specifically upregulates proteasome-related genes along with a subset of antioxidant response genes. As expression of several proteasome genes was also induced in an Nrf1-dependent manner in another human cell line, MCF10A, it is likely that Nrf1-dependent induction of proteasome genes is a general mechanism utilized by various types of cells, although there is some variation among cell lines in response to proteasome inhibition (data not shown).

Identification of CK2 as a suppressor of Nrf1-mediated transcription. It is conceivable that regulating the transcriptional activity of Nrf1 is of critical importance in controlling cellular proteasome activity. To understand regulatory mechanisms of Nrf1 activity, we conducted a mass spectrometric analysis and identified a wide variety of proteins as Nrf1-binding proteins (see Table S1 in the supplemental material) (19). We focused on the protein kinase CK2 because protein kinases are often the critical regulators for diverse transcription factors. CK2 was the only protein kinase identified in our analysis, and both the catalytic α subunit and the regulatory β subunit of CK2 were identified (see Tables S1 and S2 in the supplemental material). CK2 is known to form a heterotetrameric complex composed of two α (and/or α′) subunits and two β subunits (29). To further investigate the interaction of Nrf1 with the CK2 holoenzyme, we performed coimmunoprecipitation assays with COS7 cells. The results clearly demonstrate that CK2β was coimmunoprecipitated with Nrf1

FIG 2 CK2 regulates the Nrf1-dependent expression of proteasome genes. (A) Physical interaction of Nrf1 with CK2. Whole-cell extracts of COS7 cells expressing 3×Flag-tagged Nrf1 (3×Flag Nrf1), HA-tagged CK2α (HA CK2α), and HA CK2β were subjected to immunoprecipitation (IP) with anti-Flag antibody (αFlag), followed by immunoblot (IB) analysis with the indicated antibodies. (B) siRNA-mediated knockdown of CK2 subunits. HeLa cells were transfected with the indicated siRNAs. The mRNA expression levels of the indicated genes were determined by real-time quantitative PCR. The values were normalized to 18S rRNA values and presented as the means plus SD ($n = 3$). (C) The siRNA-mediated knockdown of CK2α, CK2α′, and CK2β was determined by immunoblot analysis. (D) Knockdown of the CK2 subunits enhances the Nrf1-dependent induction of proteasome genes. HeLa cells transfected with control (Ctrl), both CK2α and α′ (CK2α), or CK2β siRNA were treated with Nrf1 siRNA (+ Nrf1) or left untreated and treated with DMSO or 1 μM MG132 for 16 h. The mRNA expression levels were determined by real-time quantitative PCR analysis. The values were normalized to 18S rRNA values and presented as the means plus SD ($n = 3$). Values that are significantly different are indicated by asterisks and bars as follows: *, $P < 0.05$; **, $P < 0.01$; ***, $P < 0.001$. (E) Knockdown of the CK2 subunits enhanced the recruitment of Nrf1 to the AREs of proteasome gene promoters. HeLa cells were transfected with the indicated siRNAs and treated with DMSO or 1 μM MG132 for 16 h. The cells were subjected to chromatin immunoprecipitation (ChIP) analysis using normal rabbit IgG (IgG) or anti-Nrf1 antibody (αNrf1). The recruitment of Nrf1 to the AREs of *PSMB6*, *PSMC4*, and *PSMA4* was determined by real-time quantitative PCR. The promoter region of *RPL30* served as a negative control. The values were presented as the means plus SD ($n = 3$). Values that are significantly different are indicated by asterisks and bars as follows: *, $P < 0.05$; **, $P < 0.01$.

(Fig. 2A). Of note, CK2α was coimmunoprecipitated with Nrf1 only in the presence of CK2β (Fig. 2A). Thus, Nrf1 may bind to the CK2 holoenzyme through its regulatory β subunit. To examine whether CK2 regulates the transcriptional activity of Nrf1, we assessed the effect of an siRNA-mediated knockdown of the CK2 subunits on the Nrf1-dependent expression of the proteasome subunit genes. siRNAs for CK2α, CK2α′, a paralogous isoform of CK2α, and CK2β efficiently downregulated the expression of their target mRNAs (Fig. 2B). Efficient knockdown of CK2α, CK2α′, and CK2β was also confirmed by Western blotting (Fig. 2C). The siRNA-mediated knockdown of both CK2α and CK2α′ enhanced the MG132-induced expression of proteasome subunit genes such as *PSMC4*, *PSMB6*, *PSMA4*, and *PSMC6* (Fig. 2D). Knockdown of CK2β had similar effects on the expression of these genes (Fig. 2D). These enhancements were not observed when Nrf1 was downregulated simultaneously by siRNA (Fig. 2D). These results indicate that CK2 suppresses the Nrf1-dependent expression of proteasome subunit genes that are induced by proteasome inhibition. To further evaluate whether Nrf1 mediates the effect of CK2 knockdown on the transcription of proteasome genes, we performed chromatin immunoprecipitation (ChIP) assays using an anti-Nrf1 antibody. We examined the recruitment of Nrf1 to the AREs, which are located in the proximal promoter of *PSMC4* and *PSMB6* and in the first intron of *PSMA4* (16, 17). siRNA-mediated knockdown of CK2α and CK2β significantly augmented the recruitment of Nrf1 to the AREs, both with and without MG132 treatment (Fig. 2E; see Discussion). The 5′-upstream region of *RPL30* served as a negative control of Nrf1 binding. As siRNA-mediated knockdown of Nrf1 markedly decreased the amount of precipitated ARE regions of the proteasome subunit promoters (Fig. 2E), the observed ChIP signals should reflect Nrf1-ARE binding. These data collectively indicate that CK2 suppresses the transcriptional activity of Nrf1 by regulating the recruitment of Nrf1 to its target AREs.

The Nrf1-mediated transcriptional regulation of the proteasome subunit genes should control the total cellular proteasome activity. To investigate the effect of a CK2 knockdown on the detailed time profile of proteasome activity under conditions of proteasome inhibition, we performed real-time monitoring of proteasome activity in living cells. We utilized a ubiquitin-fused luciferase reporter (Ub-FL) as the indicator of endogenous proteasome activity (20). In this system, high reporter activity corresponds to low proteasome activity. The addition of the proteasome inhibitor epoxomicin resulted in a gradual increase of the reporter activity, which was greatly enhanced by siRNA-mediated knockdown of Nrf1 (Fig. 3A). In contrast, the knockdown of either CK2α or CK2β suppressed the epoxomicin-induced stabilization of the reporter protein (Fig. 3A). Similar results were obtained by measuring the properly normalized reporter activity in cell lysates that were prepared 16 h after the addition of epoxomicin (Fig. 3B). We also measured endogenous proteasome activity by using a luminogenic substrate Suc-LLVY-aminoluciferin for the chymotrypsin-like activity. The result demonstrates that Nrf1 knockdown cells show lower proteasome activity than control cells 24 h after epoxomicin treatment (Fig. 3C). On the other hand, CK2α or CK2β knockdown cells show slightly higher proteasome activity than control cells, although the difference in proteasome activity is moderate compared with the results in Fig. 3A and B. These results suggest that CK2-mediated suppression of

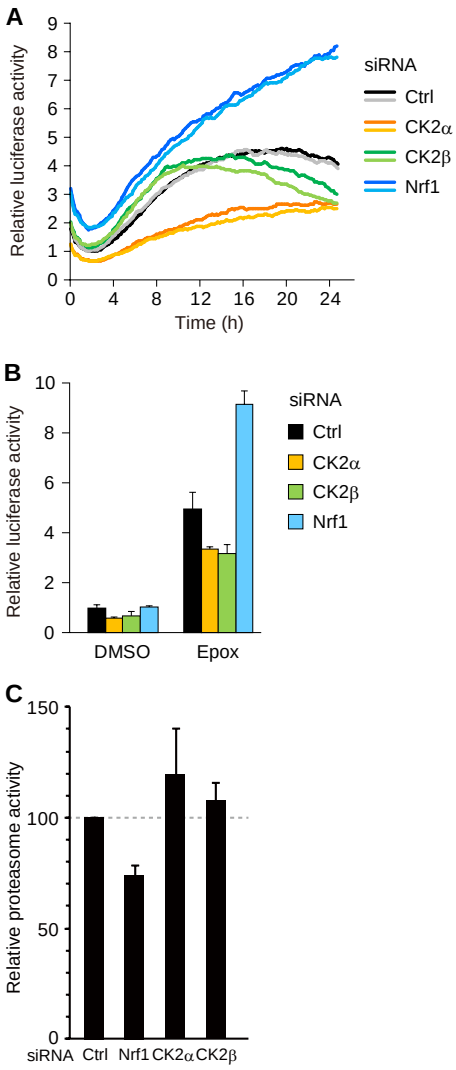

FIG 3 Knockdown of the CK2 subunits or Nrf1 affects degradation of ubiquitinated proteins. (A) HeLa cells transfected with the Ub-FL reporter plasmid and the indicated siRNAs were treated with 0.1 mM D-luciferin. Real-time monitoring of the reporter activity was performed using a photomultiplier. Epoxomicin was added to the culture medium 1 to 2 h after the start of measurement. The darker and lighter lines indicate duplicate traces of two independent samples. Representative data are shown. (B) HeLa cells transfected with the Ub-FL reporter plasmid, the control *Renilla* luciferase reporter, and the indicated siRNAs were treated with DMSO or 10 nM epoxomicin (Epox) with D-luciferin for 16 h. The cells were lysed and subjected to a luciferase assay. The values were normalized to *Renilla* luciferase activity values and presented as the means plus SD ($n = 3$). (C) HeLa cells transfected with control (Ctrl), Nrf1, CK2α, or CK2β siRNA were treated with 10 nM epoxomicin for 24 h. The proteasome activity was determined by using a luminogenic substrate Suc-LLVY-aminoluciferin for the chymotrypsin-like activity. The values were shown as the percent changes of proteasome activity over the control siRNA-treated cells (means plus SD, $n = 9$).

Nrf1 activity leads to the downregulation of proteasome activity in cells.

CK2 phosphorylates Nrf1 at a specific serine residue. Next, we focused on the underlying mechanisms of the CK2 regulation of Nrf1. We assumed that CK2 directly phosphorylates Nrf1 and regulates its transcriptional activity. To test this hypothesis, we performed an *in vitro* kinase assay using recombinant CK2α and a

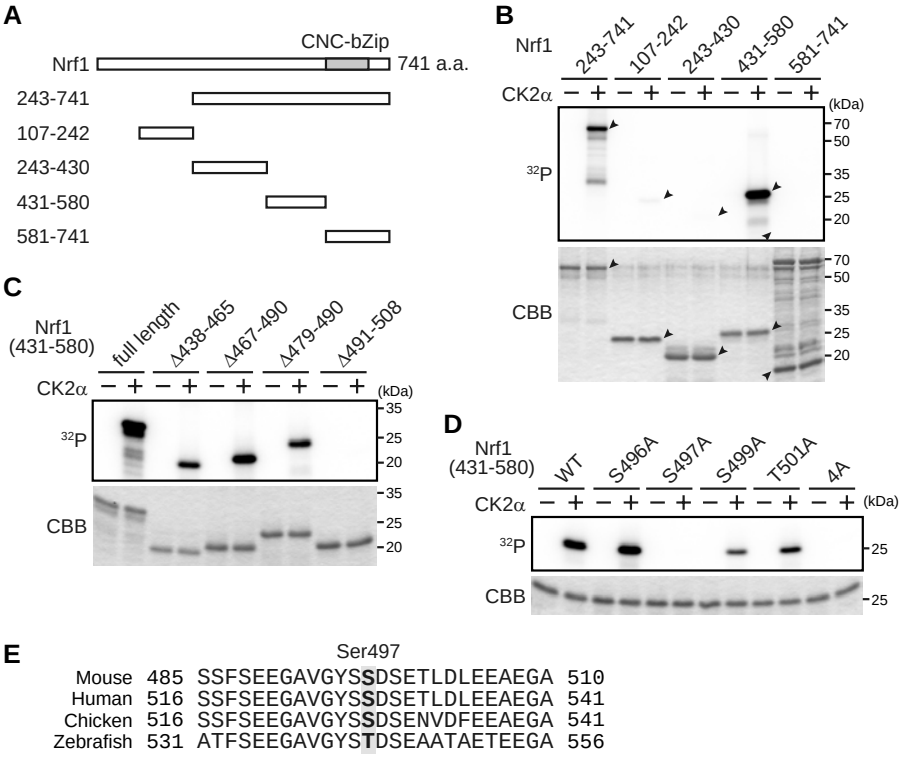

FIG 4 CK2 phosphorylates Nrf1 at Ser 497. (A) Schematic structures of the Nrf1 fragments. a.a., amino acids. (B) CK2 phosphorylates residues 431 to 580 of Nrf1. The purified Nrf1 fragments were incubated in the presence of [γ-^{32}P]ATP with (+) or without (−) recombinant CK2α. The autoradiograph was analyzed with a phosphorimager. The indicated input proteins were analyzed by Coomassie brilliant blue (CBB) staining. The positions of input proteins are indicated by black arrowheads. (C) CK2 phosphorylates residues 491 to 501 of Nrf1. The Nrf1 fragments (residues 431 to 580) with the indicated internal deletions were subjected to an *in vitro* phosphorylation assay. (D) CK2 phosphorylates Ser 497 of Nrf1. The Nrf1 fragments (residues 431 to 580) with the indicated point mutations were subjected to an *in vitro* phosphorylation assay. WT, wild type; 4A, all four of the candidate serine/threonine residues were replaced by alanine. (E) Conservation of Nrf1 sequences among the species around the CK2-mediated phosphorylation site.

series of Nrf1 fragments (Fig. 4A). Among the constructed fragments, Nrf1 (residues 431 to 580) was specifically phosphorylated by CK2α (Fig. 4B). Additional experiments narrowed the phosphorylation site to a small region (residues 491 to 508) of Nrf1 (Fig. 4C). We introduced an alanine substitution at each of the four candidate phosphoacceptor sites (Ser 496, Ser 497, Ser 499, and Thr 501). Of the constructed mutants, only the Ser 497 to Ala (S497A) mutant was not phosphorylated by CK2α *in vitro* (Fig. 4D). Thus, we concluded that Ser 497 of Nrf1 is the primary target for phosphorylation by CK2α *in vitro* (Fig. 4E).

The CK2 phosphorylation site mutant enhances the transcriptional activity of Nrf1. To investigate the effect of the CK2-mediated phosphorylation of Nrf1, we compared the transcriptional activity of the S497A mutant with wild-type Nrf1 (Nrf1-WT). We used a luciferase reporter that was driven by three tandem copies of the ARE from the PSMA4 promoter (17). Forced expression of Nrf1 increased the reporter activity in a dose-dependent manner (Fig. 5A). Notably, the S497A mutant exhibited enhanced transcriptional activity compared to wild-type Nrf1 (Fig. 5A). Similar results were obtained with the reporter assay using pRBGP2 luciferase reporter that was driven by three tandem copies of the MARE (Fig. 5A) (21). Furthermore, forced expression of the Nrf1-S497A mutant increased expression of endogenous proteasome genes such as PSMC4 and PSMA4 much more than Nrf1-WT, although expression of PSMB6 did not increase significantly (Fig. 5B). As the steady-state level and the degradation rates of these proteins were comparable (Fig. 5C), the enhanced activity of the S497A mutant is not merely due to the elevated expression and/or stabilization of the Nrf1 proteins. In addition, there was no difference in the subcellular localization and physical interaction with MafK, a heterodimerization partner of Nrf1, between wild-type Nrf1 and the S497A mutant (data not shown). We next examined whether the enhanced transcriptional activity of the S497A mutant could affect endogenous proteasome activity. The Ub-FL reporter plasmid with either wild-type Nrf1 or the S497A mutant expression plasmid was transfected into HeLa cells, and the reporter activity was monitored in cells treated with epoxomicin. The forced expression of wild-type Nrf1 prevented the increase in reporter activity that was induced by epoxomicin in a dose-dependent manner (Fig. 5D). This result suggests that the upregulation of the proteasome activity by the Nrf1-mediated induction of proteasome expression confers tolerance for proteasome inhibition on cells. Importantly, compared to wild-type Nrf1, the S497A mutant had a greater ability to prevent the increase in reporter activity (Fig. 5D). Similar results were obtained by measuring the properly normalized reporter activity in cell lysates prepared 16 h after the addition of epoxomicin (Fig. 5E). These results clearly demonstrate that the CK2 phosphorylation site mutant of Nrf1 has a greater ability to upregulate proteasome expression and activity than wild-type Nrf1. To evaluate the im-

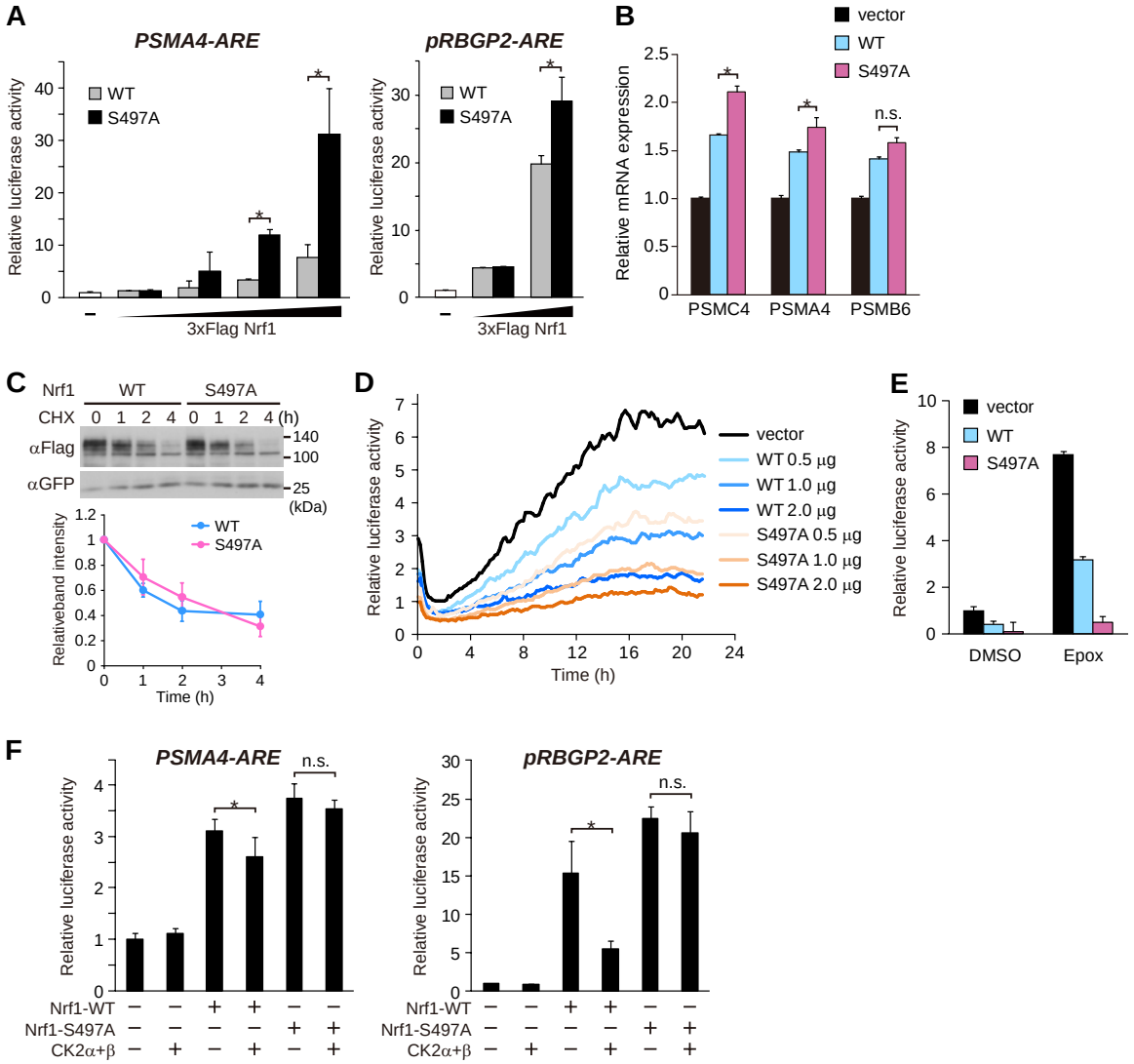

FIG 5 The Nrf1-S497A mutant has enhanced transcriptional activity and prevents the accumulation of ubiquitinated proteins. (A) The S497A mutant has enhanced transcriptional activity. COS7 cells transfected with either wild-type (WT) plasmid or S497A mutant plasmid in combination with a luciferase reporter containing three tandem copies of the AREs of *PSMA4* or a pRBGP2 reporter. The levels of luciferase activity were normalized to the *Renilla* luciferase activity of an internal control pRL-TK and presented as the means plus SD ($n = 3$). Values that are significantly different ($P < 0.05$) are indicated by a bar and asterisk. (B) The S497A mutant upregulates expression of endogenous proteasome genes. HeLa cells were transfected with either wild-type (WT) or S497A mutant plasmid. The mRNA expression levels were determined by real-time quantitative PCR analysis. The values were normalized to 18S rRNA values and presented as the means plus SD ($n = 5$). Values that are significantly different ($P < 0.05$) are indicated by a bar and asterisk. Values that are not significantly different are indicated by a bar labeled n.s. (C) Protein stability is comparable in the wild type and the S497A mutant. COS7 cells transfected with the expression plasmid for the wild-type 3×Flag Nrf1 protein or the S497A mutant of 3×Flag Nrf1 in combination with the GFP expression plasmid were treated with 20 μg/ml cycloheximide (CHX). The cells were lysed at the indicated time points and subjected to immunoblot analysis with anti-Flag or anti-GFP antibodies. The data were normalized to cotransfected GFP values and are presented as the means ± standard errors (SE) ($n = 3$). (D and E) The S497A mutant has a greater ability to repress the accumulation of ubiquitinated proteins than wild-type Nrf1. (D) HeLa cells transfected with the Ub-FL reporter plasmid in combination with the indicated amount of wild-type or S497A mutant Nrf1 plasmid were treated with 10 nM epoxomicin and D-luciferin. Real-time monitoring of the reporter activity was performed using a photomultiplier, and representative data are shown. (E) HeLa cells transfected with the Ub-FL reporter plasmid and the control *Renilla* luciferase reporter in combination with the wild-type or S497A mutant plasmid were treated with DMSO or 10 nM epoxomicin with D-luciferin for 16 h. The cells were lysed and subjected to a luciferase assay. The values were normalized to the values for *Renilla* luciferase activity and presented as the means plus SD ($n = 3$). (F) CK2 suppresses the transcriptional activity of Nrf1-WT but not that of the Nrf1-S497A mutant. COS7 cells were transfected with the indicated plasmids in combination with the *PSMA4*-ARE reporter or a pRBGP2 reporter. The levels of luciferase activity were normalized to the values for *Renilla* luciferase activity of an internal control pRL-TK and presented as the means plus SD ($n = 3$). Statistical significance is indicated as follows: *, $P < 0.05$; n.s., not significant.

portance of phosphorylation at Ser 497 in the regulation by CK2, we examined whether CK2 affects the transcriptional activity of Nrf1-WT and Nrf1-S497A. The results demonstrate that CK2 suppresses the PSMA4 reporter activity induced by Nrf1-WT but not by the Nrf1-S497A mutant (Fig. 5F, left graph). Similar results were obtained using the pRBGP2 reporter (Fig. 5F, right graph). These results collectively suggest that CK2 suppresses the transcriptional activity of Nrf1 via phosphorylation of Nrf1 at Ser 497.

The CK2 phosphorylation site mutant of Nrf1 suppresses the formation of p62-positive inclusion bodies. Proteasome dysfunction is associated with the formation of juxtanuclear inclusion bodies such as aggresomes (1). These inclusion bodies contain p62 and function to sequester unfolded and misfolded proteins that could not be degraded by the proteasome (30). The phosphorylation state of Ser 497 of Nrf1 may affect the efficiency of the formation of such inclusion bodies. To assess this possibility, we examined the effect of forced expression of the S497A mutant of Nrf1 on the formation of p62-positive inclusion bodies. Treatment of cells with epoxomicin led to the formation of p62-positive juxtanuclear inclusion bodies in HeLa cells (Fig. 6A). Similar results were obtained when MG132 was used instead of epoxomicin (data not shown). Strikingly, the siRNA-mediated knockdown of Nrf1 markedly enhanced the inclusion body formation (Fig. 6A). This result indicates that Nrf1 plays an important role in preventing the formation of juxtanuclear inclusion bodies. These p62-positive inclusion bodies were also ubiquitin positive, indicating the accumulation of ubiquitinated proteins (Fig. 6B). Knockdown of Nrf1 did not affect the total amount of p62 but caused an increase in the autophagic marker LC3-II (Fig. 6C). This finding suggests that the downregulation of Nrf1 leads to the accumulation of autophagosomes that are involved in an alternative degradation pathway for misfolded proteins. We tested the effect of Nrf1 overexpression on inclusion body formation. Forced expression of wild-type Nrf1 decreased the efficiency of formation of the p62-positive juxtanuclear inclusion bodies that were induced by epoxomicin (Fig. 6D). Importantly, forced expression of the S497A mutant reduced inclusion body formation more effectively than that of wild-type Nrf1 (Fig. 6D). These results suggest that the phosphorylation state of Ser 497 affects the formation efficiency of the p62-positive juxtanuclear inclusion bodies that are induced by proteasome inhibition.

DISCUSSION

Significance of CK2 as a regulator of Nrf1 transcriptional activity. In this study, we demonstrate that CK2 interacts with and phosphorylates Nrf1 and suppresses its transcriptional activity, thereby regulating the expression of proteasome subunits. Nrf1 is localized to the endoplasmic reticulum (ER) membrane and is constitutively degraded by the proteasome under normal conditions (18, 19). Inhibition or dysfunction of the proteasome may induce the stabilization and nuclear translocation of Nrf1 proteins. Our results have implicated CK2 in the regulatory mechanisms of Nrf1 activity. Given that knockdown of the CK2 subunits facilitates the recruitment of Nrf1 to the AREs of their promoters and increases the expression of Nrf1 target genes even without proteasome inhibition (Fig. 2D and E), CK2 may suppress the transcriptional activity of Nrf1 and thus prevent the unnecessary expression of Nrf1 target genes under physiological conditions. As we have no data indicating that phosphorylation of Ser 497 is altered in response to proteasome inhibition, it remains to be elucidated whether CK2-mediated phosphorylation of Nrf1 is regulated during Nrf1 activation. Our preliminary data demonstrate that the expression of CK2α is reduced upon inhibition of the proteasome (data not shown). Although the mechanism underlying the decrease in CK2α expression is unclear, it is possible that Nrf1 phosphorylation is decreased upon proteasome inhibition, resulting in efficient transcriptional activation of stabilized Nrf1 proteins.

Nrf1 exists as multiple isoforms, including TCF11 (transcription factor 11), a longer isoform found in humans (31). The regulatory mechanism for TCF11 might differ from that of Nrf1, as TCF11 has the nuclear export signal that is not present in Nrf1. In this study, we used the expression plasmid for mouse Nrf1 but not the expression plasmid for TCF11. Thus, it remains to be elucidated in future studies whether human TCF11 can be regulated by CK2 and whether there is any difference in CK2-mediated regulation between mouse Nrf1 and human TCF11. In addition to a known proteasome-mediated regulation of Nrf1 activity, we propose that CK2-mediated phosphorylation of Nrf1 acts as another layer of Nrf1 regulation to fine-tune its transcriptional activity.

Effect of CK2-mediated direct phosphorylation of Nrf1. The phosphorylation of Nrf1 Ser 497 is likely to enhance its transcriptional activity but not affect its stability, subcellular localization, or ability to bind MafK proteins. Our data indicate that Ser 497 has an important role in CK2-dependent suppression of Nrf1 transcriptional activity. Given that CK2 knockdown enhances the recruitment of Nrf1 to its target AREs, it is likely that CK2-mediated phosphorylation of Ser 497 controls the recruitment of Nrf1 to the AREs of the target promoters. However, it remains to be investigated how phosphorylation of Ser 497 suppresses Nrf1 recruitment. As Ser 497 resides in the Neh6-like domain and are located next to the CNC-bZip domain, phosphorylation may induce a conformational change of the Nrf1 protein, compromising its binding to the target DNA.

Ser 497 of mouse Nrf1 is conserved in mouse Nrf2 (Ser 365), but it is not known whether CK2 can phosphorylate Nrf2 at Ser 365. It has been reported that Nrf2 is phosphorylated by CK2 and that this phosphorylation regulates the transcriptional activity of Nrf2 (32, 33). The effect of the CK2-mediated phosphorylation on Nrf2 activity is controversial, but several reports have shown that CK2 inhibition results in Nrf2 inactivation (32, 34, 35). The CK2-mediated phosphorylation of Nrf2 facilitates its nuclear translocation and the upregulation of Nrf2 target gene expression. Thus, it seems likely that the role of CK2-dependent regulation in Nrf2 may be different from that in Nrf1.

The CK2-Nrf1 axis as a new therapeutic target for diseases associated with proteasome dysfunction. The regulation of proteasome activity is an established strategy for cancer treatment, and it is expected to be a promising approach to ameliorate some age-related disorders, such as neurodegenerative diseases. Supporting this notion, a previous study has demonstrated that a small-molecule inhibitor of USP14, a proteasome-associated deubiquitinating enzyme, increases the proteasome activity and enhances the degradation of several neurodegenerative disease-associated proteins such as tau and TDP-43 (36). Thus, the upregulation of proteasome activity should alleviate the accumulation of aggregate-prone proteins. In addition, it has been reported that overexpression of a proteasome subunit gene increases proteasome activity, decreases the accumulation of ubiquitinated proteins, and ameliorates the response to oxidative stress (37–39). Therefore, the fact that Nrf1 regulates the expression of most of the proteasome subunit genes may provide a new approach, transcriptional upregulation of the proteasome, to treat human diseases associated with the accumulation of abnormal proteins. Our findings that Nrf1-S497A exerts a more significant effect on the inhibition of p62-positive inclusion body formation than wild-type Nrf1 does strongly suggest that the CK2-mediated phosphor-

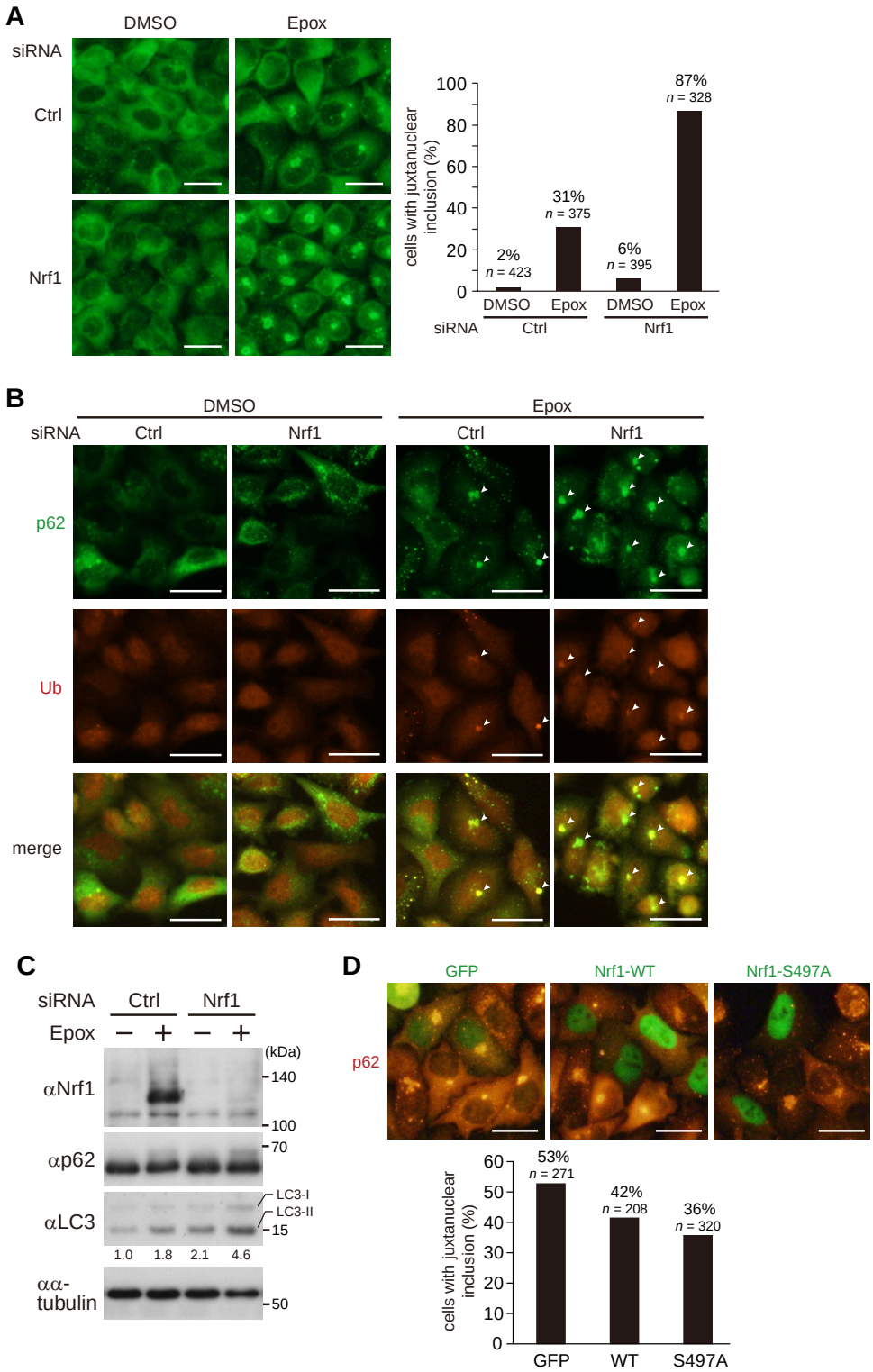

FIG 6 Nrf1 has the ability to ameliorate the formation of p62-positive inclusion bodies in HeLa cells. (A) Knockdown of Nrf1 causes enhanced formation of p62-positive inclusion bodies. HeLa cells transfected with control (Ctrl) or Nrf1 siRNA were treated with DMSO or 10 nM epoxomicin for 24 h. The cells were immunostained with anti-p62 antibody, and the percentage of cells containing juxtanuclear inclusion bodies were calculated. Bars, 50 μm. (B) p62-positive inclusion bodies formed by proteasome inhibition are ubiquitin positive. HeLa cells transfected with control (Ctrl) or Nrf1 siRNA were treated with DMSO or 10 nM epoxomicin for 24 h. The cells were immunostained with anti-p62 (green) and antiubiquitin (red) antibodies. Juxtanuclear inclusion bodies stained with both antibodies are indicated by small white arrowheads. Bars, 50 μm. (C) The cells treated as in panel A were lysed and subjected to immunoblot analysis with the indicated antibodies. The relative band intensities of LC3-II were quantified and normalized to α-tubulin values. (D) The S497A mutant has a greater ability to decrease the formation of p62-positive juxtanuclear inclusion bodies than wild-type Nrf1. HeLa cells transfected with the expression plasmid for GFP or wild-type or the S497A mutant of 3×Flag Nrf1 were treated with DMSO or 10 nM epoxomicin for 24 h. The cells were immunostained with anti-Flag and anti-p62 antibodies, and the percentage of cells containing juxtanuclear inclusion bodies out of total GFP- or 3×Flag Nrf1-expressing cells were calculated. Bars, 50 μm.

ylation of Nrf1 is one of the potential targets for treating proteinopathies such as neurodegenerative diseases.

CK2 has an array of substrate proteins and functions in diverse cellular processes, including cell growth and proliferation (40, 41). Recent studies have also implicated CK2 in neuronal functions and the progression of neurodegenerative diseases (42, 43). It has been reported that CK2 phosphorylates several neurodegenerative disease-related proteins, such as α-synuclein, synphilin-1, and apolipoprotein E, to enhance aggregate formation (44–46). Thus, the regulation of CK2 activity may represent a possible target for therapeutic intervention. Indeed, CK2 inhibition has been shown to exert a protective effect on neurons (44, 47, 48). In contrast, a recent report has shown that CK2 phosphorylates p62 and stimulates the clearance of protein aggregates via the autophagy-lysosome pathway (49). This finding raises the possibility that CK2 inhibition or knockdown results in the impairment of aggregate clearance. Therefore, there seem to be pros and cons to modulating CK2 activity with regard to ameliorating proteinopathies. Nevertheless, our data strongly suggest that the CK2-mediated regulation of Nrf1 can be a novel target for the treatment of diseases associated with proteasome dysfunction.

ACKNOWLEDGMENTS

We are grateful to David Piwnica-Worms and Raymond J. Deshaies for the Ub-FL plasmid and the 3xPSMA4-ARE-Luc plasmid, respectively. We also thank Noriko Noguchi and Akiko Matsumoto for research support.

This work was supported in part by grants-in-aid (A.K. and Y.T.) and the Strategic Research Foundation at Private Universities (2012 to 2016) (A.K.) from the Ministry of Education, Sports, Science and Technology, the Mochida Memorial Foundation (A.K.), the Naito Foundation (A.K.), the Suzuken Memorial Foundation (A.K.), the Takeda Science Foundation (A.K.), the Uehara Memorial Foundation (A.K.), Astellas Foundation for Research on Metabolic Disorders (A.K.), and the Inamori Foundation (Y.T.).

REFERENCES

1. **Kopito RR.** 2000. Aggresomes, inclusion bodies and protein aggregation. Trends Cell Biol. **10:**524–530.
2. **Ross CA, Poirier MA.** 2004. Protein aggregation and neurodegenerative disease. Nat. Med. **10:**S10–S17.
3. **Strnad P, Zatloukal K, Stumptner C, Kulaksiz H, Denk H.** 2008. Mallory-Denk-bodies: lessons from keratin-containing hepatic inclusion bodies. Biochim. Biophys. Acta **1782:**764–774.
4. **Glickman MH, Ciechanover A.** 2002. The ubiquitin-proteasome proteolytic pathway: destruction for the sake of construction. Physiol. Rev. **82:**373–428.
5. **Levine B, Kroemer G.** 2008. Autophagy in the pathogenesis of disease. Cell **132:**27–42.
6. **Mizushima N, Levine B, Cuervo AM, Klionsky DJ.** 2008. Autophagy fights disease through cellular self-digestion. Nature **451:**1069–1075.
7. **Rubinsztein DC.** 2006. The roles of intracellular protein-degradation pathways in neurodegeneration. Nature **443:**780–786.
8. **Kobayashi M, Yamamoto M.** 2006. Nrf2-Keap1 regulation of cellular defense mechanisms against electrophiles and reactive oxygen species. Adv. Enzyme Regul. **46:**113–140.
9. **Sykiotis GP, Bohmann D.** 2010. Stress-activated cap'n'collar transcription factors in aging and human disease. Sci. Signal. **3:**re3. doi:10.1126/scisignal.3112re3.
10. **Chan JY, Kwong M, Lu R, Chang J, Wang B, Yen TS, Kan YW.** 1998. Targeted disruption of the ubiquitous CNC-bZIP transcription factor, Nrf-1, results in anemia and embryonic lethality in mice. EMBO J. **17:**1779–1787.
11. **Kim J, Xing W, Wergedal J, Chan JY, Mohan S.** 2010. Targeted disruption of nuclear factor erythroid-derived 2-like 1 in osteoblasts reduces bone size and bone formation in mice. Physiol. Genomics **40:**100–110.
12. **Ohtsuji M, Katsuoka F, Kobayashi A, Aburatani H, Hayes JD, Yamamoto M.** 2008. Nrf1 and Nrf2 play distinct roles in activation of antioxidant response element-dependent genes. J. Biol. Chem. **283:**33554–33562.
13. **Xing W, Singgih A, Kapoor A, Alarcon CM, Baylink DJ, Mohan S.** 2007. Nuclear factor-E2-related factor-1 mediates ascorbic acid induction of osterix expression via interaction with antioxidant-responsive element in bone cells. J. Biol. Chem. **282:**22052–22061.
14. **Xu Z, Chen L, Leung L, Yen TS, Lee C, Chan JY.** 2005. Liver-specific inactivation of the Nrf1 gene in adult mouse leads to nonalcoholic steatohepatitis and hepatic neoplasia. Proc. Natl. Acad. Sci. U. S. A. **102:**4120–4125.
15. **Kobayashi A, Tsukide T, Miyasaka T, Morita T, Mizoroki T, Saito Y, Ihara Y, Takashima A, Noguchi N, Fukamizu A, Hirotsu Y, Ohtsuji M, Katsuoka F, Yamamoto M.** 2011. Central nervous system-specific deletion of transcription factor Nrf1 causes progressive motor neuronal dysfunction. Genes Cells **16:**692–703.
16. **Lee CS, Lee C, Hu T, Nguyen JM, Zhang J, Martin MV, Vawter MP, Huang EJ, Chan JY.** 2011. Loss of nuclear factor E2-related factor 1 in the brain leads to dysregulation of proteasome gene expression and neurodegeneration. Proc. Natl. Acad. Sci. U. S. A. **108:**8408–8413.
17. **Radhakrishnan SK, Lee CS, Young P, Beskow A, Chan JY, Deshaies RJ.** 2010. Transcription factor Nrf1 mediates the proteasome recovery pathway after proteasome inhibition in mammalian cells. Mol. Cell **38:**17–28.
18. **Steffen J, Seeger M, Koch A, Kruger E.** 2010. Proteasomal degradation is transcriptionally controlled by TCF11 via an ERAD-dependent feedback loop. Mol. Cell **40:**147–158.
19. **Tsuchiya Y, Morita T, Kim M, Iemura S, Natsume T, Yamamoto M, Kobayashi A.** 2011. Dual regulation of the transcriptional activity of Nrf1 by β-TrCP- and Hrd1-dependent degradation mechanisms. Mol. Cell. Biol. **31:**4500–4512.
20. **Luker GD, Pica CM, Song J, Luker KE, Piwnica-Worms D.** 2003. Imaging 26S proteasome activity and inhibition in living mice. Nat. Med. **9:**969–973.
21. **Igarashi K, Itoh K, Motohashi H, Hayashi N, Matuzaki Y, Nakauchi H, Nishizawa M, Yamamoto M.** 1995. Activity and expression of murine small Maf family protein MafK. J. Biol. Chem. **270:**7615–7624.
22. **Igarashi K, Kataoka K, Itoh K, Hayashi N, Nishizawa M, Yamamoto M.** 1994. Regulation of transcription by dimerization of erythroid factor NF-E2 p45 with small Maf proteins. Nature **367:**568–572.
23. **Miyata Y, Nishida E.** 2005. CK2 binds, phosphorylates, and regulates its pivotal substrate Cdc37, an Hsp90-cochaperone. Mol. Cell. Biochem. **274:**171–179.
24. **Kuusisto E, Suuronen T, Salminen A.** 2001. Ubiquitin-binding protein p62 expression is induced during apoptosis and proteasomal inhibition in neuronal cells. Biochem. Biophys. Res. Commun. **280:**223–228.
25. **Wang HQ, Liu HM, Zhang HY, Guan Y, Du ZX.** 2008. Transcriptional upregulation of BAG3 upon proteasome inhibition. Biochem. Biophys. Res. Commun. **365:**381–385.
26. **Zhou M, Wu X, Ginsberg HN.** 1996. Evidence that a rapidly turning over protein, normally degraded by proteasomes, regulates hsp72 gene transcription in HepG2 cells. J. Biol. Chem. **271:**24769–24775.
27. **Gamerdinger M, Hajieva P, Kaya AM, Wolfrum U, Hartl FU, Behl C.** 2009. Protein quality control during aging involves recruitment of the macroautophagy pathway by BAG3. EMBO J. **28:**889–901.
28. **Johansen T, Lamark T.** 2011. Selective autophagy mediated by autophagic adapter proteins. Autophagy **7:**279–296.
29. **Niefind K, Guerra B, Ermakowa I, Issinger OG.** 2001. Crystal structure of human protein kinase CK2: insights into basic properties of the CK2 holoenzyme. EMBO J. **20:**5320–5331.
30. **Komatsu M, Waguri S, Koike M, Sou YS, Ueno T, Hara T, Mizushima N, Iwata J, Ezaki J, Murata S, Hamazaki J, Nishito Y, Iemura S, Natsume T, Yanagawa T, Uwayama J, Warabi E, Yoshida H, Ishii T, Kobayashi A, Yamamoto M, Yue Z, Uchiyama Y, Kominami E, Tanaka K.** 2007. Homeostatic levels of p62 control cytoplasmic inclusion body formation in autophagy-deficient mice. Cell **131:**1149–1163.
31. **Husberg C, Murphy P, Bjørgo E, Kalland KH, Kolstø AB.** 2003. Cellular localisation and nuclear export of the human bZIP transcription factor TCF11. Biochim. Biophys. Acta **1640:**143–151.
32. **Apopa PL, He X, Ma Q.** 2008. Phosphorylation of Nrf2 in the transcription activation domain by casein kinase 2 (CK2) is critical for the nuclear translocation and transcription activation function of Nrf2 in IMR-32 neuroblastoma cells. J. Biochem. Mol. Toxicol. **22:**63–76.
33. **Pi J, Bai Y, Reece JM, Williams J, Liu D, Freeman ML, Fahl WE, Shugar**

D, Liu J, Qu W, Collins S, Waalkes MP. 2007. Molecular mechanism of human Nrf2 activation and degradation: role of sequential phosphorylation by protein kinase CK2. Free Radic. Biol. Med. **42:**1797–1806.
34. **Afonyushkin T, Oskolkova OV, Binder BR, Bochkov VN.** 2011. Involvement of CK2 in activation of electrophilic genes in endothelial cells by oxidized phospholipids. J. Lipid Res. **52:**98–103.
35. **Ivanov AV, Smirnova OA, Ivanova ON, Masalova OV, Kochetkov SN, Isaguliants MG.** 2011. Hepatitis C virus proteins activate NRF2/ARE pathway by distinct ROS-dependent and independent mechanisms in HUH7 cells. PLoS One **6:**e24957. doi:10.1371/journal.pone.0024957.
36. **Lee BH, Lee MJ, Park S, Oh DC, Elsasser S, Chen PC, Gartner C, Dimova N, Hanna J, Gygi SP, Wilson SM, King RW, Finley D.** 2010. Enhancement of proteasome activity by a small-molecule inhibitor of USP14. Nature **467:**179–184.
37. **Chondrogianni N, Gonos ES.** 2007. Overexpression of hUMP1/POMP proteasome accessory protein enhances proteasome-mediated antioxidant defence. Exp. Gerontol. **42:**899–903.
38. **Chondrogianni N, Tzavelas C, Pemberton AJ, Nezis IP, Rivett AJ, Gonos ES.** 2005. Overexpression of proteasome beta5 assembled subunit increases the amount of proteasome and confers ameliorated response to oxidative stress and higher survival rates. J. Biol. Chem. **280:**11840–11850.
39. **Tonoki A, Kuranaga E, Tomioka T, Hamazaki J, Murata S, Tanaka K, Miura M.** 2009. Genetic evidence linking age-dependent attenuation of the 26S proteasome with the aging process. Mol. Cell. Biol. **29:**1095–1106.
40. **Allende JE, Allende CC.** 1995. Protein kinases. 4. Protein kinase CK2: an enzyme with multiple substrates and a puzzling regulation. FASEB J. **9:**313–323.
41. **Meggio F, Pinna LA.** 2003. One-thousand-and-one substrates of protein kinase CK2? FASEB J. **17:**349–368.
42. **Blanquet PR.** 2000. Casein kinase 2 as a potentially important enzyme in the nervous system. Prog. Neurobiol. **60:**211–246.
43. **Perez DI, Gil C, Martinez A.** 2011. Protein kinases CK1 and CK2 as new targets for neurodegenerative diseases. Med. Res. Rev. **31:**924–954.
44. **Lee G, Tanaka M, Park K, Lee SS, Kim YM, Junn E, Lee SH, Mouradian MM.** 2004. Casein kinase II-mediated phosphorylation regulates α-synuclein/synphilin-1 interaction and inclusion body formation. J. Biol. Chem. **279:**6834–6839.
45. **Okochi M, Walter J, Koyama A, Nakajo S, Baba M, Iwatsubo T, Meijer L, Kahle PJ, Haass C.** 2000. Constitutive phosphorylation of the Parkinson's disease associated α-synuclein. J. Biol. Chem. **275:**390–397.
46. **Raftery M, Campbell R, Glaros EN, Rye KA, Halliday GM, Jessup W, Garner B.** 2005. Phosphorylation of apolipoprotein-E at an atypical protein kinase CK2 PSD/E site in vitro. Biochemistry **44:**7346–7353.
47. **Chen-Roetling J, Li Z, Regan RF.** 2008. Hemoglobin neurotoxicity is attenuated by inhibitors of the protein kinase CK2 independent of heme oxygenase activity. Curr. Neurovasc. Res. **5:**193–198.
48. **Moreno H, Yu E, Pigino G, Hernandez AI, Kim N, Moreira JE, Sugimori M, Llinás RR.** 2009. Synaptic transmission block by presynaptic injection of oligomeric amyloid beta. Proc. Natl. Acad. Sci. U. S. A. **106:**5901–5906.
49. **Matsumoto G, Wada K, Okuno M, Kurosawa M, Nukina N.** 2011. Serine 403 phosphorylation of p62/SQSTM1 regulates selective autophagic clearance of ubiquitinated proteins. Mol. Cell **44:**279–289.

Biochemical and Biophysical Research Communications 478 (2016) 363–370

Contents lists available at ScienceDirect

Biochemical and Biophysical Research Communications

journal homepage: www.elsevier.com/locate/ybbrc

USP15 stabilizes the transcription factor Nrf1 in the nucleus, promoting the proteasome gene expression

Kousuke Fukagai [a], Tsuyoshi Waku [a], A.M. Masudul Azad Chowdhury [a, 1], Kaori Kubo [a, 1], Mariko Matsumoto [a, 1], Hiroki Kato [a], Tohru Natsume [b], Fuminori Tsuruta [c], Tomoki Chiba [c], Hiroaki Taniguchi [a], Akira Kobayashi [a, *]

[a] Laboratory for Genetic Code, Graduate School of Life and Medical Sciences, Doshisha University, Kyotanabe, Kyoto, Japan
[b] National Institutes of Advanced Industrial Science and Technology, Biological Information Research Center (JBIRC), Tokyo, Japan
[c] Graduate School of Life and Environmental Sciences, University of Tsukuba, Tsukuba, Ibaraki, Japan

ARTICLE INFO

Article history:
Received 29 June 2016
Accepted 8 July 2016
Available online 11 July 2016

Keywords:
Ubiquitination
Deubiquitination
Proteasomal degradation
Transcription factor
Gene regulation

ABSTRACT

The transcriptional factor Nrf1 (NF-E2-related factor 1) sustains protein homeostasis (proteostasis) by regulating the expression of proteasome genes. Under physiological conditions, the transcriptional activity of Nrf1 is repressed by its sequestration into the endoplasmic reticulum (ER) and furthermore by two independent ubiquitin-proteasome pathways, comprising Hrd1 and β-TrCP in the cytoplasm and nucleus, respectively. However, the molecular mechanisms underlying Nrf1 activation remain unclear. Here, we report that USP15 (Ubiquitin-Specific Protease 15) activates Nrf1 in the nucleus by stabilizing it through deubiquitination. We first identified USP15 as an Nrf1-associated factor through proteome analysis. USP15 physically interacts with Nrf1, and it markedly stabilizes Nrf1 by removing its ubiquitin moieties. USP15 activates the Nrf1-mediated expression of a proteasome gene luciferase reporter and endogenous proteasome activity. The siRNA-mediated knockdown of *USP15* diminishes the Nrf1-induced proteasome gene expression in response to proteasome inhibition. These results uncover a new regulatory mechanism that USP15 activates Nrf1 against the β-TrCP inhibition to maintain proteostasis.

1. Introduction

The transcription factor Nrf1 (NF-E2-related factor 1 or NFE2L1) induces the expression of the proteasome subunit genes under proteasome dysfunction [1,2]. This adaptation for proteasome dysfunction is called “proteasome recovery” to sustain protein homeostasis (proteostasis). Consistently, the deletion of the *Nrf1* gene in the central nervous system of mice causes an abnormal accumulation of ubiquitinated protein aggregates in neurons, and these mice show progressive motor ataxia and severe weight loss [3,4]. These observations strongly suggest that Nrf1 plays important roles in proteostasis.

Accumulated evidence has revealed that the molecular function of Nrf1 is regulated by multiple repression mechanisms [5,6]. Under physiological conditions, Nrf1 is sequestered in the endoplasmic reticulum (ER) through its N-terminal NHB1 domain to prevent nuclear translocation and transcriptional activation [7]. Furthermore, Nrf1 is repressed by proteasomal degradation via two independent E3 ubiquitin (Ub) ligases as follows: the SCF (Skp1-Cul1-F-box protein) ubiquitin ligase that contains the β-TrCP adaptor and the endoplasmic reticulum-associated degradation (ERAD) ubiquitin ligase Hrd1, in the nucleus and cytoplasm, respectively [1,8]. It has also been reported that Fbw7 mediates the nuclear degradation of Nrf1 [9]. These findings imply that Nrf1 is activated by escaping from these proteasomal degradation mechanisms. However, the molecular bases of Nrf1 activation remain unclear.

Ubiquitin-specific protease 15 (USP15), which is a ubiquitously expressed Deubiquitinating enzyme (DUB), regulates the biological function of many substrate proteins for various cellular functions

Abbreviations: ARE, antioxidant response element; CNC, Cap'n'Collar; DUB, deubiquitinating enzyme; ER, endoplasmic reticulum; NHB1, N-terminal homology box 1; Nrf1, NF-E2-related factor 1; RT-qPCR, real time-quantitative PCR; SCF, Skp1-Cul1-F-box protein; SEM, standard error of the mean; USP, ubiquitin-specific protease.

* Corresponding author. Laboratory for Genetic Code, Graduate School of Life and Medical Sciences, Doshisha University, 1-3 Tatara Miyakodani, Kyotanabe 610-0394, Japan.
E-mail address: akobayas@mail.doshisha.ac.jp (A. Kobayashi).
[1] These authors contributed equally to this work.

http://dx.doi.org/10.1016/j.bbrc.2016.07.045
0006-291X/

[10–12]. For example, USP15 regulates the E3 ubiquitin ligase MDM2 for the tumor suppressor p53 [13] and the TGFβ-induced monoubiquitination of SMAD (R-SMAD) [14]. Furthermore, it has been reported that USP15 represses Nrf1-related factor Nrf2 through activating the Keap1-mediated ubiquitination activity by its deubiquitination [15].

For a comprehensive understanding of the physiological function of Nrf1, deciphering the molecular mechanisms underlying Nrf1 activation from multiple repression mechanisms is indispensable. We found that USP15 stabilizes Nrf1 from the β-TrCP-mediated degradation in the nucleus through its deubiquitination, ameliorating its transcription activity for the gene expression of the proteasome subunits. These results suggest that USP15 plays an important role for the regulation of Nrf1 activity to maintain proteostasis.

2. Materials and methods

2.1. Antibodies

The antibodies utilized in this study were anti-FLAG (M2; Sigma), anti-V5 antibody (46-0705; Invitrogen), anti-α-tubulin (DM1A; Sigma), anti-green fluorescent protein (anti-GFP) (B-2; Santa Cruz), anti-Nrf1 (D5B10; Cell Signaling Technology and H285; Santa Cruz), anti-USP15 (2D5; Santa Cruz), anti-hemagglutinin (anti-HA) (Y-11; Santa Cruz), and anti-Histone H3 (06-755; EMD Millipore).

2.2. Expression plasmids

3 × Flag-Nrf1, ΔNHB1 and ΔbZip have been described previously [8]. 3 × Flag-Nrf3 was generated by subcloning the PCR-amplified mouse Nrf3 cDNA into the p3 × FLAG-CMV™10 vector (Sigma). Flag-Nrf2 and Flag-p45 were kindly provided by Ken Itoh.

2.3. Cell culture and transfection

HEK293T cells and HeLa cells were cultured as described [8]. The transfection of plasmid DNA and short interfering RNA (siRNA) was performed using Lipofectamine Plus and RNAiMAX (Invitrogen), respectively, according to the manufacturer's protocols.

2.4. Cycloheximide chase experiments

HEK293T cells were transfected with the expression vectors containing wild-type or deletion mutants of 3 × Flag-Nrf1 [8], along with a GFP expression vector (Clonetech, pEGFP-N1). At 24 h after transfection, the cells were treated with 10 μg/ml cycloheximide (CHX), and the whole cell extracts were prepared at the indicated time points. Immunoblot analyses were conducted with the indicated antibodies. When USP15 siRNAs were transfected into the cells, the cells were pretreated at 32 h after the transfection with 10 μM MG132 for 8 h, followed by the CHX treatment.

2.5. Immunoprecipitation, immunoblot analysis and ubiquitination assay

The expression vectors for 3 × Flag-Nrf1 and V5-USP15 were transfected into HEK293T cells. At 24 h after transfection, whole cell extracts were prepared using lysis buffer (50 mM Tris-HCl [pH 8.0], 10% glycerol, 100 mM NaF, 50 mM NaCl, 2 mM EDTA, 2 mM sodium orthovanadate, 10 mM sodium pyrophosphate, 10 mM β-glycerophosphate, 0.1% NP-40, and 1 × protease inhibitor cocktail [Roche]). The whole cell extracts were subjected to immunoprecipitation with Protein G Sepharose 4 Fast Flow beads (GE Healthcare) and the anti-V5 antibody (2D5; Abcam) at 4 °C for 2 h by rotating. The Protein G beads were washed three times with wash buffer (50 mM Tris-HCl [pH 7.4], 150 mM NaCl and 0.1% NP-40). The immunocomplexes were visualized with immunoblot analysis using the indicated antibodies. Ubiquitination assay was performed as described [8].

2.6. Immunofluorescence staining

HEK293T cells were transfected with wild-type or deletion mutants of 3 × Flag-Nrf1 and/or V5-USP15. At 24 h after transfection, the cells were washed with PBS and fixed with 4% formaldehyde for 15 min at room temperature (RT). After the PBS washing, the cells were permeabilized with 0.5% Triton X-100 in PBS for 10 min at RT, washed with PBS and subsequently blocked with 1% skim milk (Nacalai tesque) for 1 h. A primary antibody treatment (anti-FLAG or anti-V5 antibody) was conducted at RT for 1 h. After washing with PBS, the cells were incubated with the Alexa488 or Alexa546 Fluor secondary antibody (Invitrogen) for 1 h in the dark. The nuclei were stained with 4′,6-diamidino-2-phenylindole (DAPI). The immunofluorescence was viewed using an Olympus IX7 microscope.

2.7. Luciferase assay

HeLa cells were transfected with ΔNHB1 and V5-USP15, along with a luciferase reporter plasmid containing three tandem copies of the ARE of PSMA4 [2] and pRL-TK (Promega) as an internal control. At 24 h after transfection, the luciferase activities were measured using the PicaGene luciferase assay system (Toyo Ink) and a Berthold Lumat LB9507 luminometer according to the manufacturer's protocols.

2.8. RNA extraction and real-time quantitative PCR (RT-qPCR)

Total RNA was prepared using the ISOGENII (Wako). One μg of total RNA was utilized for cDNA synthesis using random hexamer primers (Takara Bio) and Moloney murine leukemia virus (M-MLV) reverse transcriptase (Invitrogen). Real-time quantitative PCR was conducted using the FastStart Universal SYBR Green Master Mix (Roche) and the Thermal Cycler Dice Real Time System II (Takara Bio). All target gene expression levels were normalized to 18S rRNA expression. The sequences of the primers are listed in Table 1.

2.9. Proteasome fluorogenic peptidase assay

The *in vitro* measurement of proteasome activities was performed as previously described [16]. HeLa cells were transfected

Table 1
Sequences of siRNA and primers for real time PCR.

Gene	Sense strand sequence (5′–3′)	Antisense strand sequence (5′–3′)
NRF1	gggauucggugaagauuugTT	caaaucuucaccgaaucccTT
USP15-1	uauuuguuccacaaucuggTT	ccagauuguggaacaaauaTT
USP15-2	gguuggaauaaacuuugucaTT	ugacaaguuuauuccaaccTT
USP15-3	ccagucacuuaaggaacauTT	auguuccuuaagugacuggTT
Control	uucuccgaacgugucacguTT	acgugacacguucggagaaTT
Gene	**Forward primer (5′–3′)**	**Reverse primer (5′–3′)**
18S rRNA	cgccgctagaggtgaaattc	cgaacctccgactttcgttct
USP15	ggtgctgaagatccctgg	tactggaggcagggacca
NRF1	tggaacagcagtggcaagatctca	ggcactgtacaggatttcacttgc
PSMA4	cattggctgggataagca	atgcatgtggccttccat
PSMC4	ggaagaccatgttggcaaag	aagatgatggcaggtgcatt
PSMB6	ctgatggcgggaatcatc	ccaatggcaaaggactgc

with ΔNHB1 or ΔbZip along with V5-USP15. At 24 h after the transfection, the cells were treated with Epoxomicin for 16 h (10 nM) and whole cell extracts were prepared. Twenty μg of total protein of cell lysates were utilized for the assay using Suc-LLVY-AMC (Peptide Institute), Z-GGL-AMC (Santa Cruz) or Z-LLE-AMC (Peptide Institute). After incubation for 30 min at 37 °C, fluorescence (380 nm excitation, 460 nm emission) was monitored on a microplate fluorometer (Infinite 200PRO, Tecan). Protein concentration of the cell lysates was determined using the BCA protein assay (Pierce). Each peptidase activity (arbitrary unit) was expressed as [AMC fluorescence (a sample - a background)] per micro gram lysate protein.

2.10. Statistical analysis

Statistical significance was evaluated with Student's t-test for repeated measurements. All values are represented as the means ± standard error of the mean in at least three-independent experiments.

3. Results

3.1. Identification of USP15 as an Nrf1-associated factor

To elucidate the molecular mechanisms underlying Nrf1 activation, we attempted proteome analysis to identify the Nrf1-associated proteins using liquid chromatography-tandem mass spectrometry (LC-MS/MS) analysis. HEK293 cells that transiently expressed C-terminal Flag-tagged Nrf1 (Nrf1-Flag) were subjected to immunoprecipitation with an anti-FLAG antibody to isolate Nrf1 complexes, and these complexes were analyzed using LC-MS/MS [8]. We succeeded in the identification of numerous factors, such as Keap1, proteasome subunits and mitochondria-related factors (data not shown). Among these factors, we focused on the deubiquitinating enzyme USP15, as we had previously discovered that Nrf1 is degraded by two-independent ubiquitin ligases, including Hrd1 and β-TrCP [1,8]. This result allowed us to make a hypothesis that USP15 antagonistically stabilizes Nrf1 against Hrd1 or β-TrCP-mediated degradation through its deubiquitination. To address this hypothesis, we first examined an association between USP15 and Nrf1 using immunoprecipitation. Whole cell extracts of HEK293T cells expressing 3 × Flag-Nrf1 and V5-USP15 were subjected to immunoprecipitation using the anti-V5 antibody (Fig. 1A). Consistently, 3 × Flag-Nrf1 was coprecipitated with V5-USP15, indicating that USP15 physically interacts with Nrf1 in cells.

3.2. USP15 stabilizes Nrf1 through its deubiquitination

We next examined whether USP15 stabilizes Nrf1 through its deubiquitination. The overexpression of V5-USP15 markedly stabilized 3 × Flag-Nrf1 in HEK293T cells (Fig. 1B). A cycloheximide chase experiment also revealed that USP15 increases the turnover time of Nrf1 (Fig. 1C). Moreover, the siRNA-mediated knockdown of endogenous *USP15* reduced the protein turnover time of endogenous NRF1 (Fig. 1D). As a result, these data strongly suggest that USP15 stabilizes endogenous NRF1.

We further conducted a ubiquitination assay to examine whether USP15 deubiquitinates Nrf1. 3 × Flag-Nrf1 was ubiquitinated in HEK293T cells in the presence of hemagglutinin (HA)-tagged ubiquitin (HA-Ub), immunoprecipitated using the anti-FLAG antibody and visualized by immunoblot analysis using an anti-HA antibody (Fig. 1E). The coexpression of HA-Ub along with 3 × Flag-Nrf1 caused smeared bands, implying that Nrf1 is ubiquitinated in cells. Under these experimental conditions, USP15 significantly reduced the smear patterns of 3 × Flag-Nrf1, suggesting that USP15 promotes the deubiquitination of Nrf1. We concluded that USP15 is a contributing factor to the stabilization of Nrf1 through its deubiquitination.

3.3. USP15 stabilizes Nrf1 through deubiquitination in the nucleus

To confirm the colocalization of Nrf1 and USP15 in cells, we conducted immunofluorescent staining of HEK293T cells in the transient expression system (Fig. 2A). The overexpression of 3 × Flag-Nrf1 showed its nuclear localization. This result is consistent with our previous observation that 3 × Flag-Nrf1 is localized in the nucleus, despite the presence of the ER anchor domain NHB1 [8]. V5-USP15 alone was localized to both the cytoplasm and nucleus (a bottom right panel). Nevertheless, the coexpression of 3 × Flag-Nrf1 caused the nuclear translocation of V5-USP15, implying a physical interaction between USP15 and Nrf1 in cells (top panels). We further examined the colocalization of endogenous USP15 with 3 × Flag-Nrf1 using immunostaining with the anti-USP15 antibody (Fig. 2B). Indeed, endogenous USP15 also colocalized with 3 × Flag-Nrf1 in the nucleus of HEK293T cells. Collectively, these data strongly highlight that endogenous USP15 colocalizes with 3 × Flag-Nrf1 in the nucleus.

The current results further allowed us to hypothesize that USP15 stabilizes Nrf1 in the nucleus, where Nrf1 is subjected to β-TrCP-mediated degradation. To confirm this hypothesis, we investigated whether USP15 stabilizes a nuclear localizing Nrf1 mutant. We generated the 3 × Flag-tagged Nrf1 mutant vector by deleting the ER retention motif in the NHB1 domain (Fig. 2C, ΔNHB1). As a control, a cytoplasm-localizing Nrf1 mutant vector was constructed by deleting the nuclear localization signal (NLS) in the basic region of the bZip domain (ΔbZip). We verified by immunostaining that the ΔNHB1 and the ΔbZip mainly localize to the nucleus and the cytoplasm, respectively (Fig. 2D). The effects of USP15 on the turnover of these Nrf1 mutants were determined using a cycloheximide chase experiment. Predictably, USP15 stabilized ΔNHB1 but not ΔbZip (Fig. 2E). These results indicate that USP15 stabilizes Nrf1 in the nucleus but not the cytoplasm.

3.4. USP15 augments the Nrf1-mediated gene expression

We further deciphered the effect of USP15 on the Nrf1 transcriptional activity using a luciferase reporter assay (Fig. 3A). The ΔNHB1 and V5-USP15 vectors were transfected into HeLa cells, along with a luciferase reporter containing three tandem copies of *PSMA4* gene-derived ARE [2]. ΔNHB1 slightly increased the expression of the reporter. The coexpression of V5-USP15 significantly augmented the ΔNHB1-mediated reporter activity in a dose-dependent manner. This effect of USP15 was not observed in the absence of ΔNHB1 mutant. These results clearly suggest that USP15 activates the transcriptional activity of Nrf1. Furthermore, we examined whether USP15 can activate the NRF1-induced endogenous proteasome activity (Fig. 3B). HeLa cells were transfected by ΔNHB1 mutant along with V5-USP15. After Epoxomicin treatment of the cells for proteasome recovery, chymotrypsin-like or caspase-like activities of endogenous proteasome were measured using fluorogenic Suc-LLVY-AMC, Z-GGLY-AMC or Z-LLE-AMC. While ΔNHB1 alone did not affect proteasome activity, V5-USP15 ameliorated the Nrf1-dependent proteasome activity. Thus, we concluded that USP15 activates proteasome activity through regulating Nrf1 function.

We next examined whether the knockdown of endogenous USP15 reduces the NRF1-mediated expression of the proteasome subunit genes in response to proteasome inhibition (Fig. 3C–H). HeLa cells were transfected with siRNA against *USP15* and were then treated with three different proteasome inhibitors, MG132,

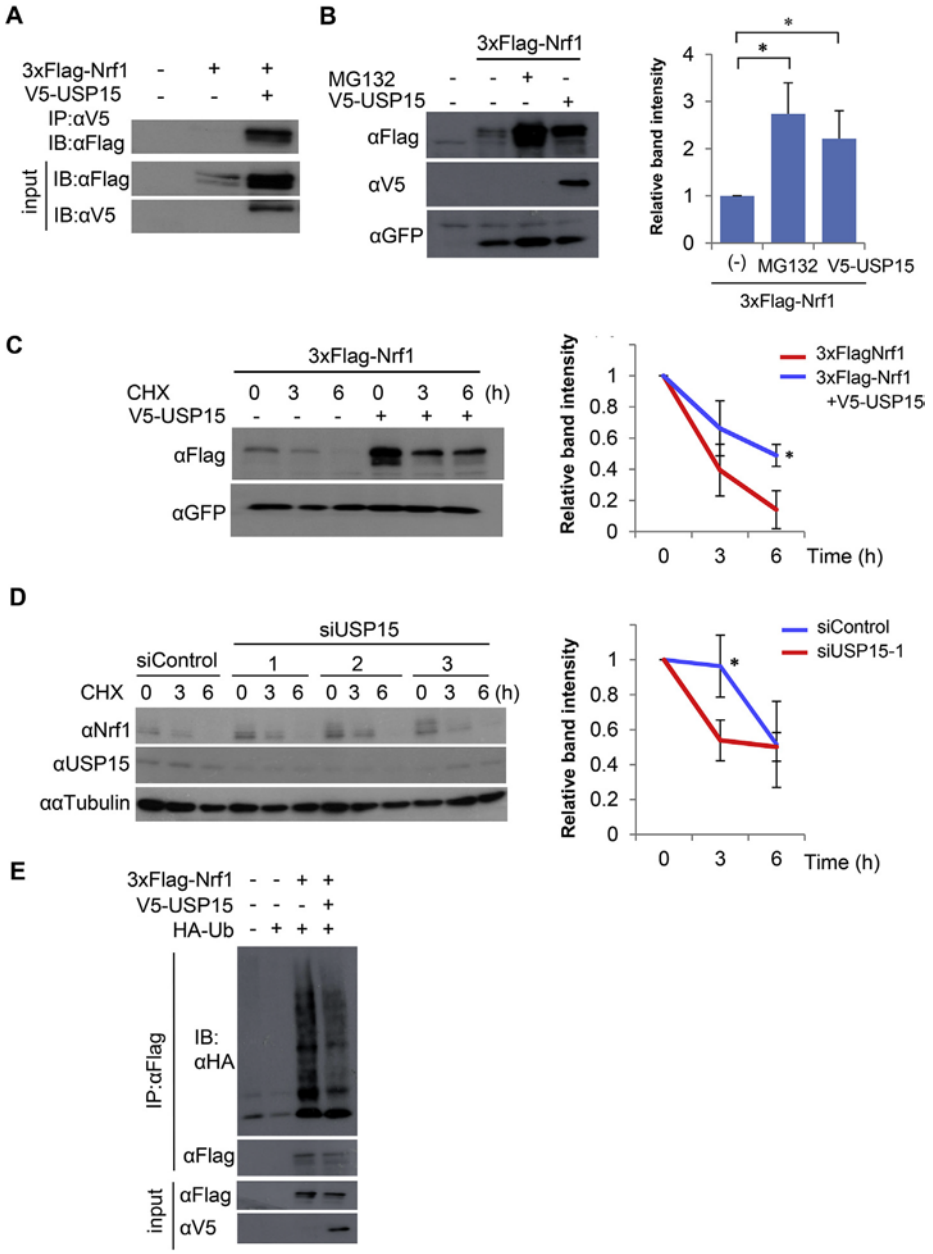

Fig. 1. USP15 stabilizes Nrf1 by its deubiquitination. (A) Nrf1 associates with V5-USP15 in HEK293T cells in immunoprecipitation analysis (IP). (B) V5-USP15 stabilizes 3 × Flag Nrf1 protein in HEK293T cells. Cells were treated with MG132 (10 μM) for 8 h before harvesting. The graph shows the quantified band intensities of 3 × Flag-Nrf1 normalized to the cotransfected GFP expression. The error bars show the standard error of the means (SEM) (n = 3). *P < 0.05 compared to 3 × Flag-Nrf1 (two-tailed unpaired *t*-test). (C) V5-USP15 stabilizes 3 × Flag-Nrf1 in the cycloheximide (CHX) chase experiments using HEK293T cells. The data were normalized to the GFP levels and presented as the means ± SEM (n = 3). *P < 0.05 compared to Control (two-tailed unpaired *t*-test). (D) Three independent USP15 siRNAs (siUSP15-1, siUSP15-2 and siUSP15-3) promote the proteasomal degradation of endogenous Nrf1 in the CHX chase experiments using HEK293T cells. The graph shows the quantified band intensities of endogenous NRF1. The data were normalized with αTubulin and presented as the means ± SEM (n = 3). *P < 0.05 compared to Control (two-tailed unpaired *t*-test). (E) V5-USP15 deubiquitinates 3 × Flag Nrf1 in HEK293T cells.

Bortezomib and Epoxomicin. The gene expression levels of *USP15*, *NRF1* and the proteasome subunits *PSMC4* and *PSMA4* were determined using real time-quantitative PCR (RT-qPCR). Consistent with previous reports [1,2,8,17], treatment with proteasome inhibitors significantly activated the gene expression of *PSMC4* and *PCMA4* (Fig. 3E and G, siControl). Unexpectedly, *USP15* siRNA alone induced the mRNA expression of *NRF1* (Fig. 3D, DMSO and siUSP15-1), thereby augmenting the expression of these proteasomal genes (Fig. 3E and G, DMSO and siUSP15-1). We also confirmed that other *USP15* siRNAs can cause the mRNA induction of *NRF1* (data not shown). Furthermore, we observed that *USP15* siRNAs significantly increased the protein expression levels of endogenous NRF1 in HeLa cells (Fig. 1D). Nevertheless, *USP15* siRNA significantly reduced the induction of proteasome genes by the proteasome inhibitors (Fig. 3F and H). All proteasome gene induction was silenced by *NRF1* siRNA, implying their NRF1-dependency. Collectively, we concluded that endogenous USP15 enhances the NRF1-mediated gene expression for proteasome recovery.

3.5. *USP15 stabilizes Nrf1 and p45 among the CNC family proteins*

Finally, we examined the biological relationship between USP15

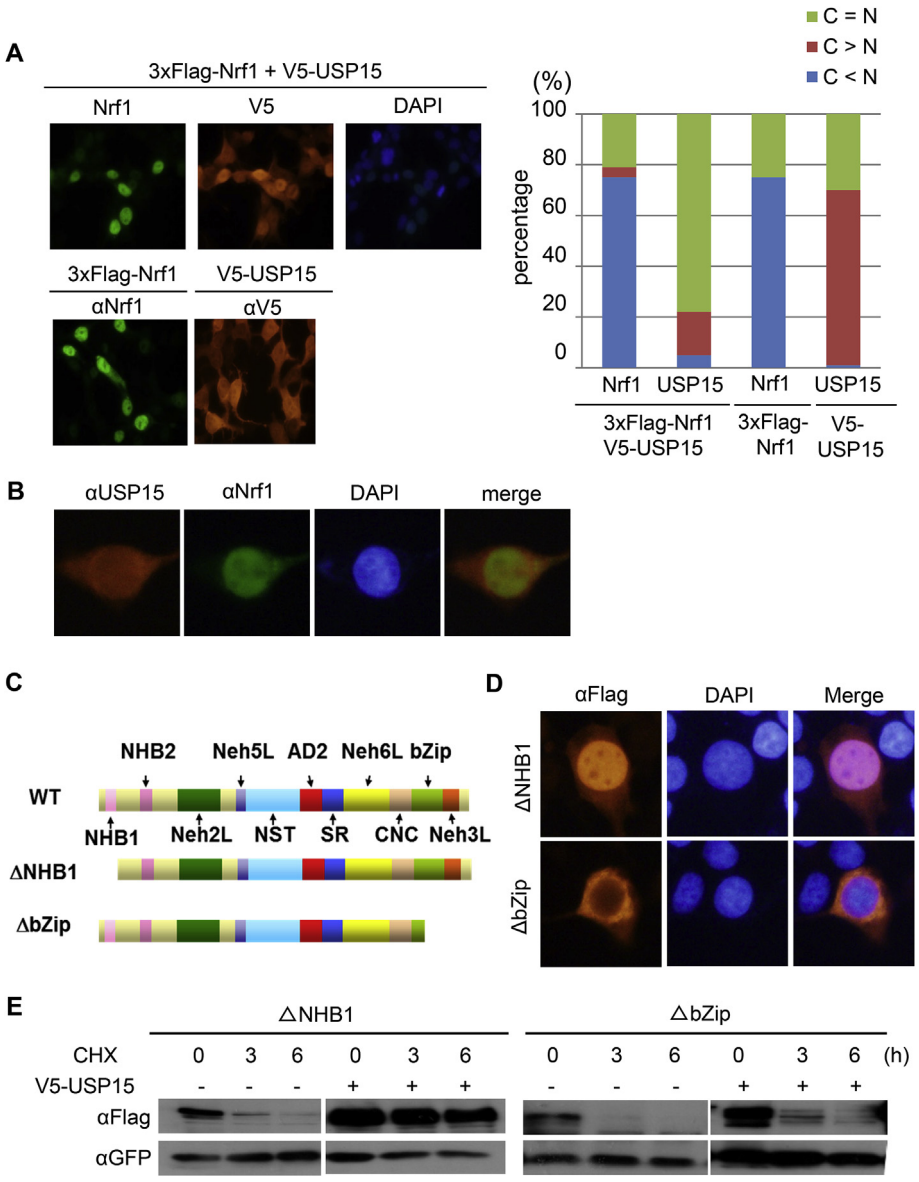

Fig. 2. The overexpression of Nrf1 causes the nuclear translocation of USP15. (A) Immunostaining of HEK293T cells expressing the indicated proteins with the anti-V5 antibody and the anti-Nrf1 antibody (CST D5B10). 10× magnification. The bar graph shows the results of the quantitative analysis of the subcellular localization of V5-USP15 and 3 × Flag-Nrf1. The localization was classified into three categories: roughly equal localization between the cytoplasmic and nuclear compartments (C = N, green bars), predominantly cytoplasmic localization (C > N, red bars), and predominantly nuclear localization (C < N, blue bars). (B) The colocalization of endogenous USP15 with 3 × Flag-Nrf1 in HEK293T cells. The nuclei were stained with DAPI. 40× magnification. (C) The schematic structures of the 3 × Flag-tagged nuclear- and cytoplasm-localizing Nrf1 deletion mutants (ΔNHB1 and ΔbZip). (D) The subcellular localization of ΔNHB1 or ΔbZip in HEK293T cells was verified by immunostaining using the anti-FLAG antibody. 40× magnification. (E) USP15 specifically stabilizes Nrf1 in the nucleus in the CHX chase experiments using HEK293T cells.

and other Cap'n'Collar (CNC) family proteins. Nrf1 belongs to a member of the CNC family, which contains Nrf1, Nrf2, Nrf3 and p45/NF-E2 [5,6]. V5-USP15 was transiently expressed in HEK293T cells, along with the CNC family proteins Nrf2, Nrf3 and p45, and the protein level of each was determined using immunoblot analysis (Fig. 4A). Under our experimental conditions, USP15 also stabilized p45, as well as Nrf1. We did not observe a USP15-driven reduction in Nrf2, although USP15 has been reported to destabilize Nrf2 by activating the Keap1-mediated ubiquitination activity by its deubiquitination [15]. The reason for this discrepancy between our results is unknown. Further examination is required to determine the molecular basis of the USP15-mediated regulation of the CNC family proteins.

4. Discussion

This study demonstrates a new molecular mechanism of Nrf1 activation by the deubiquitination enzyme USP15 (Fig. 4B). USP15 stabilizes Nrf1 in the nucleus through its deubiquitination and consequently augments its transcriptional activity. It has been identified that the β-TrCP-based E3 ubiquitin ligase causes proteasomal degradation of Nrf1 in the nucleus [8]. Therefore, our current data reveal the presence of competitive regulation of Nrf1 stability by β-TrCP and USP15 in the nucleus. Under physiological conditions, Nrf1 is repressed by its ER sequestration and proteasomal degradation. This implies the presence of stresses and/or signals that activate Nrf1 from these repression mechanisms, although such stress is still missing, except for proteasomal

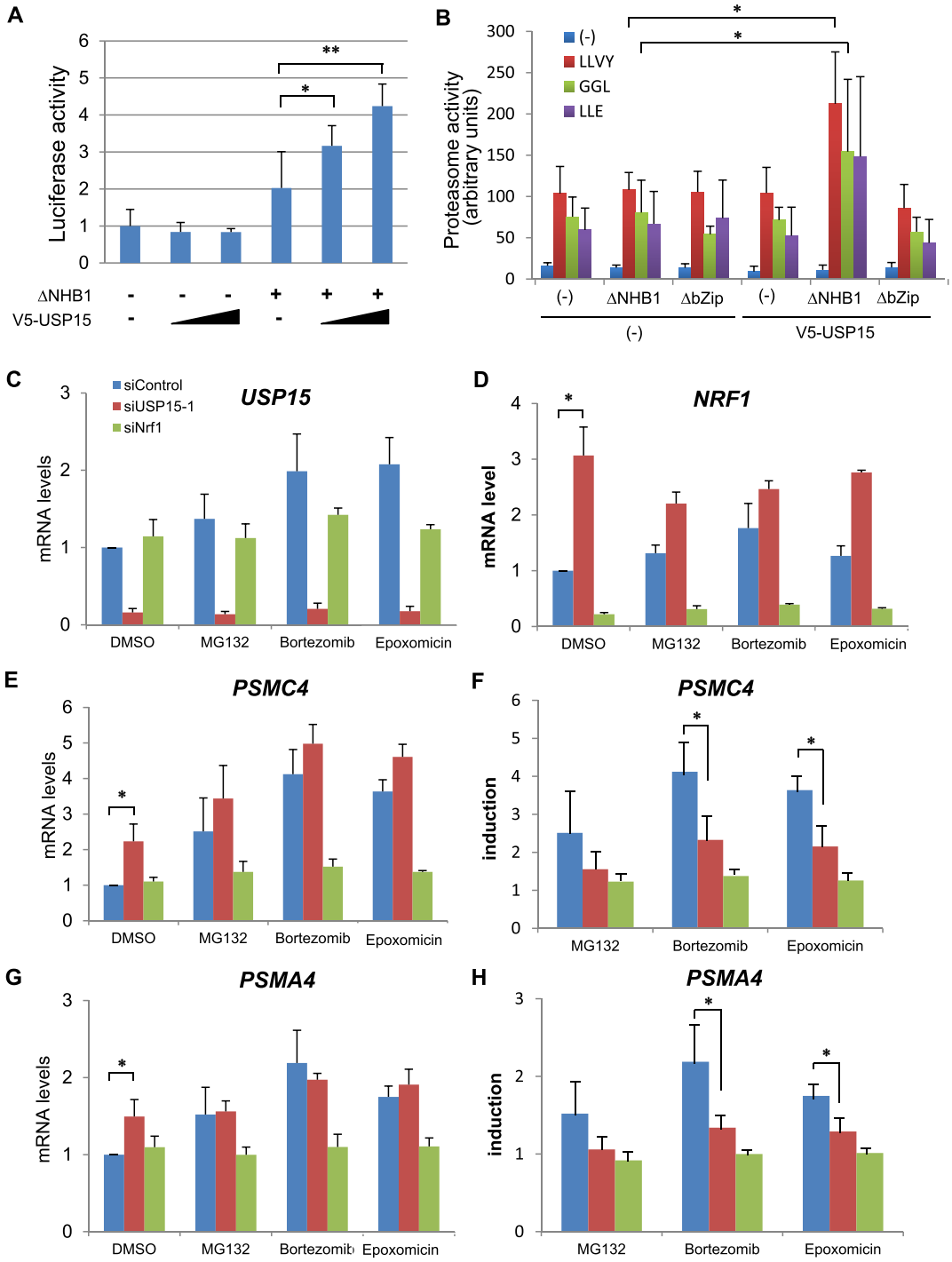

Fig. 3. USP15 promotes the Nrf1-induced proteasome gene expression. (A) Effects of V5-USP15 on the transcription activity of Nrf1 ΔNHB1 mutant were determined using a luciferase reporter containing three tandem copies of *PSMA4* gene-derived ARE. The data were normalized using *Renilla* luciferase and presented as the means ± SEM (n = 3). *P < 0.05, **P < 0.01 compared to 3 × Flag-Nrf1 (two-tailed unpaired *t*-test). (B) Whole cell extracts of HeLa cells expressing ΔNHB1 or ΔbZip along with V5-USP15 were subjected to the proteasome fluorogenic peptidase assay using Suc-LLVY-AMC (LLVY), Z-GGL-AMC (GGL) or Z-LLE-AMC (LLE). The cells were treated with Epoxomicin (10 nM) for 16 h before preparing the cell extracts. Means ± SEM (n = 3). *P < 0.05. (C–H) HeLa cells were transfected with siControl, siUSP15 or siNrf1, followed by treatment with the indicated proteasomal inhibitors for 16 h. The mRNA expression levels were determined by real-time quantitative PCR analysis. The data were normalized using 18S rRNA and presented as the means ± SEM (n = 3). The fold changes in the mRNA expression compared with values of DMSO treatment were shown as an induction (F, H). *P < 0.05 compared to siControl (two-tailed unpaired *t*-test).

inhibition. We surmise that Nrf1-activating stresses facilitate the USP15-mediated deubiquitination rather than the β-TrCP-mediated ubiquitination, thereby promoting the expression of Nrf1 target genes.

The data presented show that USP15 significantly activated the Nrf1-mediated luciferase reporter (Fig. 3A) and endogenous proteasome activity (Fig. 3B) in the transient transfection experiments and the knockdown of *USP15* reduced the induction of proteasome

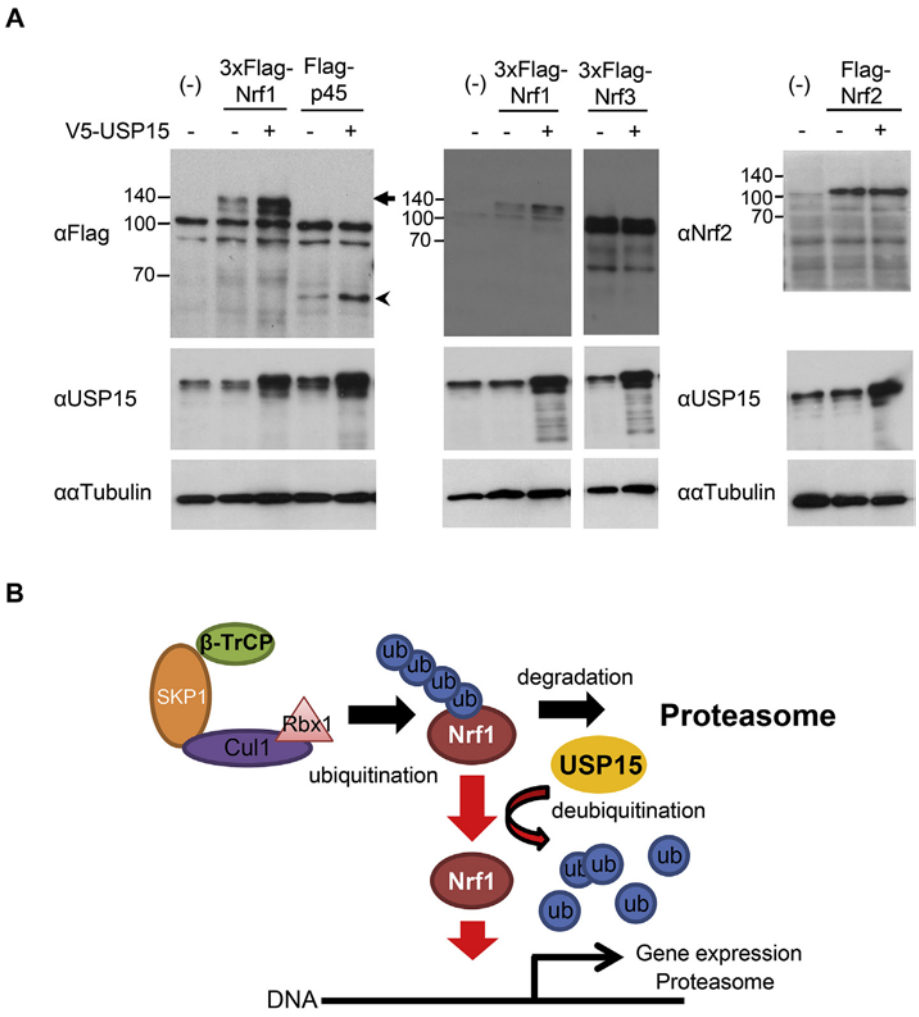

Fig. 4. Biological relevance between USP15 and CNC family proteins. (A) V5-USP15 stabilizes 3 × Flag-Nrf1 and Flag-p45 but not Flag-Nrf2 or 3 × Flag-Nrf3 in HEK293T cells. The arrow and arrowhead stand for 3 × Flag-Nrf1 and Flag-p45 expression, respectively. (B) A schematic model of the new Nrf1 activation mechanism by USP15 for the proteasome gene expression. In the nucleus, β-TrCP and USP15 competitively regulate the Nrf1 stability for the proteasome gene expression.

gene expression by endogenous Nrf1 in response to proteasome inhibition (Fig. 3F and H). Hence, these results strongly suggest that USP15 mediates the transcriptional activities of Nrf1. Intriguingly, we found that the knockdown of USP15 induced both the mRNA and protein expression levels of Nrf1 (Figs. 3D and 1D, respectively). Consequently, *USP15* siRNA activated the expression of proteasome genes, such as *PSMC4* and *PSMA4*. Nevertheless, we observed that the knockdown of *USP15* significantly reduced the Nrf1-mediated proteasome gene induction. These results imply that the Nrf1-USP15 axis comprises multiple negative and positive feedback loops. In this regard, we consider that the induction of NRF1 mRNA by USP15 knockdown compensates reduced protein expression level of NRF1, although the detailed mechanism remains to be elucidated. Collectively, the presence of multiple feedback loops in the Nrf1-USP15 axis further strengthens the fact that USP15 actually functions as a positive regulator for Nrf1.

We surmise that USP15 could endow Nrf1 and Nrf2 with distinct physiological roles, because a recent report described that USP15 negatively regulates the Nrf1-related factor Nrf2 [15]. Under physiological conditions, Nrf2 is degraded by the Keap1-Cul3 Ub ligase [18–21]. USP15 activates ubiquitin ligase activity by deubiquitinating Keap1 as its adaptor, promoting the proteasomal degradation of Nrf2. We did not observe that USP15 has any effects on Nrf2 stability (Fig. 4A), although the reason for this is unknown. Nevertheless, these data could imply opposite effects of USP15 on the transcriptional activities of Nrf1 and Nrf2. It has been recently reported that oxidative stress inhibits the deubiquitination activity of USP15 *in vitro* [22]. Given that Nrf2 exerts gene regulation in the oxidative stress response, it is quite reasonable that oxidative stress could repress the Keap1-mediated proteasomal degradation of Nrf2 by suppressing USP15. On the contrary, oxidative stress might eliminate Nrf1 on ARE genes for the Nrf2 binding by inhibiting the function of USP15 because Nrf1 binds to the ARE of *NQO1* and proteasome subunit genes under physiological conditions [6,17]. The accumulated data of mouse gene targeting experiments strongly support that Nrf1 and Nrf2 play distinct roles in the activation of ARE-dependent genes [5,6]. Collectively, these data provide an attractive hypothesis that USP15 possesses physiological roles that enable it to switch between Nrf1 and Nrf2.

USP15 regulates the stabilization of many substrate proteins in diverse cellular processes, such as MDM2 [13] and TGF-β receptor I [23]. Most of reports reveal the biological function of USP15 in the cytoplasm. We report that USP15 also exerts a function in the nucleus. Supporting our observation, one report found that USP15 deubiquitinates R-SMAD in both the cytoplasm and nucleus [14]. Furthermore, the overexpression of Nrf1 markedly promotes the

nuclear translocation of USP15 (Fig. 2A), similar to the case of the nuclear protein Tip110 [24]. Taken together, it is fully possible that USP15 deubiquitinates Nrf1 in the nucleus.

Acknowledgements

We would like to thank Drs. Stefano Piccolo, Raymond J. Deshaies, Ken Itoh and Naoto Saitoh for providing the V5-USP15, 3xPSMA4-ARE-Luc plasmid, Flag-Nrf2 and Flag-p45 and a fluorometer, respectively. This work was supported in part by grants-in-aid (AK, 26116725, 16H03265) and the Strategic Research Foundation at Private Universities (2012–2016) (AK, S1201009) from the Ministry of Education, Culture, Sports, Science, and Technology, Japan.

Transparency document

Transparency document related to this article can be found online at http://dx.doi.org/10.1016/j.bbrc.2016.07.045.

References

[1] J. Steffen, M. Seeger, A. Koch, E. Krüger, Proteasomal degradation is transcriptionally controlled by TCF11 via an ERAD-dependent feedback loop, Mol. Cell 40 (2010) 147–158.
[2] S.K. Radhakrishnan, et al., Transcription factor Nrf1 mediates the proteasome recovery pathway after proteasome inhibition in mammalian cells, Mol. Cell 38 (2010) 17–28.
[3] A. Kobayashi, et al., Central nervous system-specific deletion of transcription factor Nrf1 causes progressive motor neuronal dysfunction, Genes Cells 16 (2011) 692–703.
[4] C.S. Lee, et al., Loss of nuclear factor E2-related factor 1 in the brain leads to dysregulation of proteasome gene expression and neurodegeneration, Proc. Natl. Acad. Sci. U. S. A. 108 (2011) 8408–8413.
[5] G.P. Sykiotis, D. Bohmann, Stress-activated cap'n'collar transcription factors in aging and human disease, Sci. Signal. 3 (2010) re3.
[6] M. Bugno, M. Daniel, N.L. Chepelev, W.G. Willmore, Changing gears in Nrf1 research, from mechanisms of regulation to its role in disease and prevention, Biochim. Biophys. Acta. 1849 (2015) 1260–1276.
[7] Y. Zhang, D.H. Crouch, M. Yamamoto, J.D. Hayes, Negative regulation of the Nrf1 transcription factor by its N-terminal domain is independent of Keap1: Nrf1, but not Nrf2, is targeted to the endoplasmic reticulum, Biochem. J. 399 (2006) 373–385.
[8] Y. Tsuchiya, et al., Dual regulation of the transcriptional activity of Nrf1 by β-TrCP- and Hrd1-dependent degradation mechanisms, Mol. Cell. Biol. 31 (2011) 4500–4512.
[9] M. Biswas, D. Phan, M. Watanabe, J.Y. Chan, The Fbw7 tumor suppressor regulates nuclear factor E2-related factor 1 transcription factor turnover through proteasome-mediated proteolysis, J. Biol. Chem. 286 (2011) 39282–39289.
[10] A.Y. Amerik, M. Hochstrasser, Mechanism and function of deubiquitinating enzymes, Biochim. Biophys. Acta Mol. Cell Res. 1695 (2004) 189–207.
[11] F.E. Reyes-Turcu, K.H. Ventii, K.D. Wilkinson, Regulation and cellular roles of ubiquitin-specific deubiquitinating enzymes, Annu. Rev. Biochem. 78 (2009) 363–397.
[12] R.N. De Jong, et al., Solution structure of the human ubiquitin-specific protease 15 DUSP domain, J. Biol. Chem. 281 (2006) 5026–5031.
[13] Q. Zou, et al., USP15 stabilizes MDM2 to mediate cancer-cell survival and inhibit antitumor T cell responses, Nat. Immunol. 15 (2014) 562–570.
[14] M. Inui, et al., USP15 is a deubiquitylating enzyme for receptor-activated SMADs, Nat. Cell Biol. 13 (2011) 1368–1375.
[15] N.F. Villeneuve, et al., USP15 negatively regulates Nrf2 through deubiquitination of Keap1, Mol. Cell 51 (2013) 68–79.
[16] D. Vilchez, et al., Increased proteasome activity in human embryonic stem cells is regulated by PSMD11, Nature 489 (2012) 304–308.
[17] Y. Tsuchiya, et al., The CK2-Nrf1 axis controls the clearance of ubiquitinated proteins by regulating proteasome gene expression, Mol. Cell. Biol. 33 (2013) 3461–3471.
[18] A. Kobayashi, et al., Oxidative stress sensor Keap1 functions as an adaptor for Cul3-based E3 ligase to regulate proteasomal degradation of Nrf2, Mol. Cell. Biol. 24 (2004) 7130–7139.
[19] D.D. Zhang, S.-C. Lo, J.V. Cross, D.J. Templeton, M. Hannink, Keap1 is a redox-regulated substrate adaptor protein for a Cul3-dependent ubiquitin ligase complex, Mol. Cell. Biol. 24 (2004) 10941–10953.
[20] S.B. Cullinan, J.D. Gordan, J. Jin, J.W. Harper, J.A. Diehl, The Keap1-BTB protein is an adaptor that bridges Nrf2 to a Cul3-based E3 ligase: oxidative stress sensing by a Cul3-Keap1 ligase, Mol. Cell. Biol. 24 (2004) 8477–8486.
[21] M. Furukawa, Y. Xiong, BTB protein Keap1 targets antioxidant transcription factor Nrf2 for ubiquitination by the Cullin 3-Roc1 ligase, Mol. Cell. Biol. 25 (2005) 162–171.
[22] J.-G. Lee, K. Baek, N. Soetandyo, Y. Ye, Reversible inactivation of deubiquitinases by reactive oxygen species in vitro and in cells, Nat. Commun. 4 (2013) 1568.
[23] P.J.A. Eichhorn, et al., USP15 stabilizes TGF-β receptor I and promotes oncogenesis through the activation of TGF-β signaling in glioblastoma, Nat. Med. 18 (2012) 429–435.
[24] K.A. Timani, Y. Liu, A. Suvannasankha, J.J. He, Regulation of ubiquitin-proteasome system-mediated Tip110 protein degradation by USP15, Int. J. Biochem. Cell Biol. 54 (2014) 10–19.

Biochemical and Biophysical Research Communications 484 (2017) 176–183

Contents lists available at ScienceDirect

Biochemical and Biophysical Research Communications

journal homepage: www.elsevier.com/locate/ybbrc

Possible roles of the transcription factor Nrf1 (NFE2L1) in neural homeostasis by regulating the gene expression of deubiquitinating enzymes

Hiroaki Taniguchi [a, 1], Shota Okamuro [a, 1], Misaki Koji [a, 1], Tsuyoshi Waku [a], Kaori Kubo [a], Atsushi Hatanaka [a], Yimeng Sun [a], A.M. Masudul Azad Chowdhury [a], Akiyoshi Fukamizu [b], Akira Kobayashi [a, *]

[a] Laboratory for Genetic Code, Graduate School of Life and Medical Sciences, Doshisha University, Kyotanabe, Kyoto, Japan
[b] Center for Tsukuba Advanced Research Alliance, University of Tsukuba, Tsukuba, Ibaraki, Japan

ARTICLE INFO

Article history:
Received 30 December 2016
Accepted 9 January 2017
Available online 11 January 2017

Keywords:
Proteostasis
Ubiquitination
Deubiquitination
Neurodegeneration
Gene regulation

ABSTRACT

The transcription factor Nrf1 (NFE2L1) maintains protein homeostasis (proteostasis) by regulating the gene expression of proteasome subunits in response to proteasome inhibition. The deletion of the *Nrf1* gene in neural stem/progenitor cells causes severe neurodegeneration due to the accumulation of ubiquitinated proteins in Purkinje cells and motor neurons (*Nrf1* NKO mice). However, the molecular mechanisms governing this neurodegenerative process remain unclear. We demonstrate herein that the loss of *Nrf1* leads to the reduced gene expression of the deubiquitinating enzymes (DUBs) but not proteasome subunits in *Nrf1* NKO mice between P7 and P18. First, we show that K48-linked polyubiquitinated proteins accumulate in *Nrf1*-deficient Purkinje cells and cerebral cortex neurons. Nevertheless, loss of *Nrf1* does not alter the expression and proteolytic activity of proteasome. A significantly reduced expression of deubiquitinating enzymes was also demonstrated in *Nrf1*-deficient cerebellar tissue using microarray analysis. The genome database further reveals species-conserved ARE, a Nrf1 recognition element, in the regulatory region of certain *DUB* genes. Furthermore, we show that Nrf1 can activate *Usp9x* gene expression related to neurodegeneration. Altogether these findings suggest that neurodegeneration in *Nrf1* NKO mice may stem from the dysfunction of the ubiquitin-mediated regulation of neuronal proteins.

1. Introduction

The transcription factor Nrf1 (NFE2L1), a member of the CNC-bZip transcription factor family, maintains protein homeostasis (*e.g.*, proteostasis) [1,2]. Nrf1 induces the gene expression of proteasome subunits through the antioxidant response element (ARE) by heterodimerizing with a small Maf protein in response to proteasome inhibition [3,4]. Consistently, previous papers have reported that the deletion of the *Nrf1* gene in neural cells leads to severe neurodegeneration and the accumulation of ubiquitinated proteins in mice [5,6]. Late-stage *Nrf1* gene deletion in neuronal cells prompts late-onset neurodegeneration. The pathogenesis of this neurodegeneration process is due to the dysfunction of the proteasome. We also conducted conditional *Nrf1* gene targeting in neural stem cells and progenitor cells using the *Nestin* gene promoter-driven *Cre* transgenic mice (*Nrf1* NKO mice). *Nrf1* NKO mice show severe neurodegenerative disease with the concomitant accumulation of polyubiquitinated proteins in neurons. These mice all die within three weeks of their birth. However, the molecular mechanisms governing the neurodegeneration found in *Nrf1* NKO mice have yet to be elucidated.

The ubiquitin-proteasome pathway mediates physiological processes in many different cell types including those of the central nervous system [7,8]. The proteasome rapidly degrades substrate

Abbreviations: ARE, antioxidant response element; CNC, Cap'n'Collar; DUB, deubiquitinating enzyme; Nrf1, NF-E2-related factor 1; NFE2L1, NF-E2-like 1; qRT-PCR, quantitative real time- PCR; SD, standard deviation; TSS, transcription start site; Usp, ubiquitin-specific protease.

* Corresponding author. Laboratory for Genetic Code, Graduate School of Life and Medical Sciences, Doshisha University, 1-3 Tatara Miyakodani, Kyotanabe, 610-0394, Japan.
E-mail address: akobayas@mail.doshisha.ac.jp (A. Kobayashi).
[1] These authors equally contributed to this work.

http://dx.doi.org/10.1016/j.bbrc.2017.01.038
0006-291X/

proteins conjugated with a polyubiquitin chain by way of the E3 ubiquitin ligase. This in turn eliminates the biological function of target proteins. Deubiquitinating enzymes, in contrast, stabilize substrates by removing the polyubiquitin chain from substrates. In this regard, the key feature of ubiquitin modification is that it is rapid and reversible. This allows cells to mediate regulatory pathways in response to intrinsic and extrinsic signals. Dysfunction of the posttranslational modification system causes many human diseases, including neurodegenerative diseases [7,8]. For example, it has been reported that lower levels and activities of Usp9x may contribute to the pathogenesis of Parkinson's disease [9,10].

Here, we report that *Nrf1* NKO mice have reduced gene expression of deubiquitinating enzymes. Furthermore, polyubiquinated proteins accumulate in the nucleus and/or cytoplasm of *Nrf1*-deficient Purkinje cells in the cerebellum and in cerebral cortex neurons. We found that the expression and activity of proteasomal proteins are similar to those found in control mice at P18. Nevertheless, the expression of deubiquitinating enzymes (DUBs) is significantly reduced following *Nrf1* gene deletion. Species-conserved ARE sequences have also been found in the promoter region of certain types of *DUB* genes. Among them, Nrf1 was identified to regulate the expression of the *Usp9x* gene through the ARE. The pathogenesis of neurodegeneration in *Nrf1* NKO mice may therefore be due to an imbalance in the ubiquitination and deubiquitination of neural factors.

2. Materials and methods

2.1. Generation of neural stem and progenitor cell-specific Nrf1 knockout mice

Neural stem and progenitor cell-specific deletion of the *Nrf1* gene was accomplished as described [6]. Mice were housed in a specific pathogen-free facility, and the experimental protocol was approved and executed under the ethics review committee for animal experiments of Doshisha University.

2.2. Antibodies

The antibodies utilized in this study were anti-FLAG (M2; Sigma), anti-α-tubulin (DM1A; Sigma), anti-Calbindin (AB1778; Chemicon), anti-Nrf1 (#8052; CST), anti-p62/SQSTM1 (PM045; MBL), anti-ubiquitin (P4D1; Santa Cruz), anti-ubiquitin (Z045801; Dako), anti-K48 linked poly-ubiquitin (#4289; CST), anti-Proteasome 20S α1, 2, 3, 5, 6 & 7 subunits (Psma1-3 & 5–7) (Enzo; BML-PW8195), anti-Proteasome 20S α2 (Psma2) (Gene Tex; GTX103620) and anti-LC3 antibodies (PD014; MBL).

2.3. Cell culture and transfection

Neuro2A cells were cultured in Dulbecco's modified Eagle's medium (DMEM) (Wako) supplemented with 10% fetal calf serum (FCS) (Invitrogen), 4500 mg/l glucose, 40 μg/ml streptomycin, and 40 units/ml penicillin (Invitrogen) in a humidified incubator at 5% CO_2 and 37 °C. The transfection of plasmid DNA and short interfering RNA (siRNA) into Neuro2A cells was performed using Lipofectamine Plus and RNAiMAX (Invitrogen), respectively, according to the manufacturer's protocols. The sequences of siRNAs employed in the present study are listed in Table S1 in the supplemental material section.

2.4. RNA extraction and quantitative real-time PCR (qRT-PCR)

Total RNA was extracted from cells with ISOGEN II (311–07361; Nippon Gene) or the RNAeasy minikit (Qiagen) and subjected to cDNA synthesis with oligo dT primers and Moloney murine leukemia virus (M-MLV) reverse transcriptase (Invitrogen) according to the manufacturer's protocol. qRT-PCR was performed with FastStart Universal SYBR (Roche) and the Thermal Cycler Dice Real Time System II (TP900; Takara Bio). The PCR primers employed in this study are listed in Table S1 and 18S *rRNA* or *Gapdh* were used for normalization.

2.5. Western blotting

Whole extracts of mouse cerebellar tissues were prepared as follows. Mice were sacrificed by cervical dislocation and cerebellum tissues were immediately dissected from the brain and homogenized in SDS sample buffer (25 mM Tris-HCl [pH 6.5], 5% glycerol and 1% SDS). After sonication and centrifugation at 20,000×*g* for 5 min at 4 °C, supernatants were collected as whole cerebellum extracts. The protein concentration was determined using the Pierce BCA Protein Assay kit (Pierce). The samples were boiled in the presence of 2% 2-mercaptoethanol at 95 °C for 5 min, separated by SDS-polyacrylamide gel electrophoresis and transferred to PVDF membranes. After blocking with Blocking One (Nacalai Tesque), the membrane was incubated with a primary antibody diluted in TBST (20 mM Tris-HCl [pH 7.6], 137 mM NaCl, 0.1% Tween20) containing 10% Blocking One, followed by a secondary antibody conjugated with horseradish peroxidase and developed with ECL western blotting detection reagents (RPN2106; GE Healthcare).

2.6. Immunofluorescence staining

Mice were perfused with 4% paraformaldehyde (PFA) under anesthesia. Isolated brains were further fixed overnight with 4% PFA and kept in 0.1% sodium azide containing phosphate-buffered saline (PBS) to avoid decaying. The fixed brains were processed for vibratome sectioning (50 μm). Sliced tissues were autoclaved in 10 mM citrate buffer [pH 6.0] at 100 °C for 10 min and washed twice with PBS containing 0.1% Tween20 (PBST) for 10 min. Next, the sliced tissues were permeabilized with 0.5% Triton X-100 in PBS for 1 h at room temperature (RT), washed twice with PBST for 10 min and blocked with 10% horse serum/PBST at RT for 1 h. The sections were then incubated with primary antibodies diluted with PBST containing 1% bovine serum albumin (BSA) for 48 h at RT. After washing 4 times with PBST for 30 min, the sections were incubated with Alexa Fluor 488/546-conjugated secondary antibody (A-11029, A-11035, Invitrogen) diluted in PBST containing 1% BSA for 48 h at RT. The nuclei were then stained with 4′, 6'-diamidino-2-phenylindole (DAPI) (0.5 μg/ml) for 1 h at RT and washed 3 times with PBST for 30 min. Finally, the samples were sealed using fluorescence mounting medium (Dako). Fluorescence images were captured by a Carl Zeiss confocal microscope (LSM710).

2.7. Reporter construction and luciferase assay

A mouse *Usp9x* gene reporter was generated by inserting a 2-kbp PCR-amplified promoter region into pGL-basic (Promega). The primers were 5′-CGAAGATCTAAGGCTCAGCGCTTCTCCGCCC-3′ and 5′-GGGGTACCACATGTGCTTACCAGGCTTGTTG-3′. The reporter was transfected into Neuro2a cells along with p3xFlag mNrf1 [11] and pRL-TK (Promega) as an internal control. Forty-eight hours after transfection, luciferase activity was measured using the PicaGene luciferase assay system (Toyo Ink) and a Berthold Lumat LB9507 luminometer.

2.8. Proteasome fluorogenic peptidase assay

The *in vitro* measurement of proteasome activities was

performed as previously described [12]. Twenty micrograms of total protein of cell lysates was utilized for the assay using Suc-LLVY-AMC (Peptide Institute), Z-GGL-AMC (Santa Cruz), Z-LLE-AMC (Peptide Institute) or Ac-RLR-AMC (R&D systems). After mixing the lysate with the substrate, fluorescence (380 nm excitation, 460 nm emission) was monitored on a microplate fluorometer (Synergy HTX; BioTek) every 5 min for 1 h at 37 °C. The protein concentration of the cell lysates was determined using the BCA protein assay (Pierce). Relative proteasome activity was expressed as the slope of the linear fitting curves.

2.9. Microarray

Three independent RNA samples of the mouse cerebellum from each genotype (P7) were mixed and used for the microarray analyses. Microarray analysis was performed using slides (Affimetrix, Mouse Gene 1.0 ST Array). The data were analyzed with Expression Console and Transcriptome Analysis Console (Affimetrix). GSEA analysis was performed using open source software (v2.2.3, Broad Institute, http://software.broadinstitute.org/gsea/index.jsp) and the gene set annotated as the GO term “protein deubiquitination” (GO:0016579, http://amigo.geneontology.org/amigo/term/GO:0016579).

2.10. Statistical analyses

Statistical analyses were performed using Student's *t*-test; $P < 0.05$ was considered significant.

3. Results and discussion

3.1. Accumulation of K48-linked ubiquitinated proteins in Nrf1-deficient Purkinje cells and cerebral cortex neurons

We previously reported that polyubiquitinated proteins accumulate in various central nervous system cells including Purkinje cells in the cerebellum and cerebral cortex neurons [6]. To elucidate the characteristics of the proteins accumulated in the *Nrf1*-deficient neurons, we first determined their cellular localization by immunofluorescence staining (Fig. 1). Generally, ubiquitinated proteins accumulated in the nucleus of *Nrf1*-deficient Purkinje cells, whereas more variable patterns, including cytoplasmic accumulation and both cytoplasmic and nuclear accumulation, were found in cerebral cortex neurons. These findings may imply a specificity of the ubiquitin-conjugated proteins.

Next, we sought to determine whether the proteins that accumulated in *Nrf1* NKO Purkinje cells were conjugated with K48-linked polyubiquitin chains, which is a hallmark of proteasome substrates. We stained Purkinje cells using an antibody against the K48-linked polyubiquitin chain (Fig. 1C), indicating that the accumulated proteins were conjugated with K48-linked polyubiquitin chains. Thus, the dysfunction of Nrf1 expression leads to the accumulation of K48-typed ubiquitinated proteins in Purkinje cells.

3.2. The expression and activity of proteasome proteins are not altered in Nrf1-deficient cerebellum

A growing body of evidence reveals that Nrf1 mediates the gene expression of proteasome subunits in response to proteasomal dysfunction (*e.g.,* proteostasis) [1,2]. It has also been reported that the deletion of the *Nrf1* gene in differentiated neurons leads to neurodegeneration due to the dysregulation of proteasome genes [5]. Accordingly, we hypothesized that proteasome dysfunction promotes the accumulation of ubiquitinated proteins in *Nrf1* NKO mice. To confirm our hypothesis, we first analyzed proteasome subunit gene expression alterations in *Nrf1* NKO mice (P18) by quantitative realtime PCR (qRT-PCR) (Fig. 2A). Surprisingly, the gene expression of the proteasome subunits, *Psma2*, *Psma6* and *Psmc4* in *Nrf1*-deficient cerebellar tissue was not suppressed. The expression of these genes was slightly increased compared to that found in age-matched control mice (*Nrf1* flox/flox mice). In addition, neither the proteasome subunit protein expression levels nor the proteasomal activity, including the chymotrypsin, trypsin and caspase-like activities, were altered (Fig. 2B and C). We then performed immunostaining experiments to semi-quantitatively examine the protein levels of Psma2 in Purkinje cells (Fig. 2D). This excluded the possibility that a reduction in proteasome function and expression could be masked in whole cerebellum samples because Nrf1 is mainly expressed in cerebellar Purkinje cells [6]. Similarly, no significant reduction in the Psma2 protein levels was found in *Nrf1*-deficient Purkinje cells. Finally, western blot analyses of p62 and LC3 demonstrated that autophagy as an alternative proteostasis system was unaltered when compared to cerebellar tissue of control mice (Fig. 2E). Collectively, we concluded that the neurodegeneration observed in *Nrf1* NKO mice is not due to proteasome dysfunction. The exact cause underlying the divergent results observed between our mice and those of Chan's group mice remains unknown. Our differing results may be due, in part, to the different *Nrf1* deletion strategies employed by both groups. Our group used *Nestin-Cre* transgenic mice, while they utilized *CamK2-Cre* transgenic mice [5]. Alternatively, it is also possible that only early stage (before P7) *Nrf1* NKO mice suffer from proteasomal dysregulation, which subsequently triggers neurodegeneration.

3.3. Reduced gene expression of deubiquitinating enzymes in Nrf1-deficient cerebellar tissue

To identify the Nrf1 target gene(s) in which reduction exerts neurodegeneration, we carried out microarray analysis using cerebellar tissue from *Nrf1*-deficient mice (P7) that had not yet demonstrated an abnormal phenotype (Fig. 3). The expression of 1705 genes were reduced as a result of *Nrf1* deletion. Among them, 1198 genes possess the Nrf1-recognition ARE sequence within 2-kbp upstream and downstream regions from the transcriptional start site (Fig. 3A). Gene ontology analysis indicated that these genes possess biological functions related to mitotic nuclear division, microtubule cytoskeleton organization, mitotic cell cycle and protein deubiquitination (Fig. 3B and C). Because polyubiquitinated proteins accumulate in *Nrf1* NKO mice, we focused our attention on the protein deubiquitination genes. Indeed, the microarray data demonstrated that the expression levels of a variety of genes encoding deubiquitinating enzymes (DUBs) were reduced due to the deletion of the *Nrf1* gene (data not shown). A marked reduction in DUB expression was also confirmed by qRT-PCR in cerebellar tissue from *Nrf1* NKO mice at both P7 and P18 (Fig. 3D). Further bioinformatics analysis strengthened the physiological relevance between Nrf1 and DUBs, because the AREs of these *DUB* genes are mostly conserved within the regulatory region of several species (Table S2). Our findings demonstrate that Nrf1 may play a role in regulating *DUB* genes in the cerebellum.

3.4. Nrf1 governs neural homeostasis by regulating Usp9x gene expression

Next, we investigated the biological relationship between Nrf1 and Usp9x, because USP9X dysfunction has been noted in Lewy Body Disease and Parkinson's disease [9,10]. Interestingly, similar to Nrf1, the *Usp9x* gene is abundantly expressed in the cerebellar Purkinje cells of mice [6,9,10,13]. The ChIP-seq data from the UCSC database suggest that the ARE of *Usp9x* gene is functional because

Nrf2, a Nrf1-related factor, and its heterodimerizing partner MafK have both been shown to recognize this ARE sequence in mouse erythroleukemia CH12 cells and MEL cells (Fig. 4A). Luciferase reporter analysis was used to demonstrate that Nrf1 directly activates the *Usp9x* gene expression through the ARE (Fig. 4B). The transient expression of Nrf1 markedly activated the expression of a luciferase reporter containing the 2-kbp upstream region of the *Usp9x* gene in mouse neuroblastoma Neuro2A cells. Finally, we confirmed that siRNA-mediated Nrf1 knockdown reduces the expression of the *Usp9x* gene in Neuro2A cells (Fig. 4C).

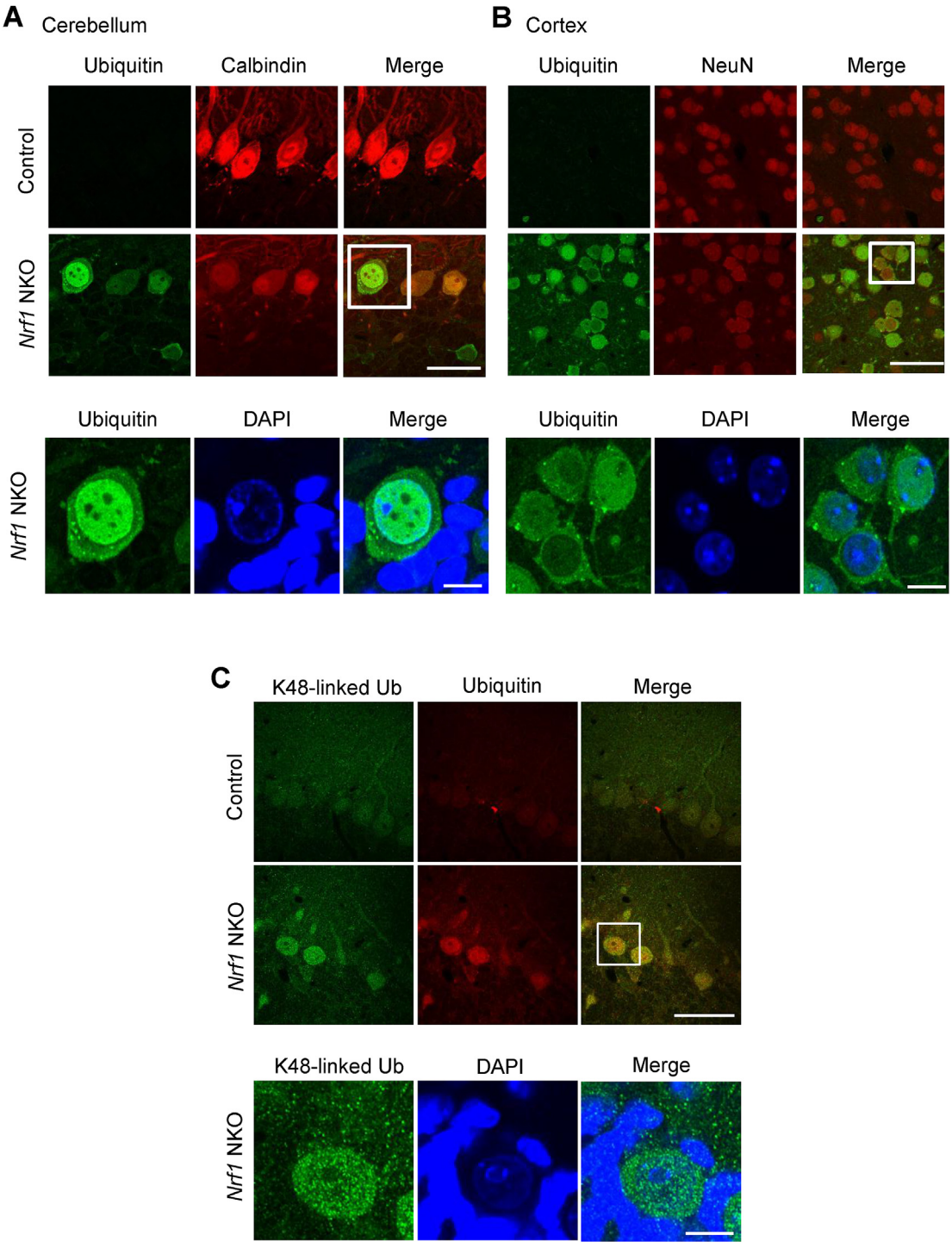

Fig. 1. *Nrf1*-deficient Purkinje cells and cortex neurons accumulate K48-linked polyubiquitinated proteins. A, B) Immunofluorescence staining of polyubiquitinated proteins in the cerebellar Purkinje cells and cortex neurons of the *Nrf1* NKO mice (P18). Purkinje cells and cortex neurons were stained with anti-Calbindin and anti-NeuN antibodies, respectively. Bottom panels are magnified images of white squares in the upper panels. Nuclei were stained with DAPI. Scale bars represent 25 μm, 50 μm (left and right of upper panels, respectively) and 10 μm (bottom panels). C) K48-linked polyubiquitinated proteins in the cerebellum were visualized by immunofluorescence staining using anti-K48Ub antibodies. Bottom panels are magnified images of the white squares in the upper panels. Nuclei were stained with DAPI. Scale bars represent 50 μm (upper panels) and 10 μm (bottom panels).

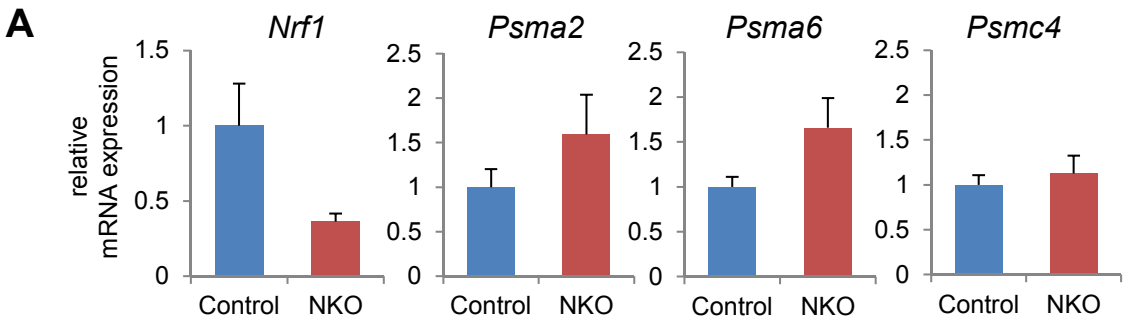
A
Nrf1
Psma2
Psma6
Psmc4
relative mRNA expression
Control
NKO

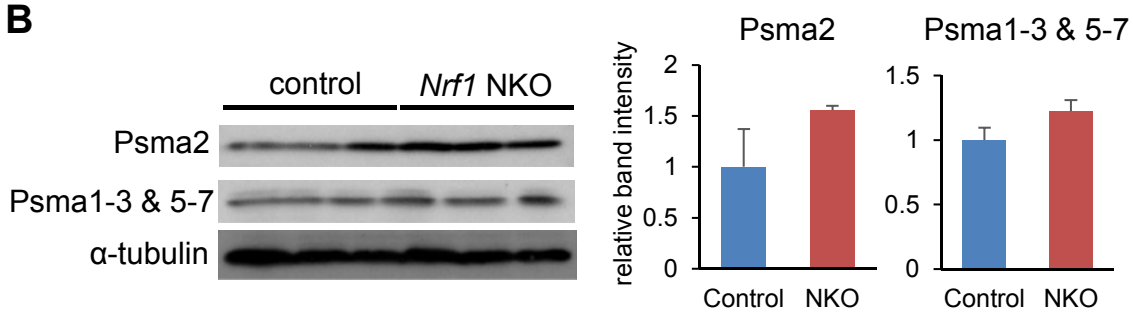
B
control
Nrf1 NKO
Psma2
Psma1-3 & 5-7
α-tubulin
relative band intensity
Psma2
Psma1-3 & 5-7
Control
NKO

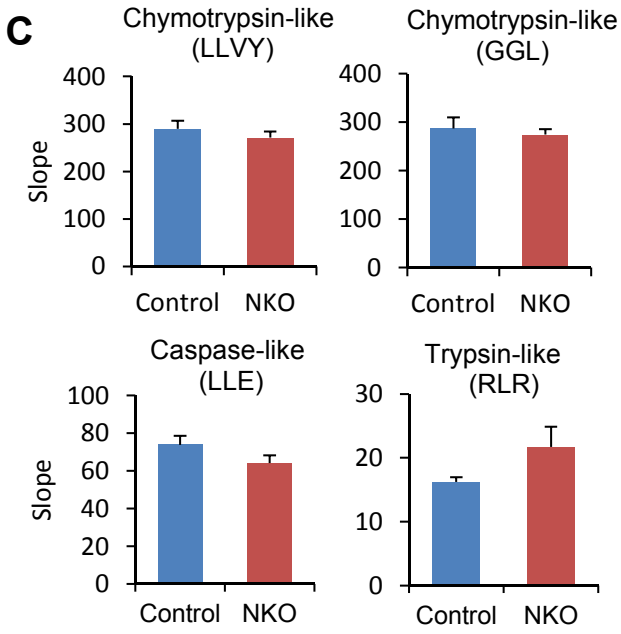
C
Chymotrypsin-like (LLVY)
Chymotrypsin-like (GGL)
Caspase-like (LLE)
Trypsin-like (RLR)
Slope
Control
NKO

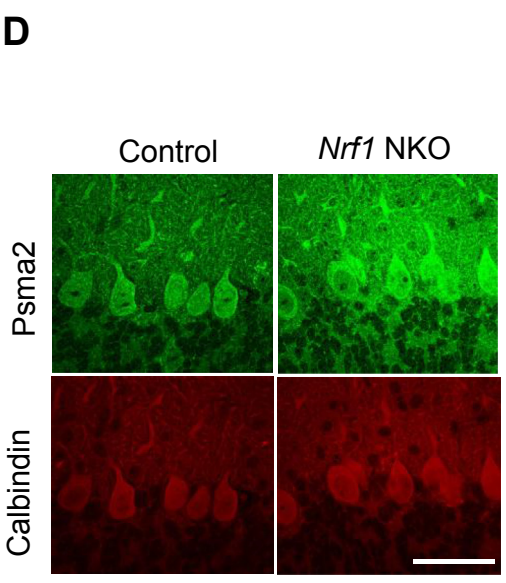
D
Control
Nrf1 NKO
Psma2
Calbindin

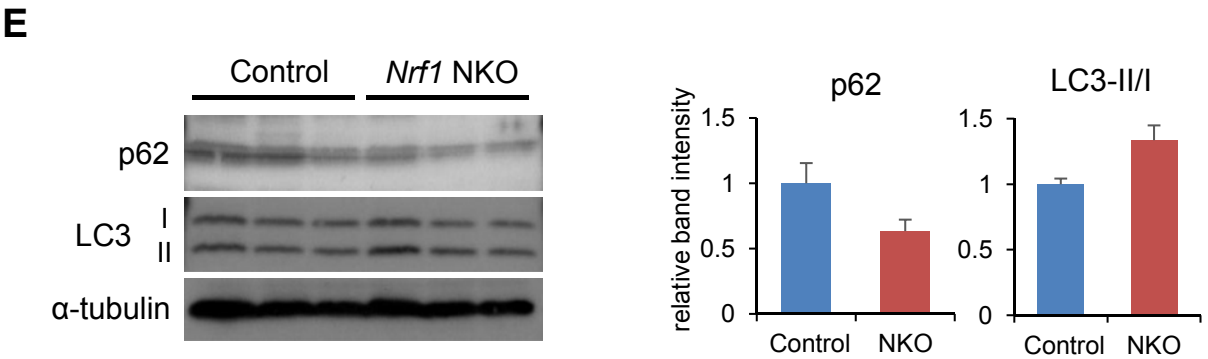
E
Control
Nrf1 NKO
p62
LC3
I
II
α-tubulin
relative band intensity
p62
LC3-II/I
Control
NKO

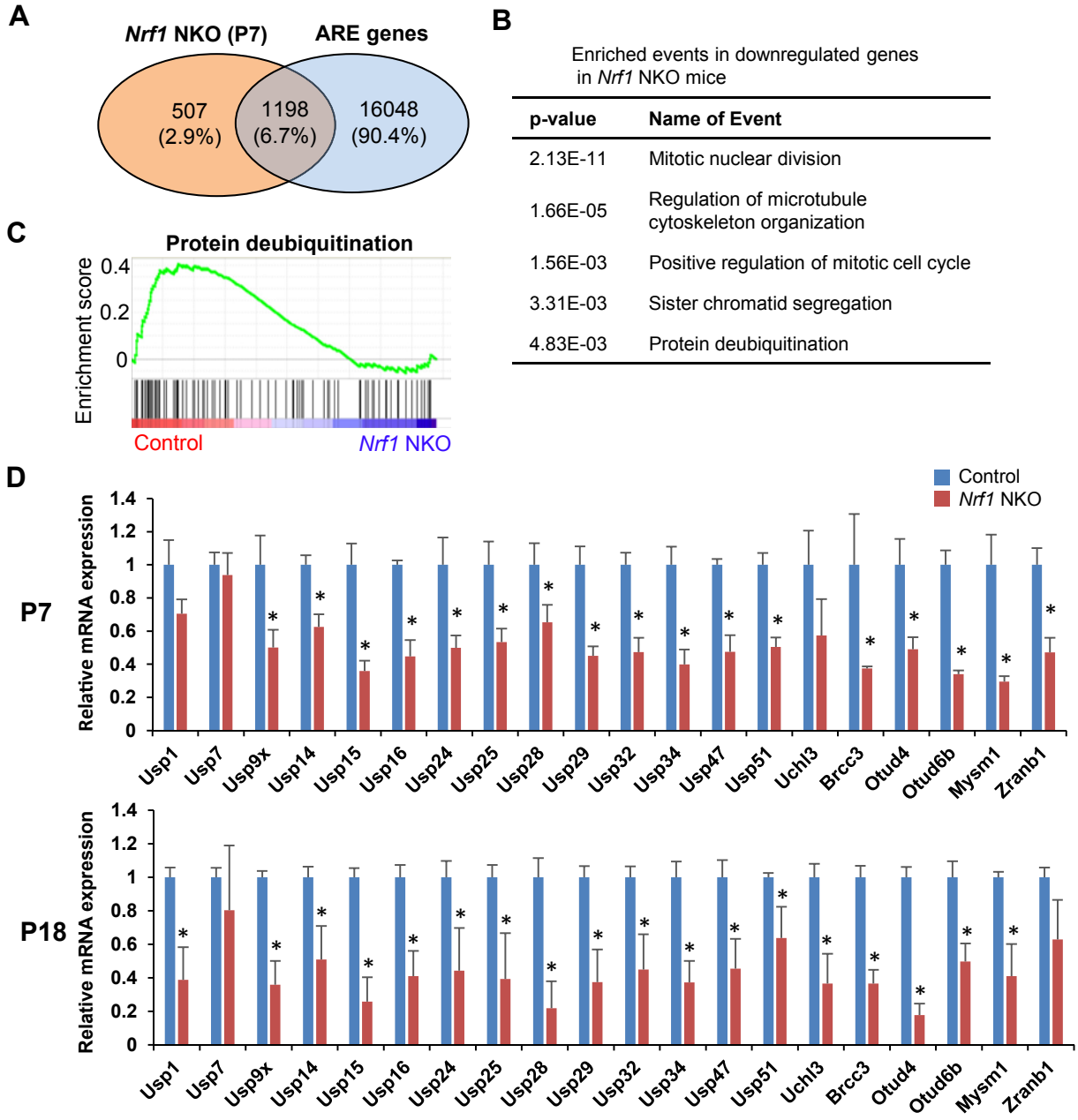

Fig. 3. Nrf1-dependent induction of *DUB* genes in the cerebellum. A) A Venn diagram showing the overlap of gene expression reduced by *Nrf1* deletion and genes containing the species-conserved ARE sequence in 2-kbp upstream and downstream regions from the transcriptional start site. B) A table of the gene ontology analysis using PANTHER significantly enriched with genes downregulated in the cerebellum of *Nrf1* NKO mice. C) Gene Set Enrichment Analysis (GSEA) histograms for the gene sets involved in protein deubiquitination. The nominal *P* values is 0.0028, and the normalized enrichment score is 1.61. D) The mRNA expression levels of the deubiquitinating enzyme genes in the cerebellum of *Nrf1* NKO or control mice were determined by qRT-PCR (P7 and P18). Values were normalized with *Gapdh* and presented as the means ± SD (P7; $n = 3$, P18; $n = 4$, *, $P < 0.05$).

Accordingly, Nrf1 may govern neural homeostasis by regulating *Usp9x* gene expression.

Our findings are consistent with a series of previous reports. *USP9X* knock down induces the formation of toxic α-synuclein inclusions in SH-SY5Y cells upon proteolytic inhibition [10]. Reduced *Usp9x* expression has been proposed to cause spinal muscular atrophy due to impaired motor neuron survival [14]. The ataxia mouse model, which exhibits severe tremors and premature death, is deficient in *Usp14* [15]. Moreover, several USPs have also been found to regulate neural activities [7,8,16–18]. Thus, the loss of *Nrf1* may lead to the imbalance of the ubiquitination status of neural proteins, causing the accumulation of polyubiquitinated proteins and, thus, the neurodegeneration observed in our study.

Fig. 2. Proteasome expression and activity are not reduced in *Nrf1*-deficient cerebellar tissue. A) Quantitative-RT-PCR (qRT-PCR) analysis showing relative mRNA expression of *Psma2*, *Psma6* and *Psmc4* in the cerebellum of *Nrf1* NKO mice (P18, n = 4). B) Western blotting demonstrating the unaltered proteasome subunit proteins in the cerebellum of *Nrf1* NKO mice (P18, n = 3). C) Proteasomal chymotrypsin, trypsin and caspase-like activity were not altered in *Nrf1*-deficient cerebellar tissue. D) No significant reduction in Psma2 protein levels was found in Purkinje cells by immunohistochemical staining using anti-Psma2 and anti-Calbindin antibodies. The scale bar represents 50 μm. E) The p62 protein expression and LC3-II/I ratio as autophagic markers were also not altered in *Nrf1* NKO cerebellar tissue in western blot analysis (P18, n = 3).

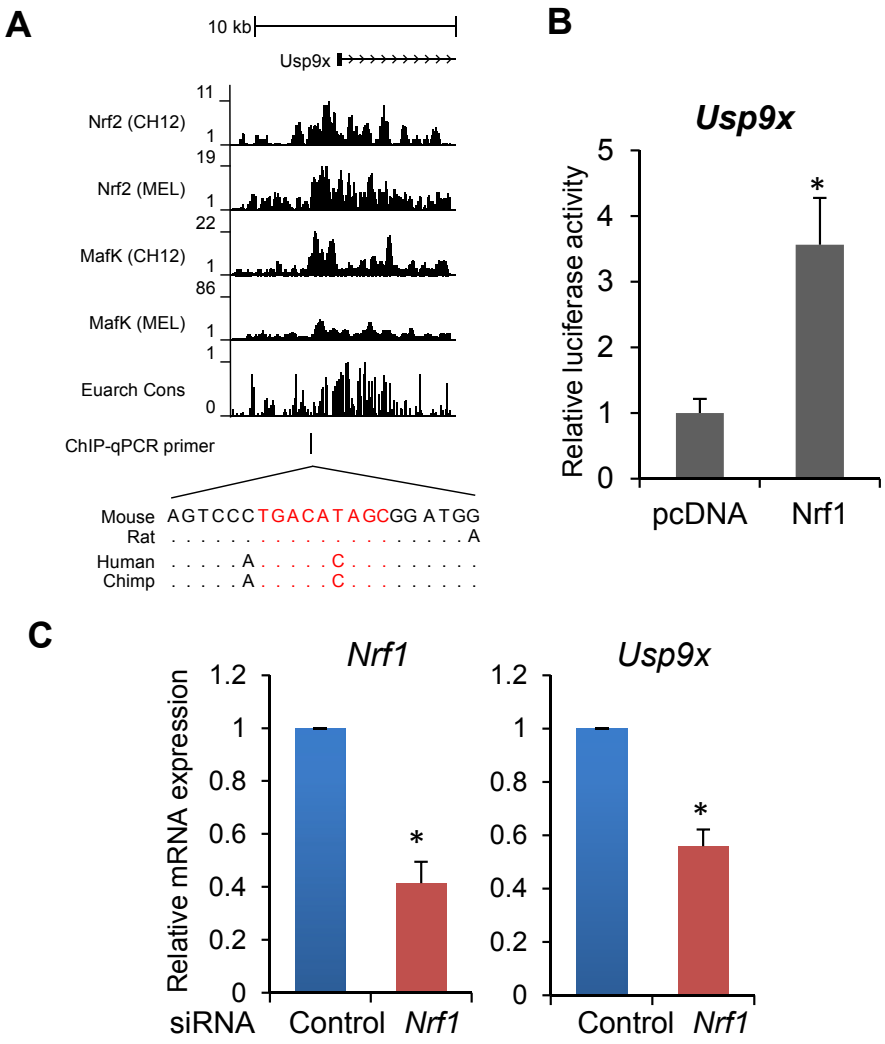

Fig. 4. Nrf1 governs *Usp9x* gene expression. (A) ChIP-seq data using the UCSC genome browser reveals species-conserved ARE sequences (red; dots stand for similar amino acids) in the *Usp9x* gene promoter region, which is recognized by Nrf2 and small Maf proteins. (B) Transient overexpression of Nrf1 activated the expression of the *Usp9x*-ARE luciferase reporter. Luciferase activity was normalized according to the *Renilla* luciferase activity of the internal control, pRL-TK, and presented as the means ± SD ($n = 3$; *, $P < 0.05$). (C) siRNA-mediated *Nrf1* knockdown reduces the gene expression of *Usp9x* in Neuro2A cells. The reduced mRNA levels were determined by qRT-PCR.

Conflict of interests

The authors declare that they have no conflicts of interests.

Acknowledgements

We would like to thank Masayuki Yamamoto for *Nrf1* flox/flox mice. We also thank Shin-ichiro Taya, Tomohiro Miyasaka, Jun Motoyama, Tatsuya Katahira, Hidenori Watanabe and Yuko Yamagata-Kikuchi for experimental supports. This work was supported in part by grants-in-aid (AK, 26116725, 16H03265) and the Strategic Research Foundation at Private Universities (2012–2016) (AK, S1201009) from the Ministry of Education, Culture, Sports, Science and Technology.

Appendix A. Supplementary data

Supplementary data related to this article can be found at http://dx.doi.org/10.1016/j.bbrc.2017.01.038.

Transparency document

Transparency document related to this article can be found online at http://dx.doi.org/10.1016/j.bbrc.2017.01.038.

References

[1] J. Steffen, M. Seeger, A. Koch, E. Krüger, Proteasomal degradation is transcriptionally controlled by TCF11 via an ERAD-dependent feedback loop, Mol. Cell. 40 (2010) 147–158.
[2] S.K. Radhakrishnan, C.S. Lee, P. Young, A. Beskow, J.Y. Chan, R.J. Deshaies, Transcription factor Nrf1 mediates the proteasome recovery pathway after proteasome inhibition in mammalian cells, Mol. Cell. 38 (2010) 17–28.
[3] M. Bugno, M. Daniel, N.L. Chepeev, W.G. Willmore, Changing gears in Nrf1 research, from mechanisms of regulation to its role in disease and prevention, Biochim. Biophys. Acta 1849 (2015) 1260–1276.
[4] Y. Zhang, Y. Xiang, Molecular and cellular basis for the unique functioning of Nrf1, an indispensable transcription factor for maintaining cell homoeostasis and organ integrity, Biochem. J. 473 (2016) 961–1000.
[5] C.S. Lee, C. Lee, T. Hu, J.M. Nguyen, J. Zhang, M. V Martin, M.P. Vawter, E.J. Huang, J.Y. Chan, Loss of nuclear factor E2-related factor 1 in the brain leads to dysregulation of proteasome gene expression and neurodegeneration, Proc. Natl. Acad. Sci. U. S. A. 108 (2011) 8408–8413.

[6] A. Kobayashi, T. Tsukide, T. Miyasaka, T. Morita, T. Mizoroki, Y. Saito, Y. Ihara, A. Takashima, N. Noguchi, A. Fukamizu, Y. Hirotsu, M. Ohtsuji, F. Katsuoka, M. Yamamoto, Central nervous system-specific deletion of transcription factor Nrf1 causes progressive motor neuronal dysfunction, Genes Cells 16 (2011) 692–703.
[7] S.V. Todi, H.L. Paulson, Balancing act: deubiquitinating enzymes in the nervous system, Trends Neurosci. 34 (2011) 370–382.
[8] G. Ristic, W.-L. Tsou, S.V. Todi, An optimal ubiquitin-proteasome pathway in the nervous system: the role of deubiquitinating enzymes, Front. Mol. Neurosci. 7 (2014) 72.
[9] M. Murtaza, L.A. Jolly, J. Gecz, S.A. Wood, La FAM fatale: USP9X in development and disease, Cell. Mol. Life Sci. 72 (2015) 2075–2089.
[10] R. Rott, R. Szargel, J. Haskin, R. Bandopadhyay, A. Lees, V. Shani, S. Engelender, α-Synuclein fate is determined by USP9X-regulated monoubiquitination, Proc. Natl. Acad. Sci. 108 (2011) 1–6.
[11] Y. Tsuchiya, T. Morita, M. Kim, S. Iemura, T. Natsume, M. Yamamoto, A. Kobayashi, Dual regulation of the transcriptional activity of Nrf1 by β-TrCP- and Hrd1-dependent degradation mechanisms, Mol. Cell. Biol. 31 (2011) 4500–4512.
[12] D. Vilchez, L. Boyer, I. Morantte, M. Lutz, C. Merkwirth, D. Joyce, B. Spencer, L. Page, E. Masliah, W.T. Berggren, F.H. Gage, A. Dillin, Increased proteasome activity in human embryonic stem cells is regulated by PSMD11, Nature 489 (2012) 304–308.
[13] J. Xu, S. Taya, K. Kaibuchi, A.P. Arnold, Spatially and temporally specific expression in mouse hippocampus of Usp9x, a ubiquitin-specific protease involved in synaptic development, J. Neurosci. Res. 80 (2005) 47–55.
[14] K.J. Han, D.G. Foster, N.Y. Zhang, K. Kanisha, M. Dzieciatkowska, R.A. Sclafani, K.C. Hansen, J. Peng, C.W. Liu, Ubiquitin-specific protease 9x deubiquitinates and stabilizes the spinal muscular atrophy protein-survival motor neuron, J. Biol. Chem. 287 (2012) 43741–43752.
[15] S.M. Wilson, B. Bhattacharyya, R. a Rachel, V. Coppola, L. Tessarollo, D.B. Householder, C.F. Fletcher, R.J. Miller, N.G. Copeland, N. a Jenkins, Synaptic defects in ataxia mice result from a mutation in Usp14, encoding a ubiquitin-specific protease, Nat. Genet. 32 (2002) 420–425.
[16] B. Bingol, J.S. Tea, L. Phu, M. Reichelt, C.E. Bakalarski, Q. Song, O. Foreman, D.S. Kirkpatrick, M. Sheng, The mitochondrial deubiquitinase USP30 opposes parkin-mediated mitophagy, Nature 509 (2014) 370–375.
[17] S. Urbe, H. Liu, S.D. Hayes, C. Heride, D.J. Rigden, M.J. Clague, Systematic survey of deubiquitinase localization identifies USP21 as a regulator of centrosome- and microtubule-associated functions, Mol. Biol. Cell. 23 (2012) 1095–1103.
[18] V.M. Gadotti, A.G. Caballero, N.D. Berger, C.M. Gladding, L. Chen, T.A. Pfeifer, G.W. Zamponi, Small organic molecule disruptors of Cav3.2-USP5 interactions reverse inflammatory and neuropathic pain, Mol. Pain 11 (2015) 12.